A Model of the Winding and Curing Processes for Filament Wound Composites

by

Jerome T.S. Tzeng

Dissertation submitted to the Faculty of the

Virginia Polytechnic Institute and State University

in partial fulfillment of the requirements for the degree of

Doctor of Philosophy

in

Engineering Mechanics

APPROVED:

Alfred C. Loos, Chairman

Mark S. Cramer

Charles E. Knight Jr.

Don H. Morris

Junuthula N. Reddy

October 1988

Blacksburg, Virginia

A Model of the Winding and Curing Processes for Filament Wound Composites

by

Jerome T.S. Tzeng

Alfred C. Loos, Chairman

Engineering Mechanics

(ABSTRACT)

The goal of this investigation was to develop a two-dimensional model which describes the winding and curing processes of filament wound composite structures. The model was developed in two parts. The first part is the cure model which relates the cure temperature, applied at the boundaries of the composite, to the thermal, chemical, and physical processes occurring in the case during cure. For a specified cure cycle, the cure model can be used to calculate the temperature distribution, the degree of cure of the resin, and the resin viscosity inside the composite case. The second part is the layer tension loss and compaction model which relates the winding process variables (i.e., winding pattern, mandrel geometry, initial winding tension, and the properties of the fiber and resin system) to the instantaneous position and tension of the fibers in each layer of the case. A finite element computer code "FWCURE" was developed to obtain a numerical solution to the model.

Verification of the cure sub-model was accomplished by measuring the temperature distributions in a 5.75 inch diameter graphite - epoxy test bottle and a 4 inch diameter graphite - epoxy tube during cure. The data were compared with the temperature distributions calculated using FWCURE. Differences between the measured and calculated temperatures was no more than 10 °C for both the test bottle and the cylindrical tube.

A parametric study was performed by using FWCURE computer code. Results of the simulation illustrate the information that can be generated by the models and the importance of different processing and material parameters on the fabrication process.

Acknowledgements

I would like to express my gratitude to Professor A. C. Loos for his guidance and encouragement throughout the course of this research and the completion of this thesis. I also thank Professor C. E. Knight for his advice in the development of the model; and Professor J. N. Reddy for his help in the numerical implementation. I am grateful to Professor D. H. Morris and Professor M. S. Cramer for their help and willingness to serve on my committee.

This work is supported by Morton Thiokol, Inc. Aerospace Group. I wish to express my thanks to Dr. D. A. Flanigan and Mr. T. F. Davidson for their continuous support and encouragement in the past four years. In addition, appreciation is extended to Mr. P. E. Rose and Ms. P. P. Alexandratos for their help in obtaining the winding and curing data.

Finally, I would like to thank my family, especially my wife Pei-Pei and my friends, Steve and Nagendra, for their encouragement and support.

Table of Contents

List of Illustrations

List of Tables

1.0 INTRODUCTION

1.1 Filament Winding

Filament winding is a widely used technique of fabricating continuous fiber-reinforced composite structures. For many years, filament wound composites have been used extensively for weight-sensitive structural components such as pressure vessels, rocket-motor cases, piping, springs, and aircraft structures. Recent achievements in filament winding technology include the launch tube for the MX missile and the re-usable solid rocket motor case for the NASA space shuttle.

One of the most crucial yet least understood area of filament winding composite manufacturing is the relationship between winding process variables, the curing process, and the final mechanical performance of the structure. Presently, filament winding is still a highly empirical technology. Processing cycles are usually obtained by trial and error by fabricating and curing small subscale structures. This procedure is time consuming and expensive. Furthermore, the process variables extrapolated from subscale components may not be suitable for the large scale structures. An

improperly processed filament wound case often results in nonuniform and incomplete cure of the matrix resin, wrinkling, local fiber buckling, nonuniform fiber/resin distributions, and high residual stresses. These defects will certainly degrade the strength of filament wound structures. Thus, structures are usually over-designed to compensate for the lack of understanding between the manufacturing process and the final mechanical properties of the structure.

A strong need exists to develop an analytical model which can simulate the fabrication process of filament wound composite structures. Thus, the objective of this project is to develop a model which describes the winding and curing processes of filament wound composite structures during fabrication. The model is expected to provide a fundamental understanding of how the winding and curing processes affect the mechanical performance of filament wound composite structures, and how the mechanical performance of the composite can be improved by choosing suitable process variables.

Filament wound structures are formed by winding continuous bands of resin impregnated fibers onto a rotating mandrel along a predetermined path. A lathe type filament winder is shown in Fig. 1. The mandrel may be made of soluble plaster, PVA sand, or segmented collapsible metal components. A suitable mandrel should be able to resist sag due to its weight and the winding tension in the fibers. The mandrel should also be easily removed from the composite case after cure. Before the composite case is wound, an elastomeric insulator is wound over the surface of mandrel and cured in a separate manufacturing step. The fiber bands are then wound over the surface of the insulator.

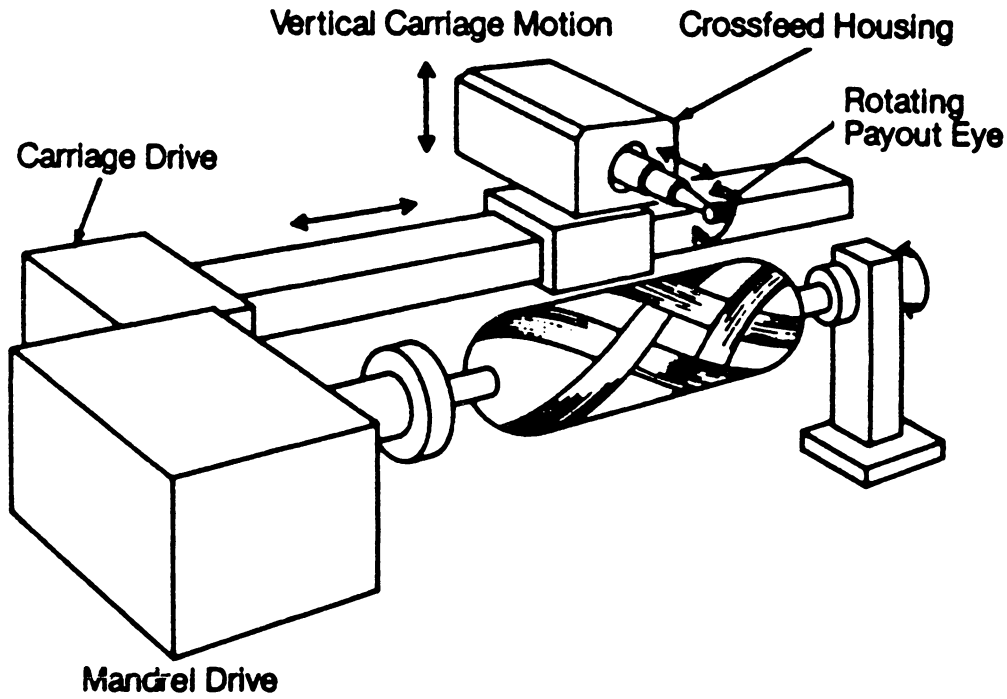

Figure 1. Lathe Type Filament Winder:

A multiaxis lathe type filament winder can wind various winding patterns and structures by controlling the speeds of the axes.

Filament winding can be characterized as either wet winding or dry winding depending on the state of the resin. In wet winding, liquid resin is applied by pulling the fiber bundles through a resin bath during winding. Dry winding, also referred as prepreg winding, utilizes fiber tows that have been preimpregnated with resin in a separate step.

Initially the resin is uncured. At the beginning of the winding process, the fiber bands impregnated with resin are exposed to the ambient temperature as they are wound onto the mandrel and begin to cure. The degree of cure of each layer in the case depends on the resin system, the ambient temperature, and the winding time. Thus, at the completion of the winding process, the degree of cure will be fairly uniform for a thin case. However, for a thick case, there can be considerable differences in the degree of cure between the inner layers and the outer layers.

Upon completion of the winding process the case is prepared for cure by wrapping a teflon release film and a porous breather cloth around the outer surface of the case. Finally, the entire mandrel - insulator - case - breather assembly is cover with a vacuum bag. When the vacuum system is activated, the bag will be drawn tightly around the composite assembly allowing compaction in the outer layers of the case. Also, the vacuum system provides a means for evacuating volatiles which may be released from the resin during cure. The bagged assembly is placed in a forced air oven or an autoclave and cured for a specified length of time. The cure temperature may vary with time in an arbitrary manner. In general, the cure process includes three stages: heating up, curing, and cooling down. The final step is to remove the mandrel from the composite case. The procedures followed in the manufacturing process are illustrated in Fig. 2.

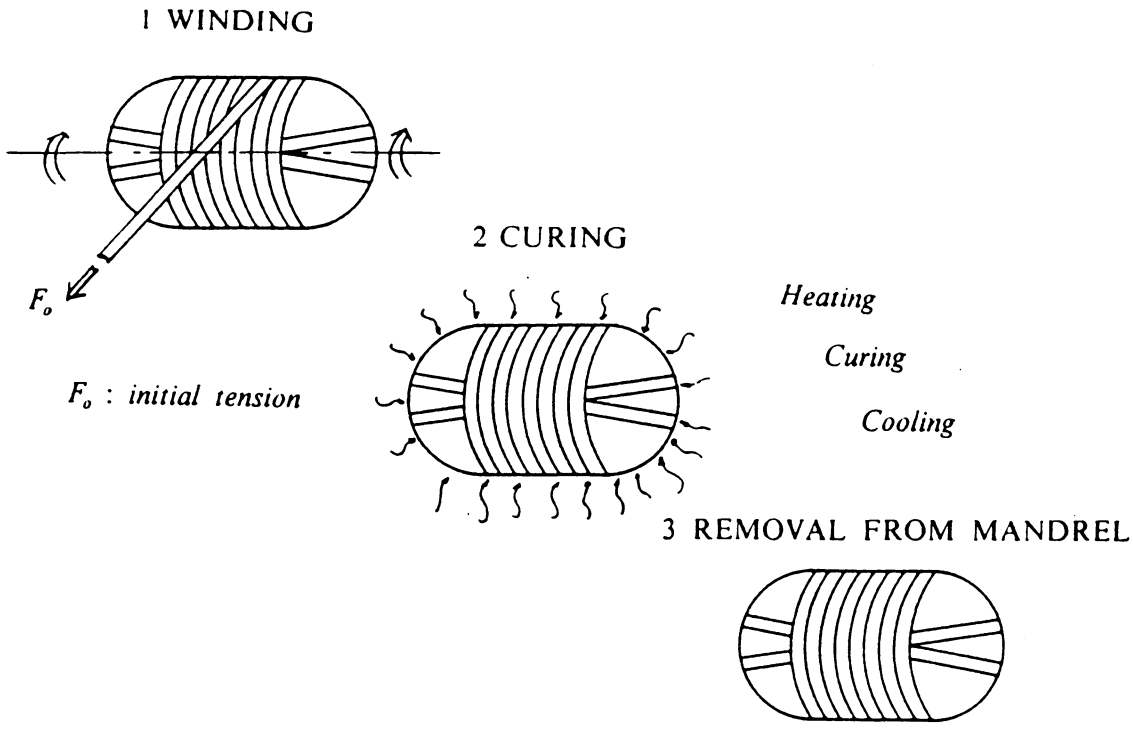

Figure 2. Manufacturing Process:

The manufacturing of filament wound composites is composed of three stages: winding, curing, and removal from mandrel. An initial winding tension, F_o is applied by stretching fibers during winding. Heat and pressure are applied to initiate and maintain chemical reactions in the composite during cure. Defects due to an improper processing are major factors which result in poor mechanical properties of filament wound composites.

The mechanical performance of filament wound composites is greatly affected by the manufacturing processes. Defects, such as delamination or debonding of the structure, porosity, high void contents, and residual stress may result from improper curing. Variables such as the cure cycle (i.e. oven temperature), cure time, and heating rate can affect the thermal process or heat transfer in the composite structure and need to be controlled during cure. During cure, heat is released due to chemical reactions in the matrix resin. The heat generation can affect the temperature distribution, the uniformity of cure, and ultimately the properties of the resin. Thus, there is a need to develop a model to simulate the thermal and chemical processes occurring in the composite structure during cure.

A very important factor in the winding process is the initial winding tension which is applied by stretching fibers during winding. During winding and in the initial stage of cure, the matrix resin is soft or liquid. The curvature of the tensioned fibers in the circumferential direction results in a force acting radially inward on each fiber layer. If the resin has not gelled, the radial force acting on the fiber will cause an inward motion of the fiber layer. The only resistance opposing the fiber motion is the drag caused by the fibers moving through the viscous resin. As the fibers migrate inward, resin will be displaced outward. The inward motion of the fiber layer will continue until a) the tension in the fibers is lost, b) the resin begins to gel, or c) the fiber layer is fully compacted. The inward fiber motion can cause tension loss in the fibers and compaction of the fiber layer in the composite structure during fabrication. An improper initial winding tension will result in a poor fiber tension distribution which results in delamination, wrinkles, high residual stresses, and fiber buckling problems. Fig. 3 illustrates the fiber tension loss during the fabrication of the filament wound composite case.

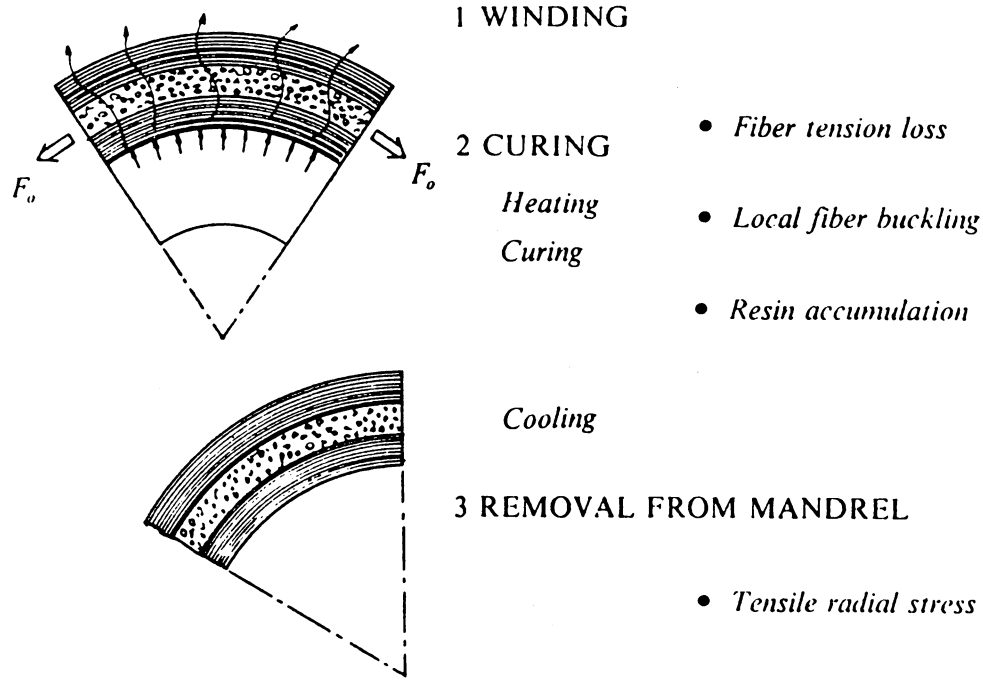

Figure 3. Winding Tension Loss in the Fabrication:

The winding tension decreases when the inward fiber motion occurs due to the resin flow in the manufacturing process. The fiber tension variation influences fiber buckling, wrinkling, resin accumulation, delamination, residual stress, and mechanical performance of FWC structures.

The winding pattern is the other important and complex variable in the manufacturing process of filament wound composites. A winding pattern is designed by choosing a suitable winding path depending on the geometry of the structure and the strength requirements of the structure. The winding path may vary from layer to layer to meet the design requirements. Improper design of the winding pattern may cause misalignment, overlaps, and gaps in placement of the fiber bands degrading the mechanical strength of the case. The winding pattern also influences many other manufacturing parameters. The pressure distribution and amount of layer compaction inside the case greatly depend on the winding pattern. During cure, anisotropic heat conduction and resin flow are also affected by the fiber path.

For pressure vessels or rocket motor cases with integrally wound end closures, two winding patterns are commonly used. These include a geodesic path and a planar path. The winding pattern and the calculation of the winding angle are fully discussed in Appendix A.

1.2 Problem Statement

The objective of the research is to develop a model which simulates the fabrication process of a filament wound composite motor case with integrally wound end closures. The model relates the winding process variables and the cure cycle to the thermal, chemical, and physical processes occurring during manufacturing.

The model was originally developed as two separate submodels. The first submodel is the cure model which will be used to obtain the temperature distribution, resin

degree of cure, and resin viscosity of the matrix inside the composite case during cure. The second submodel is the layer tension loss model which calculates resin flow, fiber displacement, fiber tension variation, and the fiber/resin distribution for each layer of the composite case during winding and cure. The models are combined into a single comprehensive fabrication model.

A second objective was to obtain test data which can be used to verify the models. A third objective was to demonstrate the use of the model establishing the fabrication procedure which results in a composite case that has the desired mechanical performance.

A fourth objective was to integrate the cure/layer tension loss model with a thermomechanical stress model currently being developed by Nguyen and Knight [1]. The model calculates residual stresses in a filament wound case due to mechanical and thermal deformations occurring during the manufacturing process. The combined model is a comprehensive fabrication model for filament wound composites.

In the report, an overview of the cure model is illustrated in Chapter 2 and the layer tension loss model is discussed in Chapter 3. In Chapter 4, the calculation procedures and the input parameters are described in detail. Experimental verification of the model and a parametric study are illustrated in Chapter 5. Chapter 6 is the summary and conclusions.

2.0 CURE MODEL

2.1 Introduction

Thermosetting resins are commonly used as matrix resins for high performance composites, because of their good mechanical properties, low shrinkage, ability to bond to other materials, and environmental stability. Composites using thermosetting resins such as epoxies must undergo a curing process where the resin is transformed from a soft, liquid, and uncured state to a tough and hard thermoset solid. This conversion, called polymerization, also forms a permanent bond between matrix and fibers.

The cure mechanism depends on the type of resin and the addition of a chemically active compound known as a curing agent (i.e. hardener, activator, and catalyst). The composite cure temperature varies depending on the resin and curing agent. High performance composite structures usually require application of external heat and pressure during the curing process. The temperature-time and pressure-time pro-

grams that are applied to the composite during cure are referred to as the "cure cycle".

Application of external heat will initiate and maintain the chemical cure reactions resulting in polymerization of the composite resin. During cure, heat is generated due to exothermic reactions. The total heat released per unit mass is defined as the heat of reaction or the heat of polymerization. The heat of polymerization is a constant for a specific resin system. During cure, the temperature of the composite will increase substantially above the cure temperature if heat is generated at a higher rate than it can be dissipated. This temperature increase is referred to as an exotherm [2].

The degree of cure, defined as the ratio of the amount of the heat evolved from the beginning of the reaction to some intermediate time to the total heat of reaction, is used to evaluate the progress of the composite curing process. A kinetics model will be developed to simulate the cure rate, degree of cure, and heat generation during the composite curing process.

The kinetic behavior of epoxy resins was studied by Ryan and Dutta [3], who developed a mathematical kinetics model for thermosetting resins. Lee, Loos, and Springer [4] developed a kinetic and viscosity model for a Hercules 3501-6 epoxy resin. Hou [5] proposed a chemoviscosity model in the rheological study of thermosetting resin. Halpin [6] developed a model to describe the prepreg manufacturing process from impregnating through curing process.

A mathematical model for the composite curing process was proposed by Loos and Springer [7]. The model characterized the thermal, chemical, and physical processes occurring in a composite plate during cure. Recently, Calius and Springer [8] devel-

oped a cure model for an open-ended filament wound composite cylinder. However, the Calius-Springer model is one-dimensional and does not include the effects of curvature and anisotropic conduction. In this investigation, a two-dimensional cure model is developed for axisymmetric filament wound composite cases with integrally wound end closures. The model includes the effects of material anisotropy due to fiber orientation and can be applied to a complex structural geometry.

2.2 Mathematical Approach

Consider the mandrel - insulator - composite case - outer layer assembly referred to as the FWC assembly (Fig. 4). The FWC assembly is cured in a forced air oven or an autoclave. The outer surface of the assembly is heated by force convection heat transfer and heat is conducted into the assembly. During the curing process, the temperature of the assembly increases which initiates and maintains exothermic chemical reactions inside the composite. The temperature variation in the assembly can be described by transient conduction heat transfer which includes internal heat generation in the composite case and forced convection heat transfer at the outer boundary.

In formulating the cure model, the assumption is made that the effects of layer compaction and resin displacement due to fiber tension, vacuum bagging, and external pressure are neglected. Accordingly, convection due to resin flow is neglected in composite region during cure. Thermal conduction is the only significant heat trans-

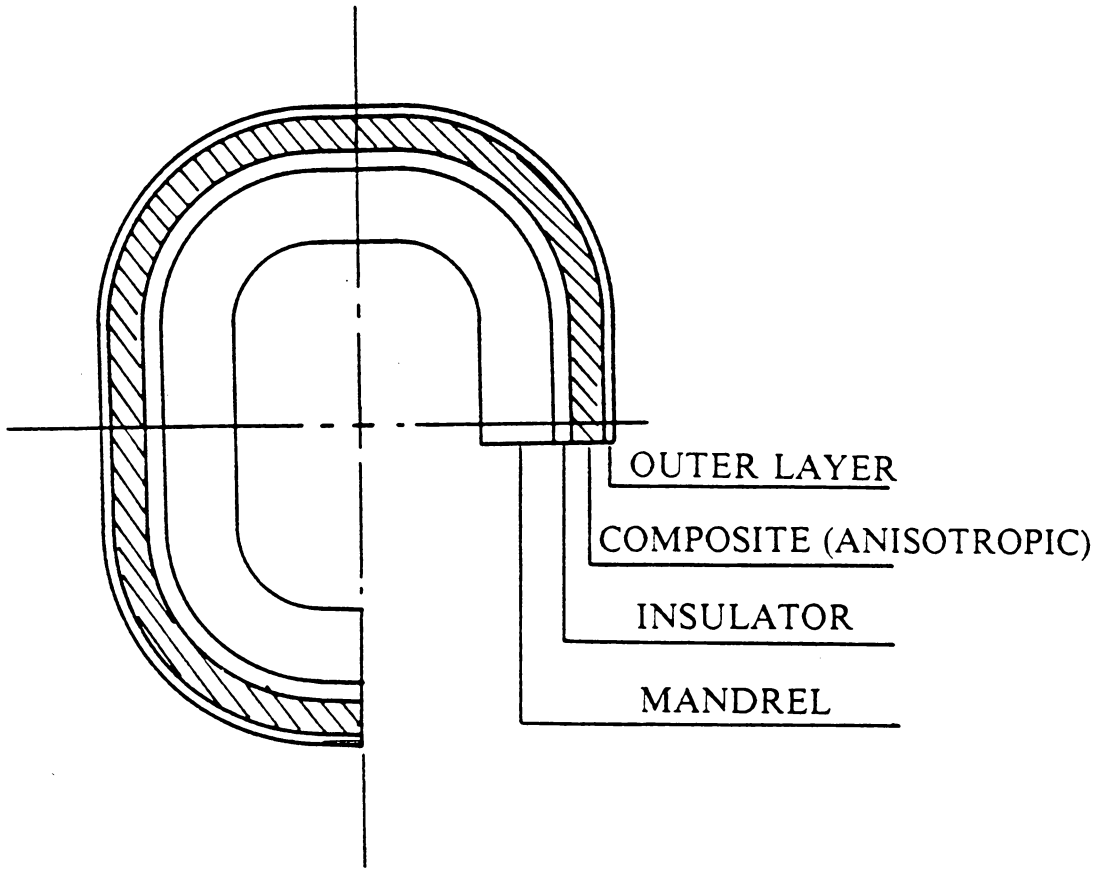

Figure 4. FWC Assembly:

The FWC composite assembly is composed of four regions: mandrel, insulator, composite case, and outer layer. The outer surface of the assembly is heated by forced convection when the assembly is cured in a forced air oven or an autoclave.

fer mode. In fact, the resin flow caused by fiber tension is small and does not significantly affect heat transfer in the composite.

In the composite region, heat conduction is anisotropic due to changes in fiber orientation. Heat generation due to exothermic chemical reactions will be considered as internal heat source. In other regions (i.e. mandrel, insulator, and outer layer), the conduction is isotropic with no heat generation.

The cure model is composed of three sub-models: a heat transfer model, a kinetics model, and a viscosity model. The heat transfer model is used to calculate the temperature distribution in the FWC assembly as a function of position and time during cure. The kinetics model calculates cure rate and heat generation due to exothermic chemical reactions. Integration of the cure rate with respect to time results in the degree of cure of the composite. The viscosity model can be used to obtain the viscosity of resin which depends on the degree of cure and temperature in the composite. The viscosity of matrix affects resin flow and winding tension loss during winding and cure.

2.3 Heat Transfer Model

The temperature distribution during winding and cure of the FWC assembly can be determined from the unsteady heat conduction equation which includes anisotropic conduction and heat generation in the composite case. The transient Fourier equation can be written as follows [9] :

$$\rho C_p \frac{\partial T}{\partial t} - \vec{\nabla} \cdot (\tilde{K} \cdot \vec{\nabla} T) - \dot{q} = 0 \qquad (2.1)$$

where ρ is the density of material, C_p is the specific heat, $\tilde{K}$ is the thermal conductivity tensor, $\dot{q}$ is the internal heat source, T is the temperature, and t is time. The temperature is a function of position and time.

Because of the nature of the manufacturing process, filament wound composite structures are usually axisymmetric. Pressure vessel type structures with integrally wound end-closures are the major interest of this project.

For an axisymmetric case, it is assumed that the temperature distribution in the case and heat convection on the boundary do not vary in the circumferential direction (i.e., θ direction in cylindrical coordinates (r, θ, z)). The reference coordinates system used in the development of the cure model is illustrated in Fig. 5.

Accordingly, Eq.(2.1) can be expressed in cylindrical coordinates with no temperature variation in the θ direction as follows:

In the composite region

$$\rho_c C_c \frac{\partial T}{\partial t} - \frac{1}{r}\{\frac{\partial}{\partial r}[r(K_{rr}\frac{\partial T}{\partial r} + K_{rz}\frac{\partial T}{\partial z})] + \frac{\partial}{\partial z}[r(K_{zr}\frac{\partial T}{\partial r} + K_{zz}\frac{\partial T}{\partial z})]\} - \rho_c \dot{Q} = 0 \qquad (2.2.a)$$

where ρ_c is the density of the composite, C_c is the specific heat capacity of the composite, K_{rr}, K_{rz}, K_{zr}, and K_{zz} are the components of thermal conductivity tensor for the

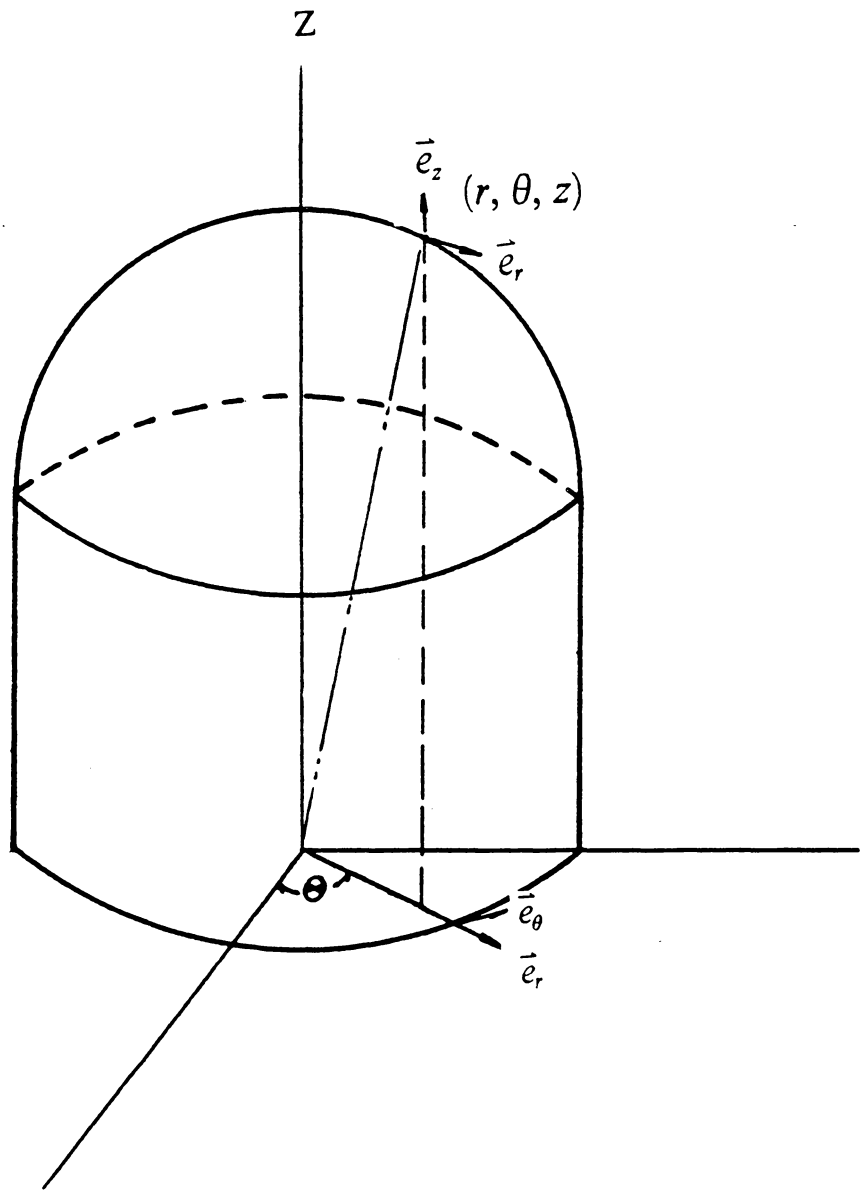

Figure 5. Reference Coordinates:

Cylindrical coordinates are used in the development of both the cure and layer tension loss models. The origin of the coordinates is located at the geometric center of the structure.

composite, $\dot{Q}$ is the rate of heat generation per unit mass due to chemical reaction in the composite, T is the temperature, and t is time.

The governing equation (Eq.(2.2.a)) is subject to

initial condition

$$T_c(0,r,z) = T_c^i(r,z) \qquad (2.2.b)$$

and boundary conditions

$$(K_{rr}\frac{\partial T}{\partial r} + K_{rz}\frac{\partial T}{\partial z})\hat{n}_r + (K_{zr}\frac{\partial T}{\partial r} + K_{zz}\frac{\partial T}{\partial z})\hat{n}_z + H(T - T_\infty) = 0 \qquad (2.2.c)$$

where $T_c^i(r,z)$ is the initial temperature as a function of position in composite region, H is the heat transfer coefficient, and T_∞ is the cure temperature or cure cycle. $\hat{n}_r$ and $\hat{n}_z$ are the components in the r and z directions, respectively, of the unit vector $\vec{n}$ which is normal to the boundary of domain.

In the other regions of the FWC assembly (see Fig.4), heat conduction is isotropic and there is no internal heat source. The governing equations in each domain are given by the following expressions :

For the mandrel region

$$\rho_m C_m \frac{\partial T}{\partial t} - \frac{1}{r}[\frac{\partial}{\partial r}(r K_m \frac{\partial T}{\partial r}) + \frac{\partial}{\partial z}(r K_m \frac{\partial T}{\partial z})] = 0 \qquad (2.3.a)$$

with initial and boundary conditions.

$$T_m(0,r,z) = T_m^i(r,z) \tag{2.3.b}$$

$$(K_m \frac{\partial T}{\partial r})\,\hat{n}_r + (K_m \frac{\partial T}{\partial z})\,\hat{n}_z + H(T - T_\infty) = 0 \tag{2.3.c}$$

For the insulator region

$$\rho_i C_i \frac{\partial T}{\partial t} - \frac{1}{r}\left[\frac{\partial}{\partial r}\left(r K_i \frac{\partial T}{\partial r}\right) + \frac{\partial}{\partial z}\left(r K_i \frac{\partial T}{\partial z}\right)\right] = 0 \tag{2.4.a}$$

with initial and boundary conditions.

$$T_i(0,r,z) = T_i^i(r,z) \tag{2.4.b}$$

$$(K_i \frac{\partial T}{\partial r})\,\hat{n}_r + (K_i \frac{\partial T}{\partial z})\,\hat{n}_z + H(T - T_\infty) = 0 \tag{2.4.c}$$

For the outer layer region

$$\rho_o C_o \frac{\partial T}{\partial t} - \frac{1}{r}\left[\frac{\partial}{\partial r}\left(r K_o \frac{\partial T}{\partial r}\right) + \frac{\partial}{\partial z}\left(r K_o \frac{\partial T}{\partial z}\right)\right] = 0 \tag{2.5.a}$$

with initial and boundary conditions.

$$T_o(0,r,z) = T_o^i(r,z) \tag{2.5.b}$$

$$(K_o \frac{\partial T}{\partial r})\,\hat{n}_r + (K_o \frac{\partial T}{\partial z})\,\hat{n}_z + H(T - T_\infty) = 0 \tag{2.5.c}$$

In Eqs.(2.3 - 2.5), ρ is the density, C is the specific heat, K is the thermal conductivity, T^i is the initial temperature, H is the heat transfer coefficient, T is the temperature, and t is time. The subscripts m, i, and o represent the mandrel, insulator, and outer layer, respectively.

The boundary conditions also require continuity of temperature and heat flux at the interface between different material regions. However, continuity of temperature and heat flux at the nodes is automatically satisfied when solution of the problem is obtained by using the finite element technique.

The forced convective heat transfer coefficient is very sensitive to the fluid velocity near the outer surface of the FWC assembly. Since the fluid velocity varies with the local geometry, the heat transfer coefficient is not a constant along the boundary and must be measured or estimated for each FWC assembly.

2.4 Kinetics Model

The rate of heat generation $\dot{Q}$ due to exothermic chemical reactions in the composite is required for solution of the heat transfer model. A kinetics model which can be used to calculate cure rate, heat generation, and resin degree of cure in composite case will be discussed in this section.

If the assumption is made that the rate of heat generation during cure is proportional to the rate of the cure reaction, then the degree of cure of the resin can be defined as

$$\alpha = \frac{Q(t)}{Q_R} \tag{2.6}$$

where Q_R is the total heat of reaction per unit mass of composite during cure and $Q(t)$ is the heat generation per unit mass of composite from the beginning of the reaction to some intermediate time t.

The heat of reaction for the composite can be expressed as

$$Q_R = \frac{\rho_r}{\rho_c} v_r H_r \tag{2.7}$$

where ρ_r and ρ_c are the densities of the resin and composite, respectively. v_r is the resin volume fraction. H_r is the heat of reaction per unit mass for the resin used in the composite. H_r is usually determined from differential scanning calorimetry (DSC) data of neat resin samples.

For an uncured resin α is zero, and for a completely cured resin, α approaches unity. Differentiating Eq.(2.7) with respect to time and rearranging gives

$$\dot{Q} = \frac{d\alpha}{dt} Q_R \tag{2.8}$$

$\frac{d\alpha}{dt}$ is defined as the reaction rate or cure rate which depends on the temperature and the degree of cure. The cure rate may be expressed symbolically as

$$\frac{d\alpha}{dt} = f(T, \alpha) \tag{2.9}$$

The exact functional form of the cure rate depends on the resin system used in the case and must be determined experimentally. Differential scanning calorimetry (DSC) is frequently used to measure the heat of reaction and the cure rate. An empirical expression for a commonly used epoxy resin system is given in references [3,4,7].

If the diffusion of chemical species is neglected, the degree of cure in the composite can be obtained by the integration of the cure rate with respect to time as follows

$$\alpha = \int_o^t \frac{d\alpha}{dt}\, dt \tag{2.10}$$

where the initial condition

$$\alpha(0,r,z) = 0$$

applies over the composite region.

2.5 Viscosity Model

In order to calculate the resin displacement and fiber motion in the composite case during cure, the resin viscosity must be known as a function of position and time. The shear viscosity of a thermosetting resin is a complex function of temperature, degree of cure (or time), and shear rate. At the present time, analytical expressions which relate the viscosity to all of the above parameters do not exist for the resin systems commonly used in composites. However, a reasonable approach to this

complex problem is to assume that the resin viscosity is independent of shear rate and to measure the resin viscosity at very low shear rates. This approach was followed to measure the viscosity of epoxy resins during cure up to the gel point. The viscosity data can then be fit to a mathematical expression relating the resin viscosity to the temperature and the degree of cure for use in numerical calculations.

A mathematical model of the resin viscosity can expressed as [4,7]

$$\mu = \mu_{\infty} \exp \left[\frac{U}{R T} + K_{\mu} \alpha \right] \tag{2.11}$$

where μ_{∞} is a constant, U is the activation energy for viscous flow, K_{μ} is a constant which accounts for the effects of the chemical reaction, R is gas constant, T is the temperature of resin, and α is the degree of cure of resin.

Once the degree of cure and temperature are known from the heat transfer and kinetics models, the viscosity of the resin can be determined as a function of position and time during cure.

2.6 Material Properties

The thermal properties of composites are fundamental to analysis of the curing process. Numerical values for these properties can be determined by physical experiments. However, some properties may not be available or are difficult to be obtained by direct measurement. A rule of mixtures model which relates the properties of the fiber and matrix to the composite properties is used to calculate thermal and material properties of the composite.

Solution of the cure model, requires that the density ρ, specific heat capacity C, and thermal conductivity [K] of the mandrel, insulator, composite case, and the outer layer be known. In addition, the heat of reaction of the composite case must be specified. In the present analysis, it is assumed that the density, specific heat, and thermal conductivity of the mandrel, insulator, and outer layer do not vary significantly with temperature. Therefore, these material properties will be treated as constants and room temperature values will be used.

The density, specific heat, thermal conductivity, and heat of reaction of the composite case depend on temperature, resin degree of cure, and fiber and resin volume fractions. In general, variations in these properties with temperature and degree of cure are not known and cannot be readily determined. However, variations in the aforementioned properties with resin and fiber contents can be calculated using a simple rule of mixtures model. The mixtures model requires that resin density, fiber density, resin specific heat, fiber specific heat, resin thermal conductivity, fiber thermal conductivity, and resin mass fraction be specified [10].

The resin volume fraction v_r, of the composite can be calculated as

$$v_r = \frac{1.0}{1.0 + \left(\frac{1.0}{m_r} - 1.0\right) \frac{\rho_r}{\rho_f}} \tag{2.12}$$

where m_r is the resin mass fraction, ρ_r is the resin density, and ρ_f is the density of the fiber. The resin mass fraction is usually specified for a prepreg roving or tape by manufacturer.

The density of the composite ρ_c, can be written as

$$\rho_c = \rho_f + (\rho_r - \rho_f)v_r \tag{2.13}$$

Eq.(2.13) assumes that the sum of the volume fractions of the resin and the fiber is unity. The specific heat capacity of the composite, C_c can be calculated from the expression

$$C_c = C_f + (C_r - C_f)m_r \tag{2.14}$$

where C_f is the specific heat capacity of the fiber and C_r is the specific heat capacity of the resin.

The thermal conductivity in the principal material directions is defined parallel and perpendicular to the fibers. The principal thermal conductivity tensor can be written as :

$$\begin{bmatrix} K_{11} & 0 & 0 \\ 0 & K_{22} & 0 \\ 0 & 0 & K_{33} \end{bmatrix} \tag{2.15}$$

The thermal conductivity of composite parallel to the fibers (K_{33}) is calculated from the mixture model as

$$K_{33} = v_r K_r + v_f K_f = K_f + (K_r - K_f)v_r \tag{2.16}$$

The thermal conductivity of the composite normal to the fibers (K_{11} and K_{22}) may be estimated from the expression [11]

$$K_{11} = K_{22} = K_r(1 - 2(\frac{v_f}{\pi})^{0.5}) + \frac{K_r}{\beta_k}\left[\pi - \frac{4}{(1 - \beta_k^2 \frac{v_f}{\pi})^{0.5}} \tan^{-1}(\frac{(\frac{1 - \beta_k^2 v_f}{\pi})^{0.5}}{(1 + \beta_k(\frac{v_f}{\pi})^{0.5})})\right] \quad (2.17)$$

where β_k is defined as,

$$\beta_k = 2.0\,(\frac{K_r}{K_f} - 1.0) \quad (2.18)$$

v_f, the fiber volume fraction, is expressed as

$$v_f = 1.0 - v_r \quad (2.19)$$

and K_r and K_f, are the thermal conductivities of the resin and the fibers, respectively.

2.7 Numerical Formulation

Solution to the cure model must be obtained by numerical methods. The finite element method is a powerful approach and is used to obtain a numerical solution of the cure model. In development of the finite element model, a variational approach is used to obtain a variational form or weak form of the governing equations stated in Section 2.3. Next, a standard finite element technique is used to develop a finite element model for the cure model. Finally, a computer code based on the finite element model is written to obtain the following information as a function of time and position for a filament wound composite case during cure.

- Temperature distribution in the FWC assembly
- Degree of cure and cure time
- Resin viscosity and gel time

2.7.1 Variational Formulation

Traditional variational methods such as the Ritz method, Galerkin method, and Least -Squares method are commonly used to obtain approximate solutions of differential equations. However, these methods are difficult to apply to solve problems which involve material discontinuities, complex boundary conditions, or domains with complex geometries and anisotropic material properties. The assumed approximate functions may be either too simple to approximate the problem accurately or too complex to be solved by the traditional variational methods. However, variational techniques can be used to approximate a solution to complex problems by introducing the finite element concept.

A variational formulation and a finite element formulation of the cure model are derived and the procedures of derivation are summarized as follows:

1. A variational form of the governing equation is derived by using variational calculus.
2. A finite element formulation is derived from the variational formulation.
3. The domain, FWC assembly (Fig. 4), is divided into a set of sub-domains (i.e. elements) called the finite element mesh. Each element in the mesh is a homogenous material and has a simple geometry. Therefore, the finite element formulation can be applied in each element accurately.

4. A standard finite element procedure is then used to construct finite element model and obtain a numerical solution.

Procedures for deriving the variational form of differential equations are given by Reddy [12]. The variational or weak forms of the governing differential equations in the heat transfer model are derived as follows :

In the composite region, considering a test function v, the variational formulation of Eq.(2.2) over a typical volume or element $V^{(e)}$ can be derived as follows :

$$\iiint_{V^{(e)}} v \left[\begin{array}{l} \rho_c C_c \dfrac{\partial T}{\partial t} \\ -\dfrac{1}{r}\left\{\dfrac{\partial}{\partial r}\left[r\left(K_{rr}\dfrac{\partial T}{\partial r}+K_{rz}\dfrac{\partial T}{\partial z}\right)\right]+\dfrac{\partial}{\partial z}\left[r\left(K_{zr}\dfrac{\partial T}{\partial r}+K_{zz}\dfrac{\partial T}{\partial z}\right)\right]\right\} \\ -\rho_c \dot{Q} \end{array} \right] dV = 0 \quad (2.20)$$

where $dV = r\, dr\, dz\, d\theta$

The finite volume, dV is shown in Fig. 6. Since the structure is axisymmetric, the dependent variable, temperature, does not vary in the θ direction. If a ring shaped element with constant cross section is used, Eq.(2.20) can be simplified by integrating the equation with respect to θ. This procedure results in the following expression :

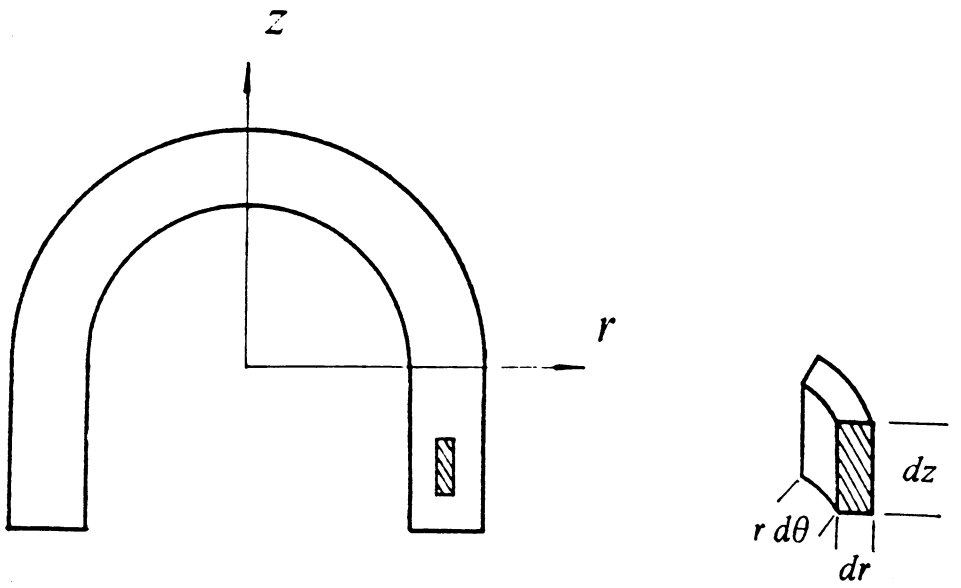

Figure 6. Finite Element Model:

A finite element formulation is developed to obtain the solution of the cure model. For an axisymmetric case, the small volume shown above can be expanded to a ring shaped element to reduce computational efforts.

$$\iint_{\Omega^{(e)}} v \left[\begin{array}{l} \rho_c C_c \dfrac{\partial T}{\partial t} \\ -\dfrac{1}{r}\left\{ \dfrac{\partial}{\partial r}\left[r\left(K_{rr}\dfrac{\partial T}{\partial r} + K_{rz}\dfrac{\partial T}{\partial z}\right)\right] + \dfrac{\partial}{\partial z}\left[r\left(K_{zr}\dfrac{\partial T}{\partial r} + K_{zz}\dfrac{\partial T}{\partial z}\right)\right]\right\} \\ -\rho_c \dot{Q} \end{array} \right] d\Omega = 0 \qquad (2.21)$$

where

$d\Omega = 2\pi\, r\, dr\, dz$

and $\Omega^{(e)}$ represents the cross sectional area of the ring element. Hence, a two-dimensional quadrilateral element is used in the following finite element formulation. Integration of Eq.(2.21) by parts and applying the natural boundary condition Eq.(2.2.c) gives the following expression

$$\begin{aligned} & \iint_{\Omega^{(e)}} v\, \rho_c\, C_c \frac{\partial T}{\partial t}\, 2\pi\, r\, dr\, dz \\ & + \iint_{\Omega^{(e)}} \left[\frac{\partial v}{\partial r}\left(K_{rr}\frac{\partial T}{\partial r} + K_{rz}\frac{\partial T}{\partial z}\right) + \frac{\partial v}{\partial z}\left(K_{zr}\frac{\partial T}{\partial r} + K_{zz}\frac{\partial T}{\partial z}\right)\right] 2\pi\, r\, dr\, dz \\ & + \int_{\Gamma^{(e)}} v\, H\, T\, 2\pi\, r\, d\Gamma \\ & = \iint_{\Omega^{(e)}} v\, \rho_c\, \dot{Q}\, 2\pi\, r\, dr\, dz + \int_{\Gamma^{(e)}} v\, H\, T_\infty\, 2\pi\, r\, d\Gamma \end{aligned} \qquad (2.22)$$

where $\Gamma^{(e)}$ represents the boundary of the element.

For the mandrel, insulator, and outer layer elements, the variational form of the governing equations can be derived following a similar procedure. Since the formulations are exactly same in the three regions, only the mandrel region will be derived. The variational formulation of Eq.(2.3) for a ring element with cross-section $\Omega^{(e)}$ can be derived as follows.

$$\iint_{\Omega^{(e)}} v\left[\rho_m C_m \frac{\partial T}{\partial t} - \frac{1}{r}\left[\frac{\partial}{\partial r}\left(rK_m \frac{\partial T}{\partial r}\right) + \frac{\partial}{\partial z}\left(rK_m \frac{\partial T}{\partial z}\right)\right]\right] d\Omega \;=\; 0 \tag{2.23}$$

Integration of Eq.(2.23) by parts and using the natural boundary condition (Eq.2.3.c) results in the following variational formulation for a typical mandrel element.

$$\begin{aligned}
&\iint_{\Omega^{(e)}} v\,\rho_m C_m \frac{\partial T}{\partial t}\, 2\pi r\, dr\, dz \\
+ &\iint_{\Omega^{(e)}} \left[\frac{\partial v}{\partial r}\left(K_m \frac{\partial T}{\partial r}\right) + \frac{\partial v}{\partial z}\left(K_m \frac{\partial T}{\partial z}\right)\right] 2\pi r\, dr\, dz \\
+ &\int_{\Gamma^{(e)}} v\, H\, T\, 2\pi r\, d\Gamma \\
= &\int_{\Gamma^{(e)}} v\, H\, T_\infty\, 2\pi r\, d\Gamma
\end{aligned} \tag{2.24}$$

The variational formulations for the insulator and outer layer regions are exactly the same as the mandrel, but have different material properties. In fact, formulation of the isotropic element (i.e. mandrel, insulator, and outer layer) is a special case of the anisotropic element (composite). The variational formulation derived above can now be used in developing the finite element model.

2.7.2 Conductivity Transformation

Before beginning the finite element formulation, the thermal conductivity of the composite must be determined. In the composite, anisotropic thermal conductivity depends on fiber orientation which is determined from the winding pattern and geometry of the structure. A tensor transformation is required to obtain the thermal conductivity for each element.

In the composite region, the winding angle, α gives the direction of the fiber path through each element. In the dome region, the element will also have a polar angle, β defined as the angle between the normal to the element surface ($\vec{n}$) and the radial coordinate direction. Both the winding and polar angle are measured from the geometric center of the element (Fig. 7).

The principal directions of the thermal conductivity tensor are defined in the direction parallel and perpendicular to the fibers. The principal conductivity tensor , $[K]$, was previously defined in Eq.(2.15) as

$$\begin{bmatrix} K_{11} & 0 & 0 \\ 0 & K_{22} & 0 \\ 0 & 0 & K_{33} \end{bmatrix} \tag{2.25}$$

where, K_{11} and K_{22} are the conductivities normal to the fiber direction and K_{33} is the conductivity along the fiber direction.

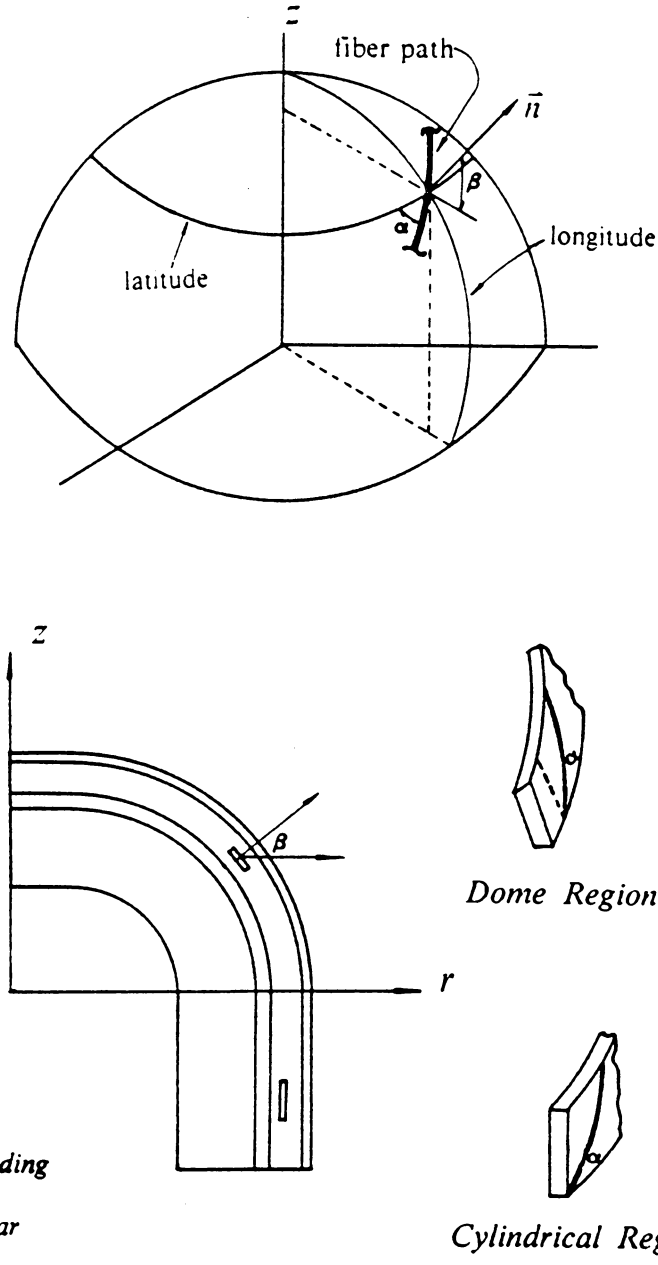

Figure 7. Winding Angle and Polar Angle:

α is winding angle defined as the angle between the winding path and the latitude of the dome. β is polar angle defined as the angle between the direction normal to the dome surface and the latitude of the dome. In each element, both the winding and polar angles are measured at the geometric center of the element.

The thermal conductivity tensor of each element can be obtained by tensor transformations from the principal conductivities, the winding angle, and the polar angle as follows :

The first transformation involves the winding angle:

$$[K]_{(\alpha)} = [A]_{(\alpha)}[K][A]^T_{(\alpha)} \tag{2.26}$$

The second transformation involves the polar angle:

$$[K]_{(\beta)} = [A]_{(\beta)}[K]_{(\alpha)}[A]^T_{(\beta)} \tag{2.27}$$

where

$$[A]_{(\alpha)} = \begin{bmatrix} 1 & 0 & 0 \\ 0 & \sin\alpha & \cos\alpha \\ 0 & -\cos\alpha & \sin\alpha \end{bmatrix} \tag{2.28a}$$

and

$$[A]_{(\beta)} = \begin{bmatrix} \cos\beta & 0 & -\sin\beta \\ 0 & 1 & 0 \\ \sin\beta & 0 & \cos\beta \end{bmatrix} \tag{2.28b}$$

α is the local winding angle and β is the local polar angle in each composite element.

Since the case is axisymetric, only four components, K_{rr} , K_{rz} , K_{zr} , and K_{zz} , are used in the cure model.

2.7.3 Finite Element Model

Based on the variational formulation derived in Section 2.7.1 , a finite element model can be constructed to find the nodal temperature in the domain. Consider a typical element and assume that the time dependent temperature field $T(r,z,t)$ is approximated by the following expression over the element

$$T(r,z,t) = \sum_{j=1}^{n} T_j(t)\, \psi_j(r,z) \tag{2.29}$$

where $T_j(t)$ is the nodal temperature and $\psi_j(r,z)$ is a linear interpolation function. The subscript " j " represents the local node number and $n = 4$, since a four node linear element is used in the model.

Substitution of the temperature field Eq.(2.29) into Eq.(2.22) and replacing v in Eq.(2.22) with the interpolation function ψ_i gives the finite element formulation in matrix form as

$$[\,C^{(e)}\,]\{\,\frac{\partial T}{\partial t}\,\} + [\,K^{(e)}\,]\{\,T\,\} = \{\,F^{(e)}\,\} \tag{2.30}$$

where the capacitance matrix $[\,C^{(e)}\,]$ and the stiffness matrix $[\,K^{(e)}\,]$ are 4 by 4 matrices and the force vector $\{\,F^{(e)}\,\}$ is a 4 by 1 vector. The components of these matrices are calculated as follows:

$$C_{ij}^{(e)} = \iint_{\Omega^{(e)}} \rho_c \psi_i \psi_j C_c \, 2\pi r \, dr \, dz$$

$$K_{ij}^{(e)} = \iint_{\Omega^{(e)}} \left[\frac{\partial \psi_i}{\partial r} \left(K_{rr} \frac{\partial \psi_j}{\partial r} + K_{rz} \frac{\partial \psi_j}{\partial z} \right) + \frac{\partial \psi_i}{\partial z} \left(K_{zr} \frac{\partial \psi_j}{\partial r} + K_{zz} \frac{\partial \psi_j}{\partial z} \right) \right] 2\pi r \, dr \, dz + \int_{\Gamma^{(e)}} \psi_i H T \, 2\pi r \, d\Gamma \tag{2.31}$$

$$F_i^{(e)} = \iint_{\Omega^{(e)}} \psi_i \rho_c \dot{Q} \, 2\pi r \, dr \, dz + \int_{\Gamma^{(e)}} \psi_i H T_\infty \, 2\pi r \, d\Gamma$$

Equations similar to Eq.(2.30) and Eq.(2.31) can be developed for the mandrel, insulator, and outer layer regions of the FWC assembly. However, in these regions the thermal conductivity is isotropic and there is no heat generation. Hence, the terms K_{rz} and K_{zr} will not appear in the stiffness matrix and the heat generation term will not appear in the force vector.

The finite element formulation for a typical element in each region of the FWC assembly (i.e. mandrel, insulator, composite, outer layer) has been derived above. Numerical integration is required to obtain the components of the $[C^{(e)}]$ and $[K^{(e)}]$ matrices and the $\{F^{(e)}\}$ vector. Following standard finite element methods, a local Cartesian coordinate system (ξ, η) is introduced and every element is mapped onto a unit master element $(-1 \leq \xi \leq 1, \quad -1 \leq \eta \leq 1)$ in the local coordinates. Numerical integrations of Eq.(2.31) for each element are calculated in the master element.

A four-node isoparametric element is used in the numerical calculation. Accordingly, the interpolation functions used to approximate the coordinates have the same form

as the functions used in the approximation of the temperature field. Temperature and coordinates r and z are approximated in local coordinates by the following expressions.

$$T = \sum_{j=1}^{4} T_j \hat{\psi}_j(\xi, \eta) \tag{2.32.a}$$

$$r = \sum_{j=1}^{4} r_j \hat{\psi}_j(\xi, \eta) \qquad z = \sum_{j=1}^{4} z_j \hat{\psi}_j(\xi, \eta) \tag{2.32.b}$$

where $\hat{\psi}_j(\xi, \eta)$ are Lagrange interpolation functions. The interpolation functions are

$$\begin{aligned} \hat{\psi}_1 &= \frac{1}{4}(1-\xi)(1-\eta) & \hat{\psi}_2 &= \frac{1}{4}(1+\xi)(1-\eta) \\ \hat{\psi}_3 &= \frac{1}{4}(1-\xi)(1+\eta) & \hat{\psi}_4 &= \frac{1}{4}(1+\xi)(1+\eta) \end{aligned} \tag{2.33}$$

Numerical integration is done by using a Gauss-Legendre quadrature and yields a set of ordinary differential equations in time. Assembly of the equations obtained from each element and the imposition of the boundary conditions results in the global governing equations for the entire space domain. The procedures of numerical integration and development of finite element programs are discussed in references [13, 14, 15].

2.7.4 Time Approximation

The formulation derived in the last section involved a separation of variables (i.e. time and space variables). The procedure which separates the time variable and the space variables is known as a semidiscrete approximation The finite element formulation in the space domain has been fully discussed and modeled in the section 2.7.3.

In time domain, finite difference methods can be employed to obtain an approximate solution. A two-point recurrence scheme for the first order differential equation can be applied to the calculation of time dependent problem [13, 14].

Consider the differential equation Eq.(2.30) at two adjacent time steps n and n+1 as follows:

$$[C^{(e)}]\{\frac{\partial T}{\partial t}\}_n + [K^{(e)}]\{T\}_n = \{F^{(e)}\}_n \tag{2.34}$$

and

$$[C^{(e)}]\{\frac{\partial T}{\partial t}\}_{n+1} + [K^{(e)}]\{T\}_{n+1} = \{F^{(e)}\}_{n+1} \tag{2.35}$$

The time derivative of the temperature, $\frac{\partial T}{\partial t}$ at two adjacent time steps n and $n+1$ is approximated by a linear interpolation of the temperature between adjacent time steps and can be expressed as follows

$$\theta\{\frac{\partial T}{\partial t}\}_{n+1} + (1-\theta)\{\frac{\partial T}{\partial t}\}_n = \frac{\{T\}_{n+1} - \{T\}_n}{\Delta t} \tag{2.36}$$

where Δt is time step. The parameter 'θ', which varies between 0 and 1.0, is a weight value in the difference scheme.

Multiplying Eq.(2.34) and Eq.(2.35) by $(1.0-\theta)$ and θ, respectively, then adding and substituting Eq.(2.36) into the resultant, we obtain

$$[\bar{C}]\{T\}_{n+1} = [\bar{K}]\{T\}_n + \{F\}_{n,n+1} \tag{2.37}$$

where $[\bar{C}]$ is the modified effective capacitance matrix, $[\bar{K}]$ is the modified thermal conductivity matrix, and $\{F\}_{n,n+1}$ is the modified thermal load vector defined as

$$[\bar{C}] = [C] + \theta\Delta t_{n+1}[K] \tag{2.38}$$

$$[\bar{K}] = [C] - (1.-\theta)\Delta t_{n+1}[K] \tag{2.39}$$

$$\{F\}_{n,n+1} = \Delta t_{n+1}[\theta\{F\}_{n+1} + (1.-\theta)\{F\}_n] \tag{2.40}$$

From Eq.(2.37) we get the solution at time step $t = t_{n+1}$ in terms of the solution known at time $t = t_n$ as follows

$$\{T\}_{n+1} = [\bar{C}]^{-1}[[\bar{K}]\{T\}_n + \{F\}_{n,n+1}] \tag{2.41}$$

At t = 0, the solution is known from the initial conditions.

Depending on the value selected for θ, various difference schemes can be chosen for Eq.(2.36). Lambert [16] suggested $\theta = 0.878$ as an optimal choice which results in more accuracy and less computation cycles.

2.7.5 Degree of Cure and Viscosity

The degree of cure $\alpha(r,t)$, can be calculated for each element from the expression defined in Eq.(2.9),

$$\alpha(r,z,t) = \int_{t=0}^{t=t} \frac{d\alpha}{dt}\, dt \qquad \forall \quad composite\ \ elements \qquad (2.42)$$

where the cure rate $\frac{d\alpha}{dt}$ can be calculated from the Eq.(2.8). Typical expressions for for the cure rate of some commonly used epoxy resins are shown in Appendix A. B

An Euler type numerical scheme was adopted to calculate the value of $\alpha^{n+1}(r,z,t)$ from $\alpha^{n}(r,z,t)$ of the previous time step

$$\alpha^{n+1}(r,z,t) = \alpha^{n}(r,z,t) + f[\,\alpha^{n}(r,z,t),\, T^{n}(r,z,t)\,]\,\Delta t \qquad (2.43)$$

where superscript n and $n+1$ represent time steps.

The degree of cure for the next time integration can be estimated from the value of the degree of cure and temperature of the previous time step in each element. In the calculations, the temperature of each element is obtained by averaging the nodal temperatures.

The viscosity of the resin is estimated from the expression defined in Eq. (2.10)

$$\mu\,(r,z,t) = \mu_{\infty} \exp\,[\,\frac{U}{R\,T\,(r,z,t)} + K_{\mu}\,\alpha\,(r,z,t)] \qquad (2.44)$$

Typical expressions for the viscosity of some commonly used epoxy resins are shown in Appendix B.

The viscosity is calculated from the value of the degree of cure and temperature in each element. This calculation is done at each time step and the viscosity is passed to the layer tension loss model to estimate the resin flow during cure.

3.0 LAYER TENSION LOSS MODEL

3.1 Introduction

Filament wound composites are fabricated by winding resin impregnated fibers over a mandrel along a predetermined winding path. In the winding process, the fiber bands are stretched and wound over the mandrel. The pretension in the fiber bands, referred to as the winding tension, can greatly affect the mechanical strength of filament wound composites. Application of an initial winding tension ensures that the fiber bundles are placed on the right path without buckling during winding. However, during winding and cure, the fibers can move away from the original position causing a reduction in the winding tension.

Due to the local curvature of the structure, the tensioned fibers layer will generate a radial pressure compacting the inner layers of the composite case. An external pressure may be applied at specific times during the winding process which further compacts the structure. Hence, excess resin and air bubbles formed between layers

during winding can be squeezed out of the composite case reducing the porosity or void content and increasing the fiber volume fraction.

During winding and in the early stages of the cure, the matrix resin is quite fluid. The curvature of the tensioned fibers in the circumferential direction results in a force acting radially inward on each fiber layer. The pretensioned fibers will migrate radially inward through the viscous resin. Fig. 8 shows the inward motion of fibers due to winding tension. As the fiber bundles move inward, resin will be displaced radially outward and the tension in the fiber will gradually decrease.

In dry winding, the resin in the prepreg is B-staged and quite viscous at room temperature. Therefore, no significant fiber tension loss results from the fiber motion or resin flow during winding. The majority of the fiber tension loss is due to the deformation of prepreg resulting from the high pressure generated by the tensioned outer fiber layers. In the heating stage of cure, the viscosity of resin decreases dramatically and the displacement of resin occurs radially outward. As the resin flows out, the fibers will migrate inward causing a significant fiber tension loss. If fiber tension is completely lost in a layer of the composite case, additional radial pressure from the tensioned outer layers still squeeze the resin out and may result in local fiber buckling.

In wet winding, significant fiber tension loss occurs during winding due to the low initial viscosity of matrix resin. Fiber motion and tension loss continue until the resin gels. When the wound composite case is heated during cure, additional resin flow and fiber tension loss may occur.

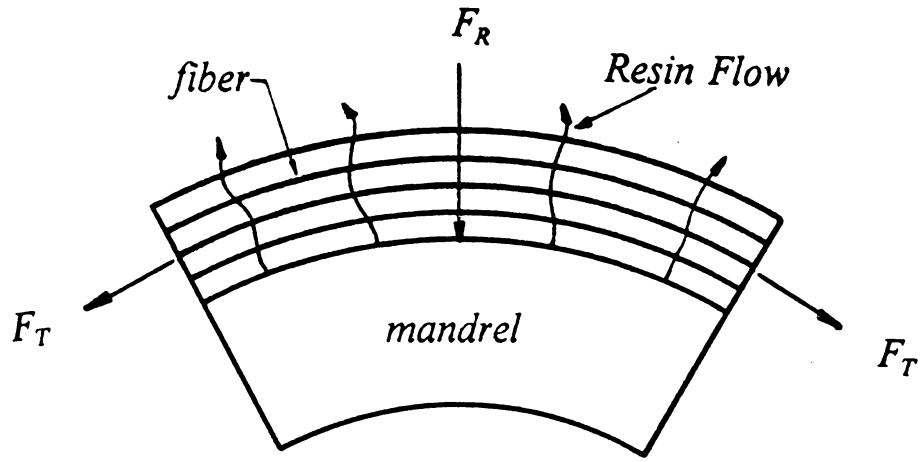

F_T : *fiber tension*

F_R : *resultant force*

Figure 8. Fiber Tension Loss:

Due to the curvature of the structure, the tensioned fiber will generate a force acting radially inward. This force results in inward fiber motion which causes fiber tension loss gradually. The fiber motion is resisted by the viscous matrix resin.

The pressure generated by the tensioned fiber layers can reach several thousand pounds per square inch in the inner region of a thick composite case. Thus, the mandrel must be sufficiently stiff to resist the pressure developed by the winding tension during winding and curing.

Initially, the mandrel is designed to provide a resistant force which can balance the pressure generated by the winding tension. The reaction force from the mandrel can result in compressive radial stresses through the thickness of the composite case. However, because of differences in the coefficient of thermal expansion between the mandrel and composite case, the composite case may separate from the mandrel during cooling. Once the separation occurs, the mandrel can no longer support the composite case. The force balance between the mandrel and the composite case disappears and the inner surface of the composite case becomes a force free surface. Accordingly, the fiber tension of the inner layers will pull the case inward causing radial tensile stresses through the thickness. The residual tensile stresses may be large enough to cause delamination in the structure.

Wrinkling is another common defect related to winding tension. Wrinkling of the structure may result from nonuniform resin flow, high residual fiber tension, and shrinkage of matrix resin during the curing process.

The displacements of the fiber bundles depend on the winding tension, the winding pattern, and the structural geometry. Different displacements of the fiber bundles in adjacent layers will cause nonuniform resin/fiber distribution. Resin accumulation will result in resin-rich areas which can degrade the mechanical strength of the composite case.

The fiber movement is resisted by the viscous resin. During winding and cure, the viscosity of the resin depends on the temperature and the degree of cure of matrix resin. Fiber motion is also affected by thermal expansion or shrinkage of the fibers during cure. The thermal strain of the fiber depends on the temperature. Thus, the temperature distribution and the resin viscosity calculated using the cure model presented in Chapter 2 will be required in the fiber motion calculations.

The fiber tension distribution in a filament wound case depends on the initial winding tension, geometry of case, winding pattern, resin viscosity, and fiber properties. The fiber tension variation will certainly affect the final mechanical performance of filament wound case. Therefore, there is a need to develop a model which can simulate fiber motion and compaction during manufacturing of a filament wound case.

In this chapter, a layer tension loss and compaction model is developed which relates the winding process variables (i.e. winding pattern, mandrel geometry, and initial winding tension), the properties of the fiber and resin system, and the applied cure temperature and pressure to the fiber tension loss, compaction, and instantaneous position of each layer in the composite case. Furthermore, the model can be used to estimate the winding time of each layer in the case.

3.1.1 Literature Review

Resin flow in flat plate composite laminates during fabrication has been studied extensively by Springer and Loos [6] who modeled the problem as resin flow through porous layers causing consolidation. Lindt [17] modeled the composite as an array

of straight aligned fibers and calculated resin flow using lubrication theory. The model also included consolidation due to fiber movement and resin flow. Hou [18] modeled resin flow in both vertical and horizontal directions in a flat laminate plate. Using the porous medium assumption, Gutowski [19] modeled the consolidation of a flat laminate plate and included the elastic effects caused by fiber deformation. Halpin [7] calculated the compaction due to three-dimensional resin flow occurring during composite fabrication. Dave, Kardos, and Dudukovic [20] proposed a three-dimensional resin flow model for unidirectional composites.

Recently, Calius and Springer [8] modeled fiber motion in an open-ended, cylindrical filament wound composite case. The model assumed that the fiber material in a layer is concentrated in a porous sheet. Darcy's law was used to calculate the resin flow due to the pressure drop across the layer. A relationship between the instantaneous position of the fiber and the fiber tension was established by modeling the fiber as a elastic wire. The fiber motion model results in a governing equation for each layer of the case representing the inward motion of the fiber bundles. However, Calius' model is a one-dimensional model which can not be applied to a case with end closures. The model also did not consider anisotropy of the resin flow and variation of the permeability due to consolidation.

In this investigation, a layer tension loss model is proposed to determine resin flow and fiber tension in a rocket motor case with end closures. The model includes variations in composite permeability caused by compaction, anisotropic flow due to various fiber orientation and geometry, and compaction resulting from the outer tensioned fiber layers.

3.2 Mathematical Approach

Consider a thin curved tensioned fiber layer in the composite case (Fig. 9). The position of the fiber layer is referred by the middle surface of the fiber layer.

Due to the curvature of the layer, the fiber tension will generate a pressure gradient across the layer. During winding and in the early stages of cure, the viscous resin is squeezed out from the fiber layer. As the resin flows out, the fibers will move radially inward causing a gradual loss of fiber tension.

If the assumption is made that the inward displacement of the fiber layer is equal to the resin displacement (Fig. 9), then the instantaneous position of the fiber layer can be determined by the resin flow through the middle surface of the fiber layer. The resin flow which can be determined by the Darcy's equation, is a function of permeability of the composite, viscosity of the resin, and pressure gradient across the layer. Once the position of the fiber layer is known, the strain in the fiber can be determined from the fiber curvature.

The fiber stress due to the initial fiber tension is around 5% to 10% of the tensile strength of the fiber. Calius and Springer [8] showed that it is reasonable to model the fiber layer as an elastic wire wound over a curved surface; therefore, the fiber tension can be calculated from the strain, elastic modulus, and cross-sectional area of the fiber layer.

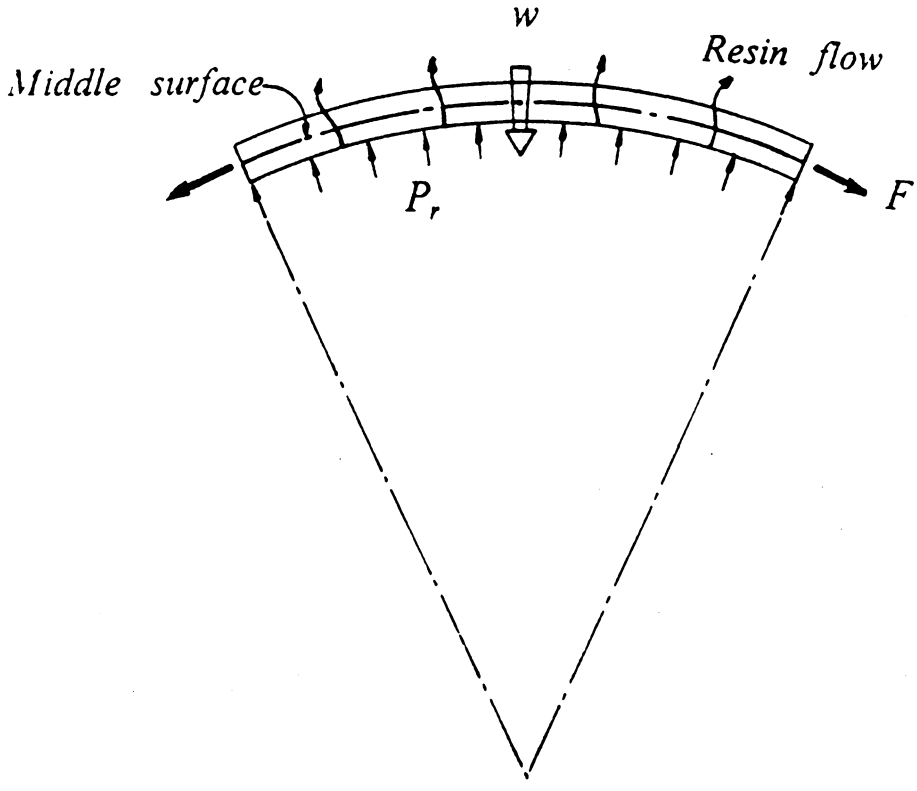

w : displacement of fiber layer

F : fiber tension

P_r : pressure

Figure 9. Resin Flow and Fiber Motion:

Instead of modeling the fiber movement through the viscous resin, we investigate how the resin passes through the fibers. The inward fiber motion of a thin layer is assumed equal to the resin flow through the middle surface of the layer along the radial direction of the fiber path. This assumption is extended to a small element which has unidirectional fiber orientation.

3.2.1 Overview of Calculation

The approach used in the model is summarized as follows :

1. Determine the resin flow and displacement in each layer of the composite case.
2. Determine the fiber motion and displacement from the resin flow in each layer.
3. Calculate fiber tension due to the resin flow.

In order to formulate the resin flow through the fiber layer, the fiber bundles impregnated with the uncured matrix resin are represented by a porous medium saturated with a viscous resin. The resin flow through the composite is a function of the permeability of composite, viscosity of resin, and pressure gradient in the composite.

In Section 3.3, an overview of the resin flow model and the governing equation used to calculate the anisotropic resin flow for an axisymmetric case are derived. A numerical solution is obtained by using finite element approach which is briefly described in Section 3.3.1.

The resin viscosity is obtained from the cure model. The major calculations of the layer tension loss model are to determine the pressure field in the composite case and to develop a permeability model. Accordingly, the resin flow rate and displacement are determined numerically using Darcy's equation.

3.3 Resin Flow Model

The following assumptions are made in the calculation of the resin flow through the composite case during the fabrication.

1. The viscous resin is assumed to be incompressible and inertial effects are neglected.
2. Each composite layer is formed instantaneously and the winding tension is assumed uniform in circumferential direction of each layer.
3. The mandrel is rigid and the insulator (rubber type material) is incompressible (i.e. deformations in the mandrel and the insulator are neglected). Hence, the fiber tension variation due to the deformation of the mandrel and the insulator is neglected. Accordingly, the pressure which causes the resin flow is assumed not to be affected by the deformation.

Darcy's law can be used to described the phenomenon of viscous flow through a porous medium. Accordingly, the resin flow rate is related to the permeability of composite, the viscosity of the resin, and the pressure gradient generated by fiber tension. The Darcy's equation for an anisotropic porous medium can be written as follows [21]

$$\vec{q} = -\left(\frac{1}{\mu}\right)[S]\,\rho\, grad\,\phi \tag{3.1}$$

where $\vec{q}$ is the resin flow rate, $[S]$ is the permeability tensor of the composite, μ is the viscosity of resin, ρ is the density of resin, and ϕ is force potential.

Neglecting body forces, Eq.(3.1) can be rewritten as :

$$\vec{q} = -\left(\frac{1}{\mu}\right)[S]\,\vec{\nabla} P \tag{3.2}$$

where P is the pressure generated by fiber tension.

In cylindrical coordinates, the matrix form of Eq.(3.2) can be expressed as

$$-\frac{1}{\mu}\begin{bmatrix} S_{rr} & S_{r\theta} & S_{rz} \\ S_{\theta r} & S_{\theta\theta} & S_{\theta z} \\ S_{zr} & S_{z\theta} & S_{zz} \end{bmatrix}\begin{bmatrix} \frac{\partial P}{\partial r} \\ \frac{1}{r}\frac{\partial P}{\partial \theta} \\ \frac{\partial P}{\partial z} \end{bmatrix} = \begin{bmatrix} q_r \\ q_\theta \\ q_z \end{bmatrix} \tag{3.3}$$

For an axisymmetric case with uniform fiber tension in the circumferential direction, the pressure does not vary in the θ direction; i.e. $\frac{\partial P}{\partial \theta} = 0$ and the resin flow along the θ direction does not affect the resin displacement in the composite case (Fig. 10). Accordingly, only resin flow in the r and z directions need to be considered in calculations of the fiber motion. Eq.(3.3) can be simplified as the following expression :

$$\begin{bmatrix} q_r \\ q_z \end{bmatrix} = -\frac{1}{\mu}\begin{bmatrix} S_{rr} & S_{rz} \\ S_{zr} & S_{zz} \end{bmatrix}\begin{bmatrix} \frac{\partial P}{\partial r} \\ \frac{\partial P}{\partial z} \end{bmatrix} \tag{3.4}$$

The viscosity of resin depends on the type of resin system and the cure cycle used in the fabrication processes. The permeability of composite can be calculated from

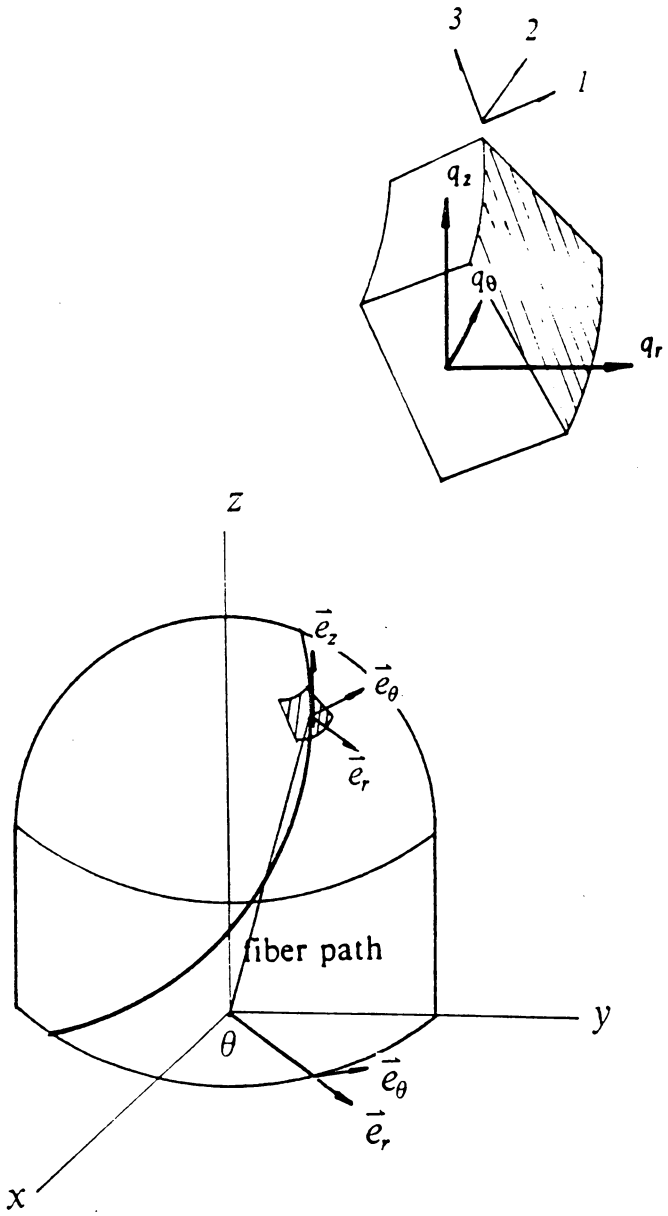

Figure 10. Resin Flow in the Composite Case:

Due to the pressure gradient, the resin flow occurs when the matrix resin melts. Anisotropic resin flow is calculated by using Darcy's law in each element. The material coordinates (1-2-3) are in the directions normal or parallel to the fibers.

the porosity and specific surface of the porous medium. The pressure gradients in the composite case are determined from the winding tension, winding pattern, structural geometry, and thermal expansion of fibers.

3.3.1 Finite Element Approach

Due to the complex geometry, anisotropic permeability, and variable material properties of the FWC case, solution to Eq.(3.4) was obtained numerically using the finite element approach. The axisymmetric finite element mesh generated for the cure model in Chapter 2 was also used for the layer tension loss model. Hence, the resin viscosity, permeabilities, and pressure gradient must be calculated for each element.

Fig. 11 shows a typical element which is reduced from a 3D ring element for axisymmetric case. The geometric center of the element can be calculated by averaging the node coordinates of the element as

$$(r_c, z_c) = \left(\frac{r_1 + r_2 + r_3 + r_4}{4} , \frac{z_1 + z_2 + z_3 + z_4}{4} \right) \qquad (3.5)$$

where r_i and z_i (i = 1,4) are the nodal coordinates. As defined in the cure model previously, each element has a winding angle and a polar angle. Both the winding angle and polar angle are measured at the geometric center of the element.

The fiber motion in each element is assumed to be equal to the resin displacement at the geometric center of the element in the direction normal to the fiber path. The

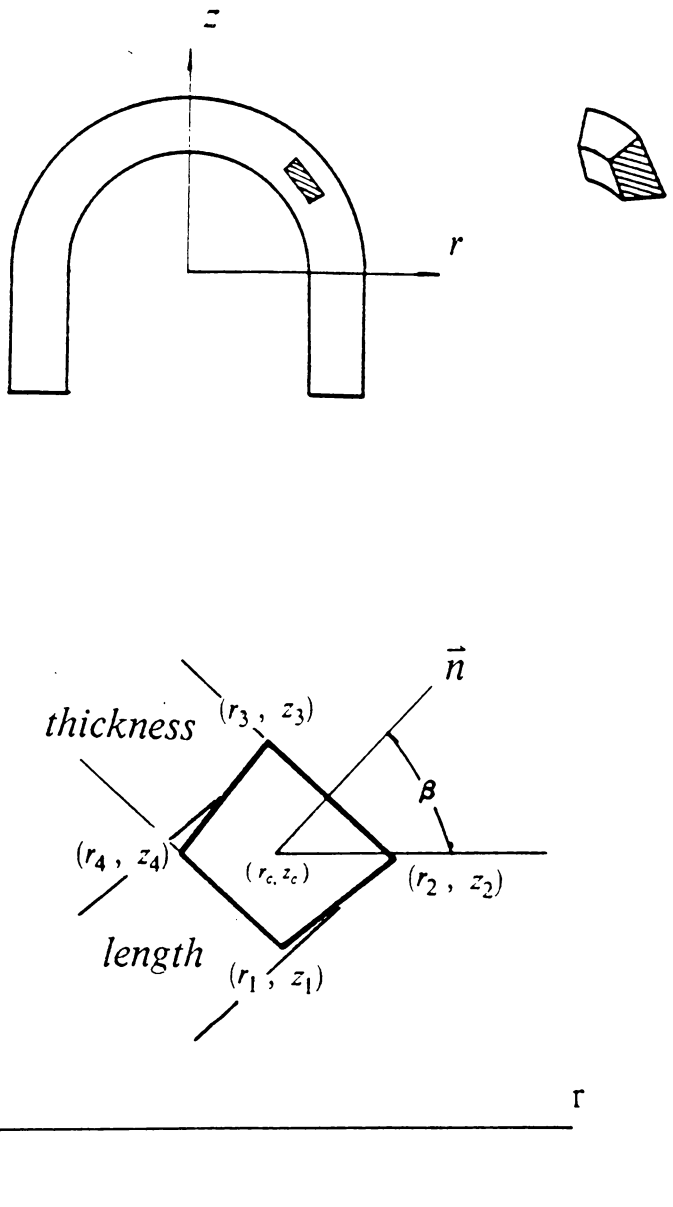

Figure 11. Typical 2D Element:

A 4 node linear element is used in the calculation of the resin flow. The geometric center is calculated from the average of the nodal coordinates. The thickness and length of the element are also estimated from the nodal coordinates and polar angle β.

resin flow at the geometric center of the the element is calculated from the resin viscosity, permeability, and pressure gradient using Darcy's equation.

The viscosity of resin is obtained from the cure model as a function of element position and time. The anisotropic permeability depends on the local fiber orientation and structural geometry which are related to the winding and polar angles in each element. Finally, the pressure gradient is calculated from the fiber tension and the curvature of the fiber path.

In Section 3.4, the pressure field generated by fiber tension will be derived for a composite case with integrally wound end closures. Therefore, the pressure gradient in each element can be calculated numerically. In Section 3.5, a permeability model is developed to estimate the permeability as a function of resin volume fraction of each composite element. The permeability, pressure gradient, and resin viscosity are then used to calculate the resin flow in each composite element in Section 3.6.

3.4 Nodal Pressure Field

In order to calculate the pressure gradient in each element, the nodal pressures must be determined. The pressure field is constructed from the following procedures.

1. The pressure due to a single tensioned element is calculated from the fiber tension, curvature of the fiber path, and thickness of the element.

2. The nodal pressure is obtained by superposing the pressure calculated from each single tensioned element. The superposition is done according to geometric location of each element (Section 3.4.3).

Once the pressure field is known, the pressure gradient through the element can be determined numerically.

3.4.1 Pressure due to a Tensioned Element

Consider the single tensioned element shown in Fig. 12. The fiber tension and curvature of the fiber path result in a pressure acting on the inner surface of the element. The pressure can be calculated from the force balance in the normal, $\vec{n}$, direction (Fig. 12) by the following expression.

$$2 \times \sigma \times \Delta r \times \cos\delta = \int_{\delta}^{\pi-\delta} P_i \frac{1}{\kappa} (\sin\varepsilon)\, d\varepsilon \qquad (3.6)$$

Integration and rearrangement of Eq. (3.6) results in the following expression for the pressure P_i

$$P_i = \sigma \times \kappa \times \Delta r \qquad (3.7)$$

where σ is tensile stress in the element, Δr is the average thickness of the element, and κ , is the curvature of the element. Initially, σ is equal to the winding tension. The average thickness of the element and the curvature of the element can be esti-

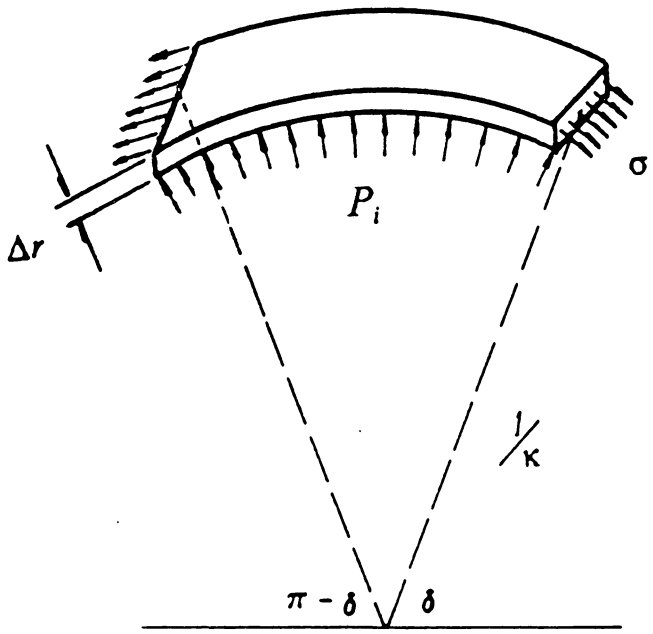

$$P_i = \sigma \times \kappa \times \Delta r$$

σ : tensile stress

κ : curvature of element

Δr : thickness of element

Figure 12. Pressure in a Single Tensioned Element:

Pressure on the inner surface of a tensioned element is equal to the reacting pressure resulting from the fiber tension and curvature. The pressure can be derived from the force balance in the normal, $\vec{n}$, direction.

mated from the node coordinates, winding path and local geometry as described in the next section.

3.4.2 Thickness and Curvature of Element

The thickness of the element can be estimated by projecting the diagonals of the element onto the the direction of the polar angle. The direction of the polar angle has been defined as the direction normal to the surface of the dome at the geometric center of the element. The thickness of the element can be estimated from the nodal coordinates and the polar angle as follows (Fig.11)

$$\frac{1}{2}\,|(r_1 - r_3)\cos\beta + (z_1 - z_3)\sin\beta| \;+\; \frac{1}{2}\,|(r_2 - r_4)\cos\beta + (z_2 - z_4)\sin\beta| \qquad (3.8)$$

where β is the polar angle of the element and r_i, z_i $i = 1,4$ are the nodal coordinates.

The length of the element (defined in Fig. 11) is also estimated from the nodal coordinates as

$$\frac{1}{2}\,[(r_1 - r_4)^2 + (z_1 - z_4)^2]^{\frac{1}{2}} \;+\; \frac{1}{2}\,[(r_2 - r_3)^2 + (z_2 - z_3)^2]^{\frac{1}{2}} \qquad (3.9)$$

The local curvature of the fiber path in each element depends on the winding path and geometry. The curvature of a typical element in the dome region can be calculated from the winding angle α and the polar angle β. A method relating the winding angle and the polar angle to the local curvature is described as follows.

The base of a right circular cone can be constructed through each element in FEM mesh (Fig. 13). The distance between the geometric center of the element and the longitudinal axis of the case defines the radius of the base of the cone. The altitude of the cone is determined from the polar angle defined as the angle between the direction normal to the element and the radius of the base.

Define plane I as the plane tangent to the fiber path at the geometric center of the element and normal to the surface of the cone. The intersection of the cone and the plane is a conic curve by the definition of conics. Depending on the angle, θ (Fig. 13) and the winding angle, α the curve is

elliptic, if $\theta > \alpha$,

parabolic, if $\theta = \alpha$, and

hyperbolic, if $\theta < \alpha$.

The angle θ is defined as $\theta = \pi/2 - \beta$.

Since the fiber path was defined, the curvature of the winding path at the center of the element can be calculated from the definition of the curvature of a conic curve. Such a method for calculating the curvature of the fiber path was developed by Nguyen [1] and is summarized below.

In the cylindrical region, θ is equal to $90°$. This is a special case and the fiber path is either an ellipse or a circle. The curvature of the fiber path can be calculated from the radius r_c and the winding angle by the following expression

$$\kappa = \{\cos^2\alpha\} \frac{1}{r_c} \tag{3.10}$$

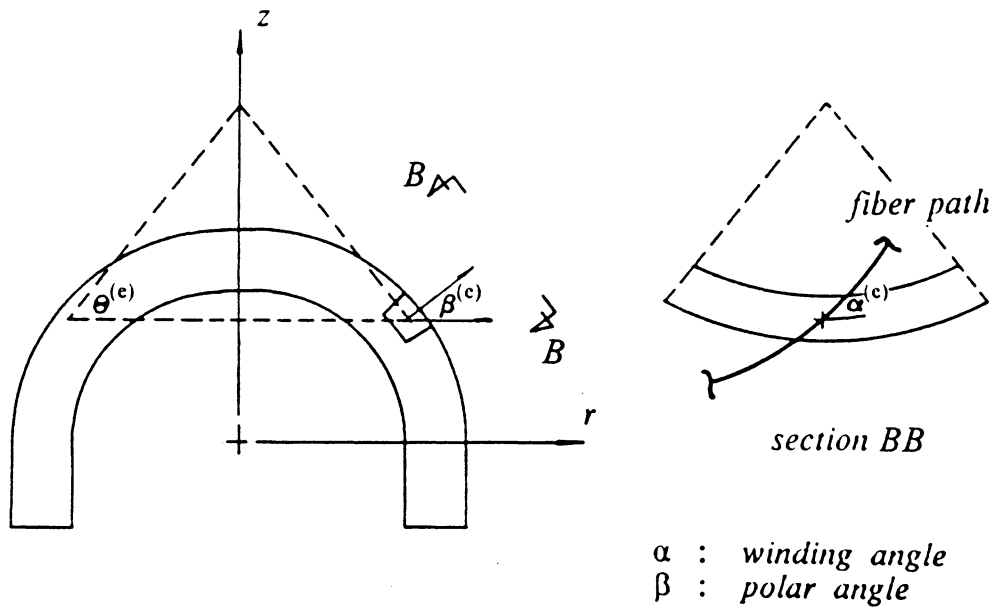

Figure 13. Curvature of Fiber Path:

A conic curve is defined by the intersection between a plane tangent to the fiber path and the cone. The curvature of the fiber path is determined by the geometry, winding angle, and polar angle in each element.

where α is the winding angle and r_c is the radial distance from the longitudinal axis of case to the center of the element.

In the dome region, the curvature of the fiber path located on plane I which is normal to the surface of the cone can not be calculated directly (Fig. 14). However, the minimum curvature located at the intersection of plan II and the cone can be determined from the winding angle α and the angle θ (Fig. 14). Accordingly, the curvature of the fiber path can be obtained by transforming the minimum curvature with respect to ω onto plane I .

The angle between the direction normal to the fiber path and the direction of the minimum curvature can be determined from geometry as

$$\omega = \theta + \alpha - 90° \tag{3.11}$$

Calculations of the fiber curvature for various cases are illustrated in reference [1]. However, the minimum curvature in the dome region for each case are summarized as follows:

elliptic

$$\kappa' = \left\{ \frac{a'b'}{\left[\left(\frac{a'}{b'} \right)^2 + \left(\frac{b'h'}{a'} \right)^2 \right]^{3/2}} \right\} \frac{1}{r_c} \tag{3.12}$$

parabolic

$$\kappa' = \left\{ \frac{\cos^2\alpha}{(\cos^2\alpha + 1)^{3/2}} \right\} \frac{1}{r_c} \tag{3.13}$$

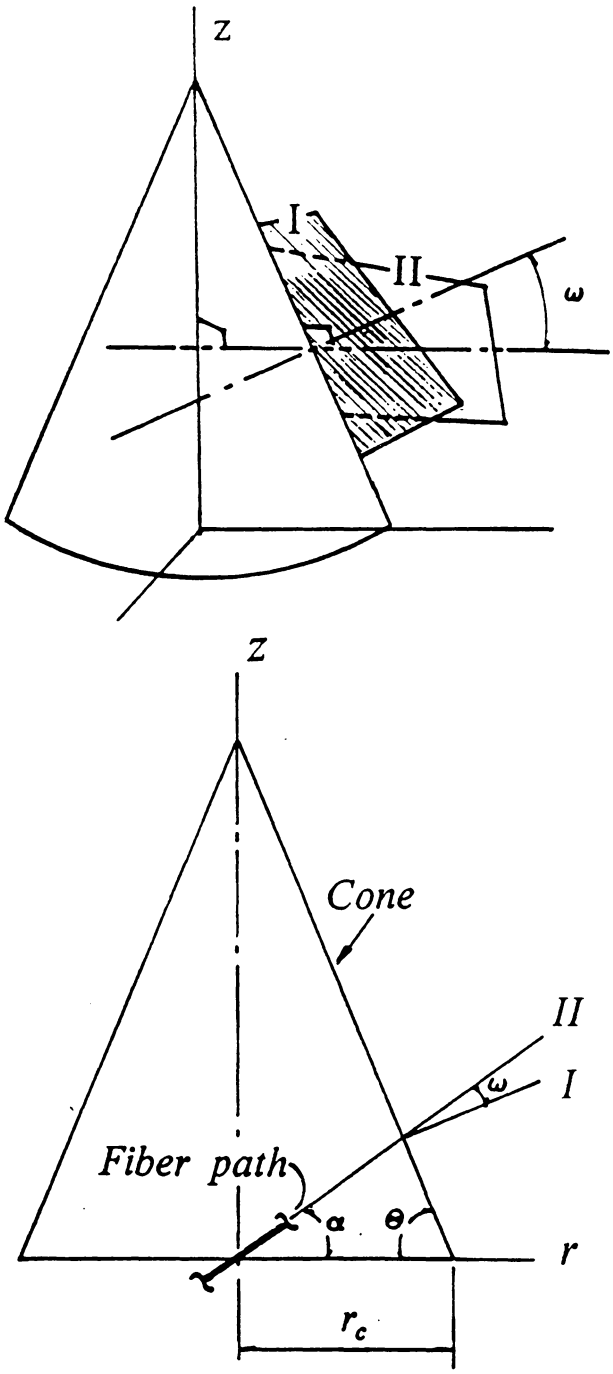

Figure 14. Minimum Curvature and Transformation:

The minimum curvature located on plane II which is normal the z-axis of the cone, is determined by the winding angle α and the angle θ . The fiber curvature located on plane I is obtained by transforming the minimum curvature with respect to angle ω.

hyperbolic

$$\kappa' = \left\{ \frac{a'b'}{\left[1 + b'^2 - a'^2 + (h' + a')^2\right]^{3/2}} \right\} \frac{1}{r_c} \tag{3.14}$$

where the α is the winding angle and r_c is the radius of the cone. The definitions of a', b', and h' can be referred from Nguyen [1] for each case.

Transformation with the angle ω results in the curvature the fiber path as follows:

$$\kappa = \kappa' \cos^2\omega \tag{3.15}$$

Hence, the pressure on the inner surface of each single tensioned element can be calculated by Eq.(3.7).

3.4.3 Superposition of Pressure

The fiber tensions in the outer elements can generate an additional pressures on the inner elements. The additional pressure is computed from force equilibrium in normal direction of element and is superposed on the inner elements to form the nodal pressure field.

The pressure field is constructed by superposing the pressures obtained from each individual tensioned element. The superposition of pressure is based on the geometric relation between the inner element and outer element.

Fig. 15 illustrates the geometric relationship between an inner element (with subscript i) and outer element (with subscript o). The geometric center of the elements are located along the same radial line which is normal to the surface of the dome.

The total pressure acting on the inner surface of the *ith* element, P_i^s, is the sum of the pressure generated by the fiber tensioned in the *ith* element plus additional pressures due to all the outer tensioned elements. The superposed pressures in the *ith* element can be obtained from the force equilibrium in the direction normal to the dome surface by the following expression

$$P_i^s = P_i + \sum_{o=i+1}^{outmost} P_o \times \frac{r_o \times l_o}{r_i \times l_i} \tag{3.16}$$

where

P_i^s is the superposed pressure acting on the inner surface of the i-th element,

P_i is the pressure generated by the i-th tensioned element itself,

P_o is the pressure generated by the o-th tensioned element,

r_i is the distance from the center of the i-th element to the longitudinal axis of case,

r_o is the distance from the center of the o-th element to the longitudinal axis of case,

l_i is the length of the i-th element, and

l_o is the length of the o-th element.

The superposed pressure calculated by Eq.(3.16) is used as the pressure acting on the inner surface of each element. The nodal pressure is then calculated by averaging the superposed pressures between the adjacent elements which are located in the same layer.

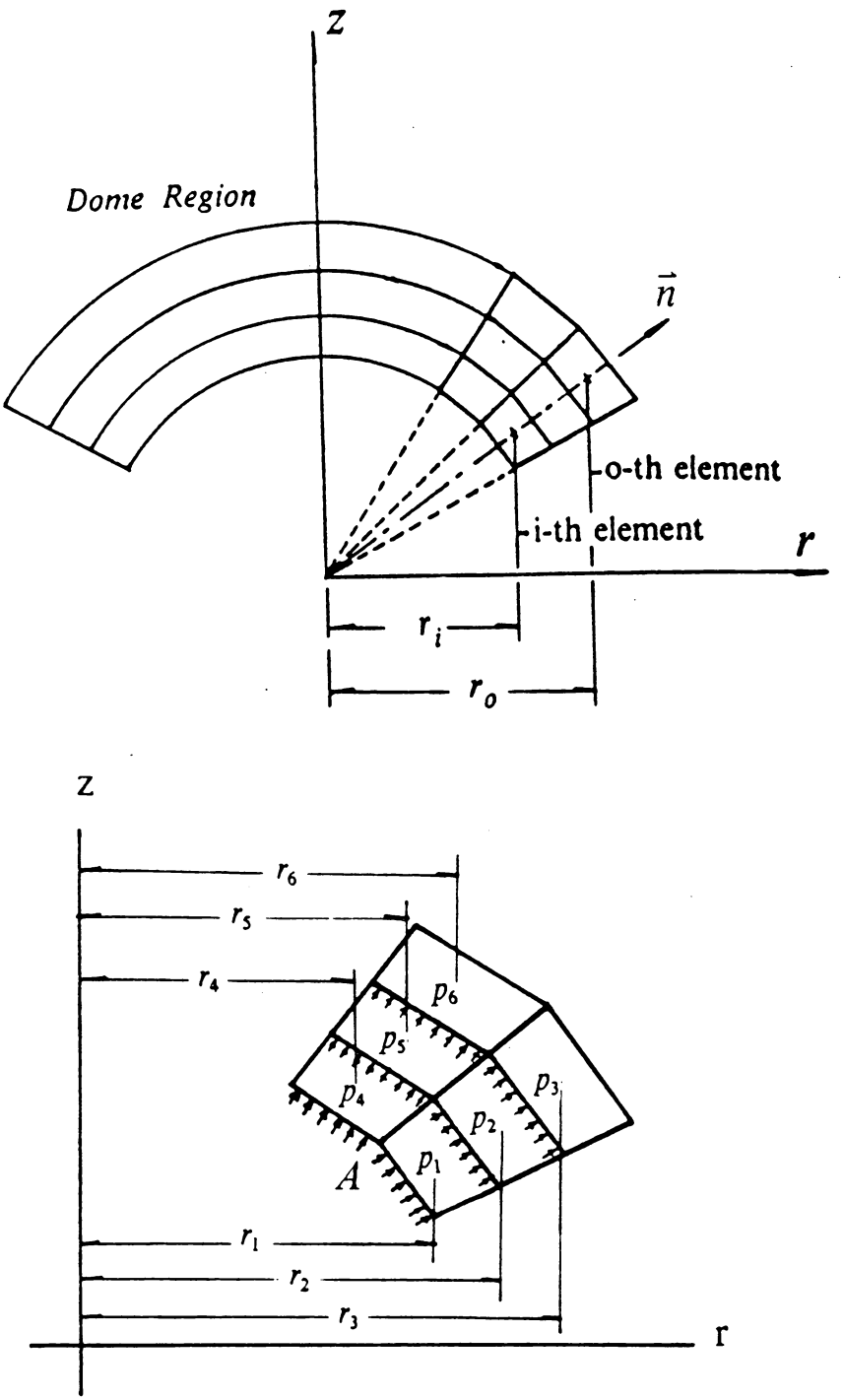

Figure 15. Pressure Superposition:

Nodal pressure field in the composite region is obtained by superposing the pressure calculated from each tensioned element. The superposition is done according to the force equilibrium in the $\vec{n}$ direction.

Consider a six element mesh in Fig. 15 . The calculation of the nodal pressure at point A is illustrated as follows :

The pressure acting on the inner surface of element 1 can be calculated as

$$P_1^S = P_1 + P_2 \times \frac{r_2 \times l_2}{r_1 \times l_1} + P_3 \times \frac{r_3 \times l_3}{r_1 \times l_1} \tag{3.17}$$

The pressure acting on the inner surface of element 4 is calculated as the following expression

$$P_4^S = P_4 + P_5 \times \frac{r_5 \times l_5}{r_4 \times l_4} + P_6 \times \frac{r_6 \times l_6}{r_4 \times l_4} \tag{3.18}$$

The variables in Eq. 3.17 and Eq. 3.18 were defined previously.

The nodal pressure at node A is obtained by averaging the pressures calculated from element 1 and element 4 as

$$P_A^N = \frac{P_1^S + P_4^S}{2} \tag{3.19}$$

where N represents the nodal pressure. Accordingly, the nodal pressure field can be constructed following the same procedures.

3.5 Permeability Model

During winding and in the early stages of cure, the permeability of the composite varies due to resin flow out of the composite causing compaction. Hence, a model

to calculate the permeability of each composite element during fabrication is required.

A relationship between permeability and the properties of a porous medium is given by the Kozeny - Carman equation [21]

$$S = \frac{P^3}{C S_o^2 (1 - P)^2} \tag{3.20}$$

where

S is the permeability of the porous medium,

C is a constant,

P is the porosity of the porous medium, and

S_o is the specific surface of the porous medium defined as the solid surface exposed to the fluid per unit solid volume.

Based on this equation, a permeability model was developed to relate the principal permeabilities to the resin volume fraction and properties and packing arrangement of the fibers in the composite. The principal directions of the permeability tensor are defined as the direction parallel or perpendicular to the fibers.

Assuming a hexagonal packing of fibers in the composite (i.e. equal distance between two centers of adjacent fibers) and specifying the resin volume fraction of the composite and the radius of the fibers, the principal permeabilities of the composite can be determined by the Kozeny - Carman equation. A unit cell assuming a hexagonal packing of fibers is shown in Fig.16 where the circles represent the cross-sections of the fibers. For a hexagonal fiber packing, the distance between two adjacent fiber centers can be calculated as follows.

$$T = \sqrt{\frac{\pi r^2}{(1 - v_r)\sin(\pi/3)}} \tag{3.21}$$

where v_r is the resin volume fraction of composite, and r is the radius of fiber.

The specific surface can be calculated as

$$S_o = \frac{2\pi r}{\pi r^2} = \frac{2}{r} = \frac{4}{d} \tag{3.22}$$

where, d is the diameter of the fiber.

The normal porosity in the parallel direction of fibers is equal to the resin volume fraction

$$P_p = v_r \tag{3.23}$$

Substituting Eq.(3.22) and Eq.(3.23) into Eq.(3.20) gives the permeability along the fiber direction

$$S_p = \frac{d^2 v_r^3}{C'(1 - v_r)^2} \tag{3.24}$$

The normal porosity in the direction perpendicular to the fibers is assumed to be

$$P_n = \frac{T - \frac{2r}{\cos(\pi/6)}}{T} \tag{3.25}$$

Substitution of Eq.(3.25) and S_o into Kozeny-Carman equation results in the permeability in the direction normal to the fibers

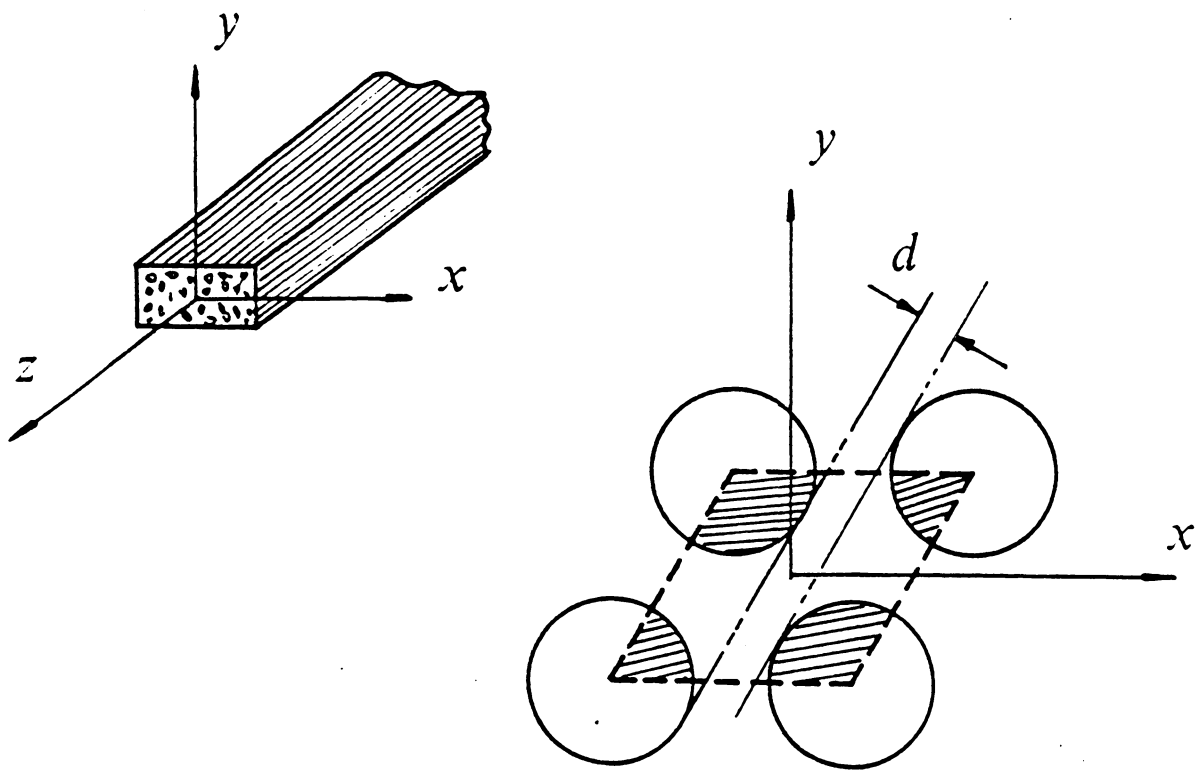

Figure 16. Permeability Model:

Assuming a hexagonal packing of fibers, a unit cell defined as the parallelogram is shown in the figure where the circles represent the fibers. The directions of the principal permeabilities are normal or parallel to the fibers (i.e. x, y, and z directions). Principal permeabilities depending on the resin volume fraction are calculated by using Kozeny-Carman equation.

$$S_n = \frac{d^2 P_n^3}{C'' (1 - P_n)^2} \tag{3.26}$$

where constants C' and C'' must be determined by experiments.

The principal permeability tensor, $[S]$, can be defined as

$$\begin{bmatrix} S_{11} & 0 & 0 \\ 0 & S_{22} & 0 \\ 0 & 0 & S_{33} \end{bmatrix} \tag{3.27}$$

where $S_{11} = S_{22}$ are the permeabilities normal to the fiber direction and S_{33} is the permeability along the fiber direction

The permeability tensor of each element can be obtained from tensor transformations relating the principal permeabilities, the winding angle, and polar angle as follows:

The first transformation involves the winding angle α :

$$[S]_{(\alpha)} = [A]_{(\alpha)} [S] [A]^T_{(\alpha)} \tag{3.28}$$

where

$$[A]_{(\alpha)} = \begin{bmatrix} 1 & 0 & 0 \\ 0 & \sin \alpha & \cos \alpha \\ 0 & -\cos \alpha & \sin \alpha \end{bmatrix} \tag{3.29}$$

The second transformation involves the polar angle β :

$$[S]_{(\beta)} = [A]_{(\beta)} [S]_{(\alpha)} [A]^T_{(\beta)} \tag{3.30}$$

where

$$[A]_{(\beta)} = \begin{bmatrix} \cos\beta & 0 & -\sin\beta \\ 0 & 1 & 0 \\ \sin\beta & 0 & \cos\beta \end{bmatrix} \tag{3.31}$$

3.6 Resin Flow

Once the nodal pressures, permeability, and viscosity of resin are known, the resin flow rate at the center of each element can be calculated using Darcy's equation. Darcy's equation in cylindrical coordinates for axisymmetric geometry is given

$$\begin{bmatrix} q_r \\ q_z \end{bmatrix} = -\frac{1}{\mu} \begin{bmatrix} S_{rr} & S_{rz} \\ S_{zr} & S_{zz} \end{bmatrix} \begin{bmatrix} \frac{\partial P}{\partial r} \\ \frac{\partial P}{\partial z} \end{bmatrix} \tag{3.4}$$

The nodal pressures were derived from the superposition of the layer pressures in the Section 3.4. Pressure across an element is approximated by differentiable interpolation functions derived from the nodal pressures. Therefore, the pressure gradient in the center of element can be calculated from derivative of the interpolation functions.

In order to simplify the calculation procedure, the element coordinates and the pressure are mapped onto an element of unit dimensions. Introducing a coordinate transformation, the coordinates r and z and the nodal pressure can be written as

$$r = r(\xi, \eta) \quad z = z(\xi, \eta) \quad P = P(\xi, \eta) \tag{3.32}$$

The coordinates (ξ, η) are referred as local coordinates. Furthermore, the mapping functions are chosen so that the element can be mapped onto a square unit element in $\xi - \eta$ plane. The unit element and the transformation functions are located in the region of

$$-1 \leq \xi \leq 1 \quad -1 \leq \eta \leq 1 \tag{3.33}$$

To be more specific, the transformation (Eq. 3.32) can be expressed by a set of linear interpolation functions as

$$r = \sum_{i=1}^{4} r_i \psi_i(\xi, \eta) \quad z = \sum_{i=1}^{4} z_i \psi_i(\xi, \eta) \quad P = \sum_{i=1}^{4} P_i \psi_i(\xi, \eta) \tag{3.34}$$

where, ψ_i are interpolation functions as follows:

$$\begin{aligned} \psi_1 &= \frac{1}{4}(1 - \xi)(1 - \eta) \quad & \psi_2 &= \frac{1}{4}(1 + \xi)(1 - \eta) \\ \psi_3 &= \frac{1}{4}(1 - \xi)(1 + \eta) \quad & \psi_4 &= \frac{1}{4}(1 + \xi)(1 + \eta) \end{aligned} \tag{3.35}$$

It is easy to realize that the inverse functions $\xi = \xi(r, z)$ and $\eta = \eta(r, z)$ are continuous, differentiable, and numerically invertible. The reduced Darcy's equation (Eq.3.4) can be rewritten in terms of the interpolation functions

$$\begin{bmatrix} q_r \\ q_z \end{bmatrix} = -\frac{1}{\mu} \begin{bmatrix} S_{rr} & S_{rz} \\ S_{zr} & S_{zz} \end{bmatrix} \begin{bmatrix} \sum_{i=1}^{4} P_i \frac{\partial \psi_i}{\partial r} \\ \sum_{i=1}^{4} P_i \frac{\partial \psi_i}{\partial z} \end{bmatrix} \tag{3.36}$$

The derivatives of the interpolation functions can be obtained from chain rule

$$\begin{bmatrix} \frac{\partial \psi_i}{\partial r} \\ \frac{\partial \psi_i}{\partial z} \end{bmatrix} = \begin{bmatrix} \frac{\partial \xi}{\partial r} & \frac{\partial \eta}{\partial r} \\ \frac{\partial \xi}{\partial z} & \frac{\partial \eta}{\partial z} \end{bmatrix} \begin{bmatrix} \frac{\partial \psi_i}{\partial \xi} \\ \frac{\partial \psi_i}{\partial \eta} \end{bmatrix} = [J] \begin{bmatrix} \frac{\partial \psi_i}{\partial \xi} \\ \frac{\partial \psi_i}{\partial \eta} \end{bmatrix} \tag{3.37}$$

where $[J]$ is referred as the Jacobian matrix

$$[J] = \begin{bmatrix} \frac{\partial \xi}{\partial r} & \frac{\partial \eta}{\partial r} \\ \frac{\partial \xi}{\partial z} & \frac{\partial \eta}{\partial z} \end{bmatrix} \tag{3.38}$$

The Jacobian matrix can not be calculated directly. However, it can be obtained from the inverse matrix $[\bar{J}]$

$$[\bar{J}] = \begin{bmatrix} \frac{\partial r}{\partial \xi} & \frac{\partial z}{\partial \xi} \\ \frac{\partial r}{\partial \eta} & \frac{\partial z}{\partial \eta} \end{bmatrix} \tag{3.39}$$

calculated from the nodal coordinates and the interpolation functions in each element

$$[\bar{J}] = \begin{bmatrix} \sum_{i=1}^{4} r_i \frac{\partial \psi_i}{\partial \xi} & \sum_{i=1}^{4} z_i \frac{\partial \psi_i}{\partial \xi} \\ \sum_{i=1}^{4} r_i \frac{\partial \psi_i}{\partial \eta} & \sum_{i=1}^{4} z_i \frac{\partial \psi_i}{\partial \eta} \end{bmatrix} \tag{3.40}$$

The resin flow rate at the center of each element can be calculated by setting $\xi = \eta = 0$. Therefore, $[\bar{J}]$ for each element can be obtained by the substitution of the nodal coordinates and $\xi = \eta = 0$ into Eq.(3.40). The inverse of the matrix $[\bar{J}]$ results in the Jacobian $[J]$.

The resin flow rates along r and z directions are calculated from the equations derived above for each element. Finally, the resin flow rate in the direction normal to the fiber path $\dot{w}$ is calculated from the polar angle and the resin flow rates q_r and q_z

$$\dot{w} = q_r \times \cos\beta + q_z \times \sin\beta \tag{3.41}$$

The resin displacement in each element is obtained by integrating the resin flow rate with respect to time.

$$w = \int_0^t \dot{w}\, dt = \sum \dot{w}\, \Delta t \tag{3.42}$$

The resin flow rate is calculated for each element at each time step. The time step and the FEM mesh used in the layer tension loss model are exactly the same as the

cure model. Therefore, the element viscosity of the resin and the temperature distribution obtained from the cure model are used directly in the resin flow calculations.

Summation of the resin displacement is done for each time step giving the fiber movement as a function of time. Fiber displacement is then used to calculate mechanical strain in the fiber which will be discussed in Section 3.8.

3.7 Compaction

In order to determine the permeability, the resin volume fraction must be known for each composite element. From the relative resin displacement between adjacent elements located in adjacent layers, the compaction and resin content of each element can be determined.

Fig. 17 shows the resin displacement in two adjacent elements. If the total resin displacement is larger for the inner element than of the outer element, resin accumulates between the layers. If the total resin displacement is smaller for the inner element than of the outer element, consolidation occurs in the outer element.

Consider the instantaneous total resin displacements of two adjacent element, w_i and w_{i+1} which are obtained from Eq. (3.42). w_i represents the resin displacement of the inner element, while w_{i+1} is the resin displacement of the outer element.

If w_i is greater than w_{i+1}, the fibers move inward faster for the inner element than for the outer element. Accordingly, the resin volume fraction of the outer element does

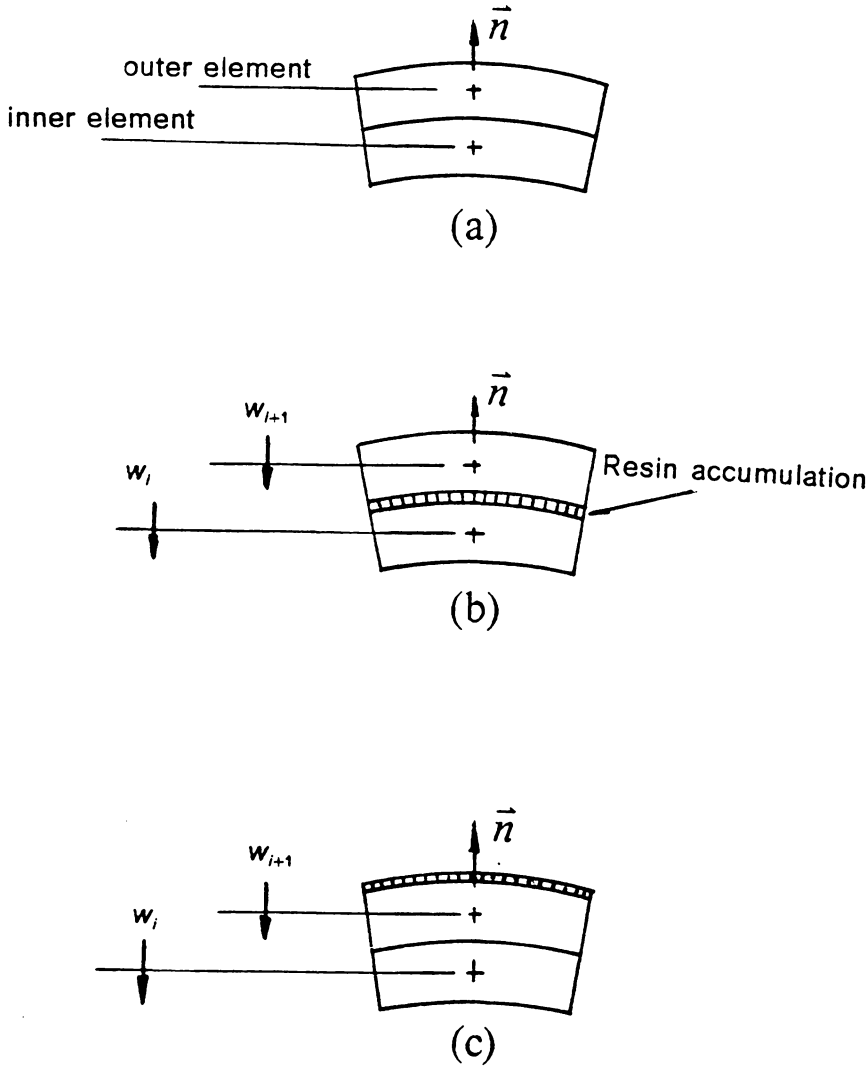

Figure 17. Compaction:

The resin volume fraction of each element is calculated from the relative resin displacements between two adjacent elements in adjacent layers. Plot (a) shows the initial positions of the two elements. Plot (b) shows that the fiber movement is greater for the inner element than for the outer element. Therefore, resin accumulates between the two layers. Plot (c) shows that the fiber movement is smaller for the inner element than for the outer element and compaction occurs in the outer element.

not change. If w_i is smaller than w_{i+1}, compaction occurs in the outer element. The new resin volume fraction of the outer element is calculated from the following expression

$$\bar{v}_{r,\,i+1} = \frac{(1 - v_{r,\,i+1})\, t_{i+1}}{t_{i+1} - w_{i+1} + w_i} \tag{3.43}$$

where t_{i+1} is the original thickness of the outer element, $v_{r,\,i+1}$ is the resin volume fraction of composite in previous time step, and w_i and w_{i+1} were defined previously as the displacement of the *ith* and $i + 1th$ elements, respectively.

Therefore, the permeability (see Section 3.5) can be updated in the calculation of the resin flow since the resin volume fraction is known for each element at any instant of time.

3.8 Fiber Tension

As previously discussed, the resin displacement normal to the fiber path at the center of the element is used to determine fiber motion. The fiber displacement is then used to calculate mechanical strain in the fibers. Because the temperature varies during cure, thermal strains occur due to thermal shrinkage or expansion of the fibers. Both the thermal and mechanical strains can affect the level of fiber tension.

Total fiber strain is obtained from the variation of fiber curvature due to the fiber displacement and thermal strain. The fiber movement is determined from the resin displacement while the thermal strain is calculated from the variation in the temper-

ature. The fiber tension first derived by Calius and Springer [8] is calculated from the following expression (Fig. 18)

$$F = E \times [(\frac{R_o - w}{R_f} - 1) - e_t] \times H \tag{3.44}$$

where E is elastic modulus of the fiber, R_o is the initial radius of curvature of fiber path, R_f is the radius of curvature of fiber when the fiber loses tension completely, w is the radial movement of fiber, e_t is the thermal strain in the fiber, and H is the cross sectional area of the fibers.

Because the fibers are continuous, fiber tension rearrangement is required to obtain a balanced fiber tension along the fiber path of each layer at each time step. If shear lag along the fiber path due to the viscous resin is neglected, tension rearrangement can be obtained from the average fiber tension F_{bal} along the same fiber path (Fig. 19) as

$$F_{bal} = \frac{\sum F_i l_i \csc \alpha_i}{\sum l_i \csc \alpha_i} \tag{3.45}$$

where l_i is the length of the element, α_i is the winding angle, and F_i is the fiber tension in the element. The balanced tension is then used to calculate pressure gradient in the next time step.

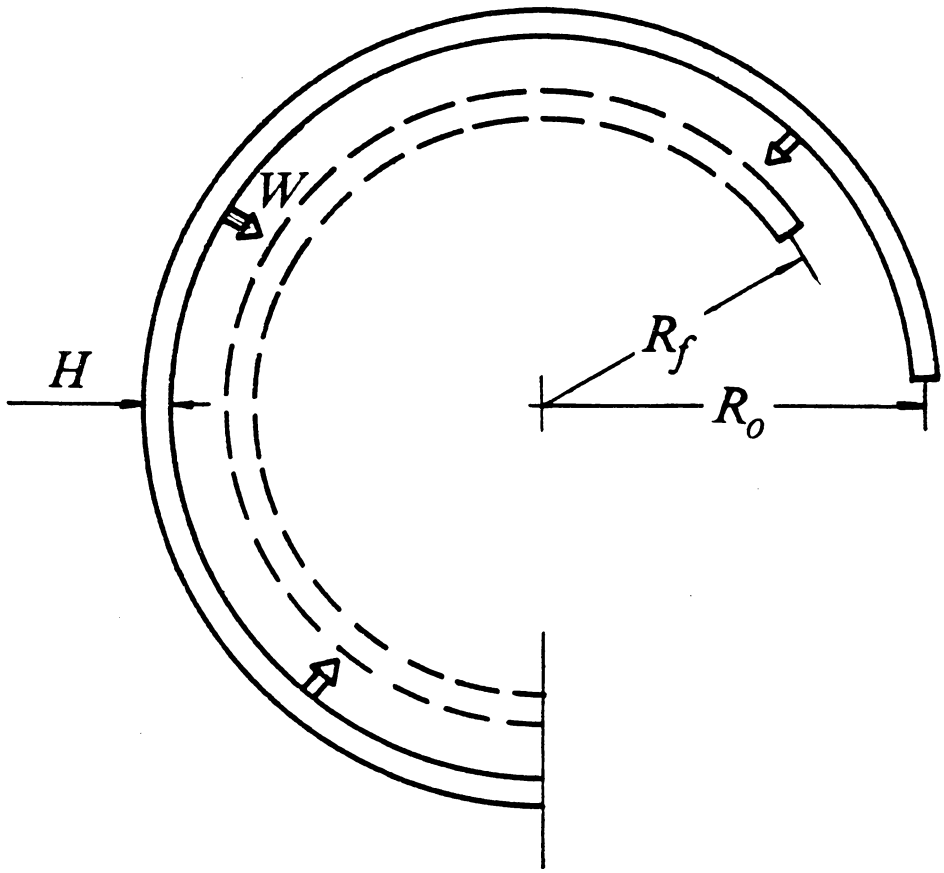

Figure 18. Fiber Tension and Position:

According the Hooke's law, the fiber tension is proportional to the strain in the fiber. The mechanical strain is obtained from the relative curvature of the fiber and the thermal strain is calculated from the change of temperature during cure.

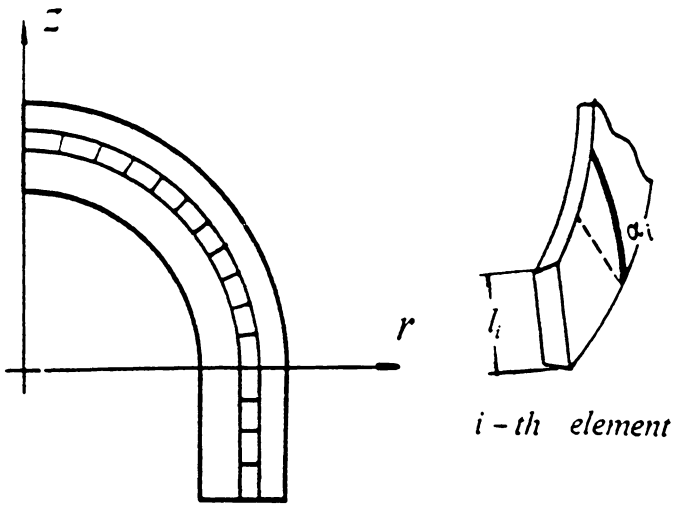

$$F_{bal} = \frac{\sum F_i \, l_i \csc \alpha_i}{\sum l_i \csc \alpha_i}$$

α_i : winding angle of the i-th element

l_i : length of the i-th element

F_i : fiber tension of the i-th element

Figure 19. Tension Rearrangement:

Tension rearrangement is carried out by averaging the fiber tension from each element along the fiber path. The length of the fiber in each element is used as a weight value and the calculation is done at each time step.

3.9 Winding Time

During the winding process, the resin is exposed to ambient temperature and begins to cure. Depending on the resin system, there may be considerable differences in the degree of cure between the inner and outer layers in a thick case. In wet winding, resin flow and tension loss occur due to a low resin viscosity during winding. Accordingly, there is a need to estimate the winding time.

The resin flow and tension loss of each layer is assumed to start when the layer is completely wound. Therefore, time required to wind each layer of the composite case needs to be estimated.

The winding time depends on the winding equipment, geometry, and winding pattern of the case . Following the winding pattern described by Lubins [22], the winding time is developed for a simple winding machine with two degrees of freedom. These include a rotating mandrel and a carriage which moves parallel to the longitudinal axis of the case.

The fiber path of a typical circuit is shown in Fig. 20 for a simple axisymmetric case with spherical end closures. If the rotation speed of mandrel (Ω) is known, the winding time for a single layer can be estimated by tracing fiber path as follows :

The revolutions of the mandrel required to complete one winding circuit can be calculated by the following expression

$$\frac{L_c \cot \alpha}{\pi R} + \frac{\theta}{\pi} \tag{3.46}$$

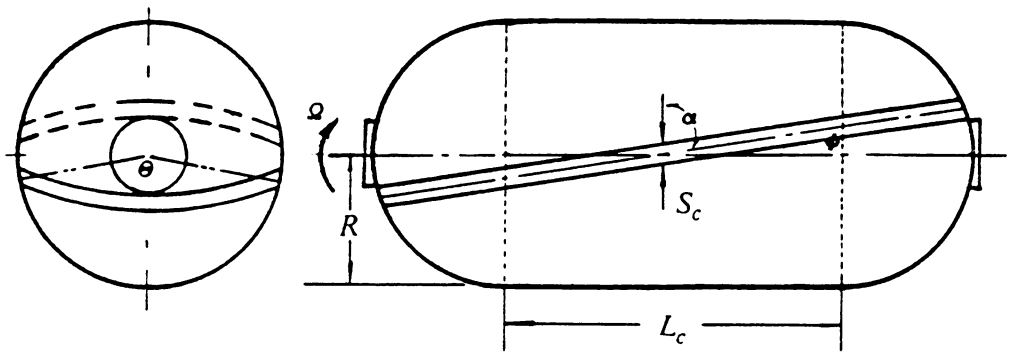

Ω : *rotation speed of mandrel*
B : width of fiber band

Figure 20. Winding Time Calculation:

Parameters used in the calculation of the winding time

where, L_c is the length of cylindrical region, α is the winding angle in the cylindrical region, R is the radius of cylinder, and θ is the dwell angle.

The circuits required per layer is given by the following expression

$$\frac{2\pi R \sin\alpha}{B} \tag{3.47}$$

where B is the band width of the fiber bundle.

Multiplying Eq. 3.46 by Eq. 3.47 , we obtain the time required to wind a complete layer

$$T_\Omega = \frac{1}{\Omega} \times \left(\frac{2\pi R \sin\alpha}{B}\right) \times \left[\frac{L_c \cot\alpha}{\pi R} + \frac{\theta}{\pi}\right] \tag{3.48}$$

where Ω is the rotational speed of the mandrel.

For a hoop winding pattern (i.e. α is small), which is wound on the cylindrical surface only, Eq. 3.48 reduces to the following expression.

$$T_\Omega = \frac{1}{\Omega} \left(\frac{L_c}{B/\sin\alpha}\right) \tag{3.49}$$

4.0 NUMERICAL IMPLEMENTATION

The formulations of the cure model and the layer tension loss model have been derived in Chapter 2 and Chapter 3. The solutions of the models must be obtained by numerical methods. As discussed in the previous chapters, the finite element method was used in the computations. In this chapter, an overview of the computational procedures will be illustrated for both the cure model and the layer tension loss model.

In formulation of the layer tension loss model, fiber motion is resisted by the viscous resin. The viscosity of the resin is greatly affected by the curing process and is calculated using the cure model. The temperature variation in the composite case causes thermal expansion or shrinkage of the fibers. The thermal strain of the fiber certainly will affect the state of the fiber tension. Accordingly, the cure model and the layer tension loss model must be combined into a comprehensive model to obtain the fiber tension loss in the composite case.

A computer code "FWCURE" based on the finite element technique was developed to obtain numerical solutions of the combined model. The step-by-step calculation procedures are discussed in the following sections.

4.1 Cure Model

The computation flow chart of the cure model is shown in the Fig. 21. The flow chart illustrates the relationships among the three submodels : the heat transfer model, kinetics model, and viscosity model.

The heat transfer model is the main element of the cure model. The model can be used to calculate the temperature distribution (i.e. nodal temperatures) in the FWC assembly. The kinetics model, constructed from the isothermal differential scanning calorimetry (DSC) data, expresses cure rate and the rate of heat generation in the matrix resin as functions of the temperature and the degree of cure of the composite. Resin viscosity is obtained from the viscosity model which relates temperature and degree of cure to viscosity. The calculation procedures is as follows :

1. The finite element mesh and the corresponding winding angles and polar angles are determined from the structural geometry.
2. The material and thermal properties for the mandrel, composite, insulator, and outer layer are specified.
3. The initial temperatures in the FWC assembly are specified and the initial degree of cure of the composite is set equal to zero.

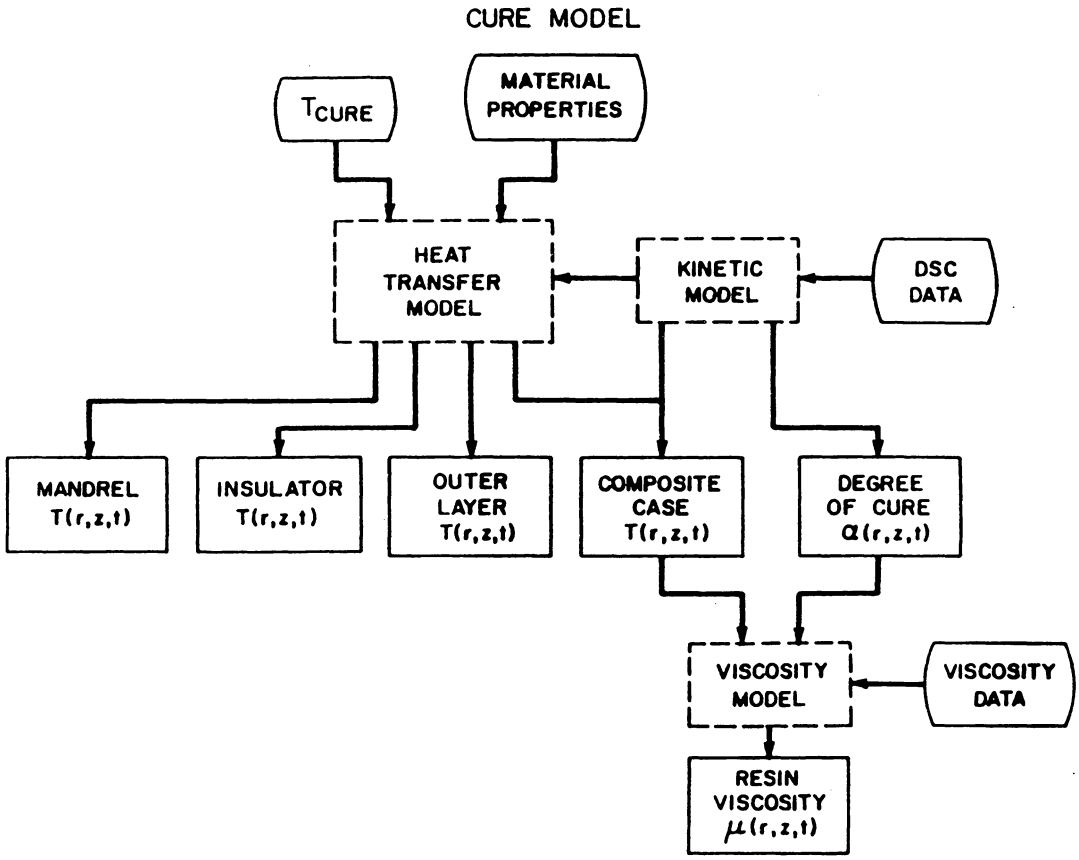

Figure 21. Computation Flow Chart of the Cure Model:

4. The cure cycle (i.e. oven temperature) is specified and the heat transfer coefficients at the boundary elements need to be predetermined.
5. The rate of the heat generation, calculated from the kinetics model, is used as an internal heat source in each composite element.
6. The nodal temperatures are obtained by the heat transfer model which computes the transient heat conduction in the FWC assembly.
7. An average temperature is calculated from the nodal temperatures for each composite element.
8. The integration of the cure rate calculated by the kinetics model gives the degree of cure of each composite element.
9. The average temperature and the degree of cure of each element are used to calculate the resin viscosity of the element from the viscosity model.

The average temperature and the resin viscosity of the element are used in the calculation of resin flow and fiber motion in the layer tension loss model.

4.2 Layer Tension Loss Model

The computation procedures for the layer tension loss model are illustrated in the flow chart (Fig. 22).

The finite element mesh and the time interval specified in the cure model are also used in the layer tension loss model. Therefore, the resin viscosity and the temperature in each composite element can be used directly in the calculation of the layer tension loss. The calculation involves the following steps.

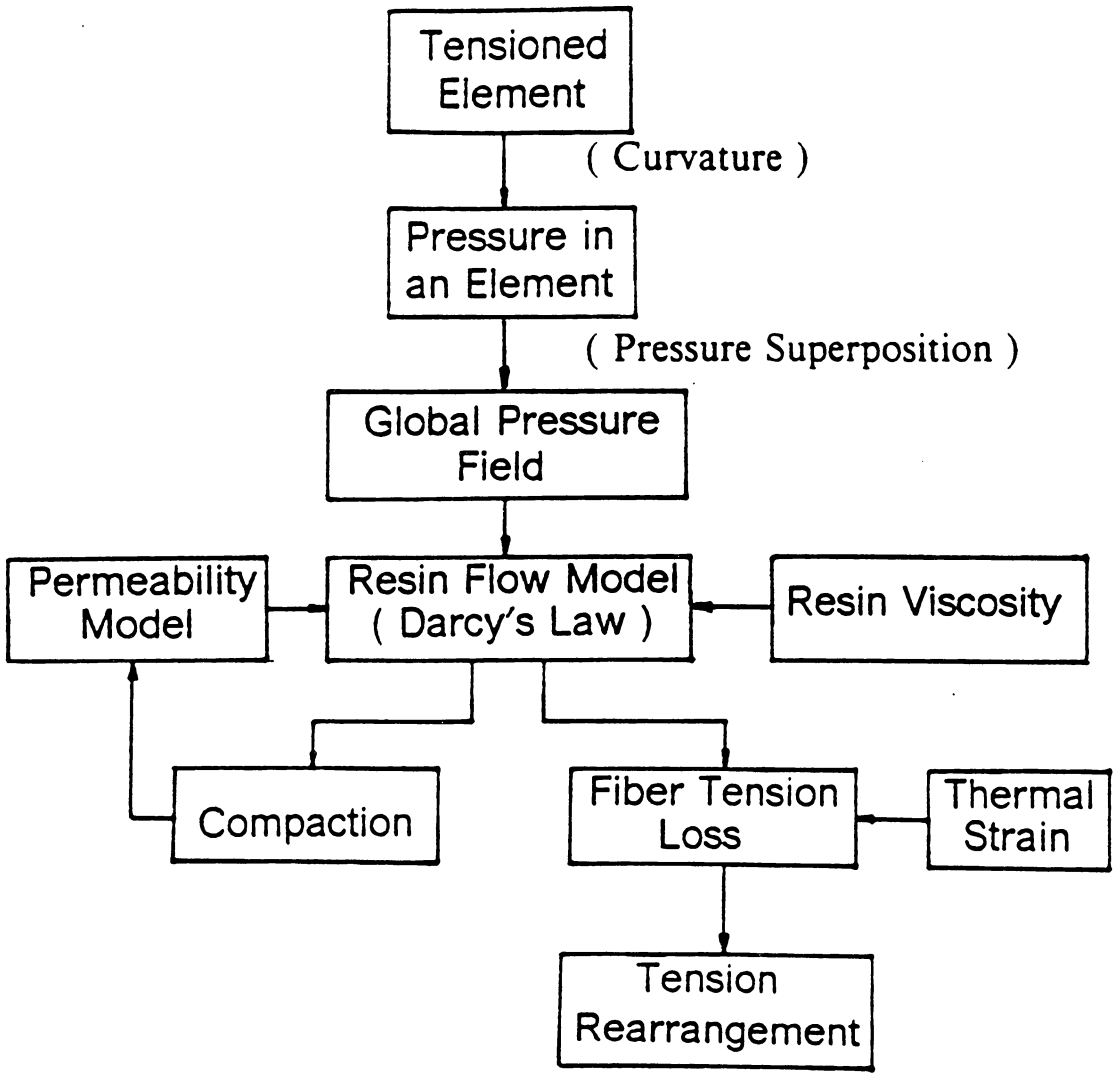

Figure 22. Computation Flow Chart of the Layer Tension Loss Model:

1. The pressure due to the tensioned element is calculated from the fiber tension and the curvature of the fiber path for each composite element.
2. The global pressure field is then obtained from the superposition of the pressures calculated from the tensioned elements.
3. The principal permeabilities of each composite element can be calculated from the resin volume fraction by using the permeability model. Furthermore, tensor transformations based on the winding and polar angles result in the permeability tensor for each element.
4. Once the pressure field, permeability, and resin viscosity are known, the resin flow rate in each element can be calculated from the anisotropic Darcy equation.
5. The resin flow in the radial direction of the fiber path at the center of the element is used to determined the fiber layer position, the fiber tension loss, and the updated resin volume fraction as discussed in Chapter 3.

4.3 Computer Code

A FORTRAN computer code "FWCURE" was written to obtain a numerical solution of the combined model. The computer code requires that the input parameters be specified. The parameters may be categorized into three groups: a) Geometry, b) Material Properties, c) Initial and Boundary Condition. A list of the input parameters required for the model is given in Table 1.

Table 1. Input Parameters for FWCURE

A) Geometry

1. Finite element mesh of the FWC assembly
2. Winding angle of element
3. Polar angle of element

B) Material Properties

a) Mandrel, Insulator, and Outer Layer

1. Density
2. Specific heat
3. Thermal Conductivity

b) Composite

1. Density
2. Specific heat
3. Principal thermal conductivities
4. Resin volume fraction
5. Heat of reaction of resin
6. Diameter of fiber
7. Thermal expansion coefficient of fiber
8. Relationship between the cure rate, temperature, and degree of cure of resin
9. Relationship between the viscosity, temperature, and degree of cure of resin

C) Initial and Boundary Conditions

1. Initial temperature distribution in the mandrel, insulator, composite case, and outer layer.
2. Initial degree of cure of resin in the composite case
3. Autoclave or oven temperature as a function of time
4. Heat transfer coefficients at the convective boundary surface of the FWC assembly.

5.0 RESULTS

Simulations of the winding and curing processes of filament wound composites were performed using the model. Verification of the cure model was accomplished by comparing the calculated solutions with data measured in the FWC assembly during cure. A parametric study was performed to illustrate the effects of processing variables and material properties on the curing process of a filament wound composite.

A 4 inch diameter graphite/epoxy tube and a 5.75 inch diameter graphite/epoxy bottle were wound and cured at Morton Thiokol Inc., Wasatch Operations. The temperature distribution in each FWC assembly was measured during cure and compared with temperatures calculated using the model. Agreement between measured and calculated temperatures was very good for both the test bottle and the cylindrical tube.

The parametric study was performed using an 18 inch diameter test bottle. This study showed how the processing parameters effect the cure and fiber tension loss in the composite case.

5.1 4 inch Tube

5.1.1 Experiment

A thick-walled cylindrical tube was wound using graphite/epoxy prepreg roving. Fig. 23 shows the schematic of the FWC tube assembly. The composite cylinder was about 1.27×10^{-2} *m* (0.5 in) thick, 10.16×10^{-2} *m* (4 in) diameter, and 0.66 *m* (26 in) long.

A. Geometry and Material

1. Mandrel

   The mandrel is a 0.96 *m* (38 in) long cylindrical steel pipe. The outer diameter is 6.08×10^{-2}*m* (2.396 in) and the wall thickness is 3.94×10^{-3} *m* (0.155 in).

2. Insulator

   The insulator was EPDM rubber with a thickness of 2.54×10^{-3} *m* (0.1 in). The insulator was wrapped onto the mandrel surface and cured in a separate step before the composite case was wound.

3. Composite Case

   The composite case was formed from prepreg rovings using a hoop winding pattern (i.e. winding angle is zero). The B-staged prepreg consisted of T-40 graphite fiber and Fiberite 982 resin. Totally, 60 layers were wound and the thickness of the case was 1.27×10^{-2} *m* (0.5 in). The initial winding tension was

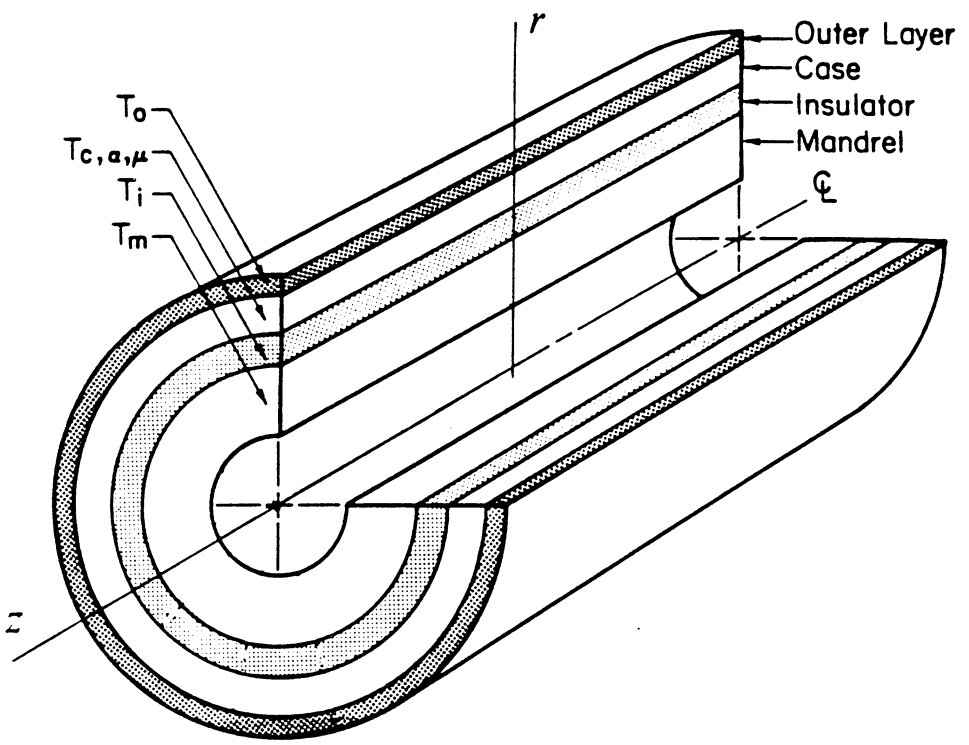

Figure 23. Schematic of FWC Tube Assembly:

The assembly consists of four regions : mandrel, insulator, composite case, and outer layer.

35.56 *nt* (8 lb) per fiber bundle with a tow cross-sectional area of $4.03 \times 10^{-7} m^2$ (6.25×10^{-4} in^2) .

4. Outer Layer

   The outer layer consists of the following material : perforated FEP film, breather cloth, Dacron release cloth, and a Nylon vacuum bag. The total thickness was measured to be 2.18×10^{-3} *m* (0.086 in).

B. Temperature Measurement and Cure Cycle

The FWC assembly was cured in an autoclave and the temperature distribution was measured during cure by thermocouples embedded through the thickness of the assembly at three axial positions (see Fig. 24). The oven temperature was monitored and recorded during the entire cure process.

The oven was heated at a constant rate of 0.52 °C/ min from the ambient temperature (21°C) to 73°C and held at 73°C for about 9 hours. The oven was then heated at 0.52°C to the final cure temperature of 123°C and held at 123°C for 5 hours. Finally, the oven was gradually cooled to the room temperature.

5.1.2 Analysis

Simulation of the fabrication process was performed using the models and associated computer code FWCURE. The material properties, finite element mesh, and kinetics

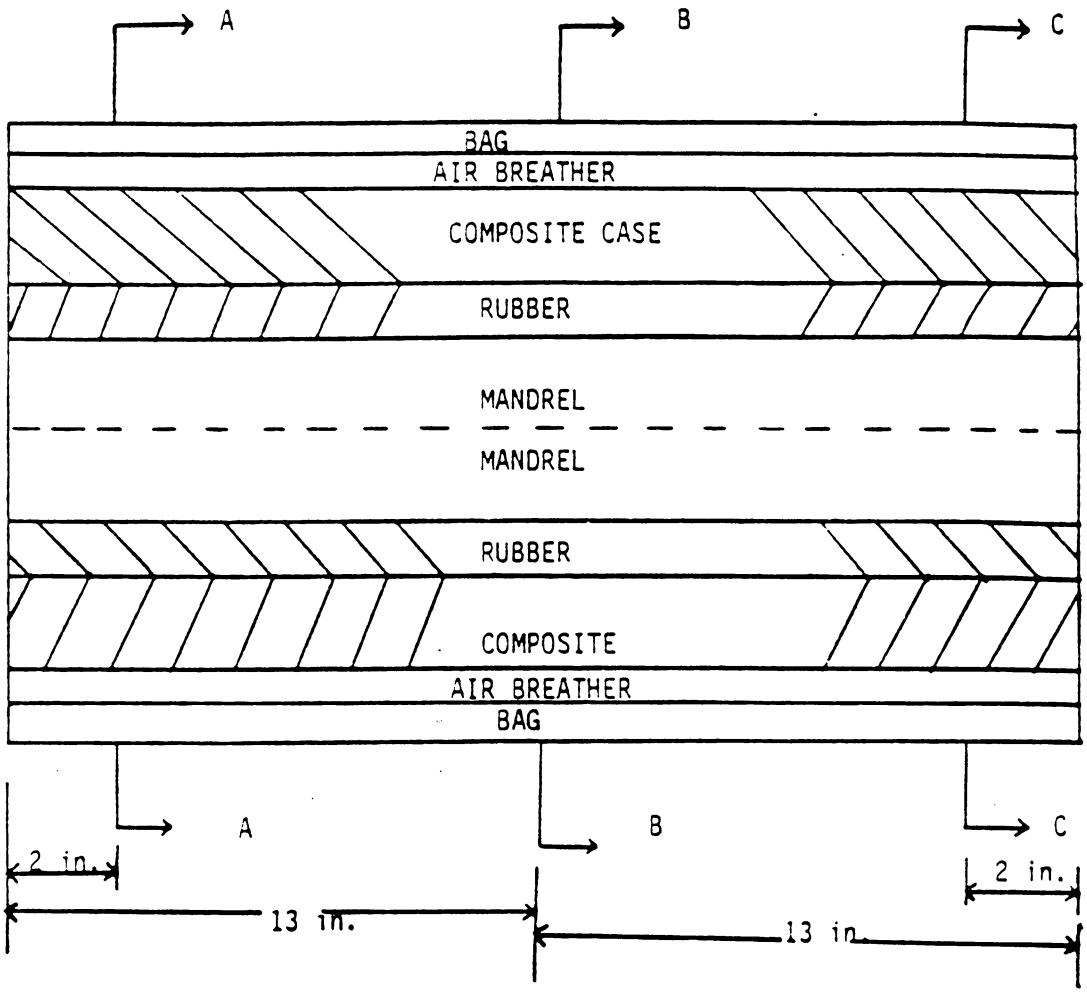

Figure 24. Thermocouples Locations:

The temperature distributions through the thickness of the assembly were measured at three axial positions (i.e. section "AA", "BB", and "CC"). (Courtesy : Morton Thiokol Inc., Wasatch Operations)

and viscosity models for the resin system must be specified and input into the computer code.

A finite element mesh was generated for the tube assembly. The nodal temperatures were taken to correspond with the experimental data at relevant locations. The degree of cure, resin viscosity, and the fiber tension variation in the tube were plotted and discussed in Section 5.1.3.

A. Material Properties

The material properties (i.e. density, thermal conductivity, and specific heat) for the mandrel, insulator, and the outer layer were obtained either from the manufacturer or handbook values were used. The properties of the composite were calculated from the properties of the fiber and resin by using the rule of mixtures equations described in Section 2.6. The properties used in the simulation are listed in Table 2.

B. Kinetics Model and Viscosity Model

The differential scanning calorimetry (DSC) experiments and the isothermal viscosity measurements for Fiberite 982 resin were performed at Morton Thiokol Inc., Wasatch Operations. The experimental data were used to develop the kinetics and viscosity models used in the simulations. The kinetics and viscosity models for Fiberite 982 resin are given in Appendix B.

C. Finite Element Mesh

Table 2. Material Properties for 4 Inch Tube

	Density	Heat Capacity	Thermal Conductivity
	ρ	C_p	K
	kg/m^3	$J/kg\,°K$	$W/m\,°K$
Mandrel	0.760×10^4	0.500×10^3	0.167×10^2
Insulator	0.110×10^4	0.176×10^4	0.207×10^0
Composite	0.159×10^4	0.148×10^4	0.741×10^0 (K_{11}) 0.741×10^0 (K_{22}) 0.412×10^1 (K_{33})
Outer layer	0.137×10^4	0.105×10^4	0.199×10^0

Constants for permeability model : $C' = C'' = 5$
Fiber diameter : $6\mu m$
Thermal expansion coefficient : -0.54×10^{-6} /°C
Young's modulus of the fiber : 2.92×10^{11} *Pa*

If we consider the symmetry of the tube, only a half of the tube needs to be analyzed. Fig. 25 shows the finite element mesh used in the simulation and the locations where the measured and calculated temperatures were compared.

The domain is divided into 15 elements in the radial direction (r-direction) : 2 mandrel elements, 2 insulator elements, 10 composite elements, and 1 outer layer element. In the longitudinal direction (z-direction), there are 14 elements which includes 13 mandrel elements and 1 outer layer element in the innermost region. Totally, there are 210 elements with 240 nodes.

In the composite region, both the winding angle and the polar angle are zero for all elements.

D. Boundary Condition

The heat transfer coefficients at the boundaries of the assembly vary with local geometry of the assembly surface. The heat transfer coefficient on the inner surface of the mandrel was assumed equal to zero because the FWC assembly was vacuum bagged and the surface was not directly heated during cure. The outer surface of the FWC tube assembly was heated by forced convection. The heat transfer coefficients were 17 W/m^2K in the cylindrical region and 15 W/m^2K on the surface of both ends. The heat transfer coefficients were obtained by matching the calculated temperatures with the measured data on the outer surface of the assembly.

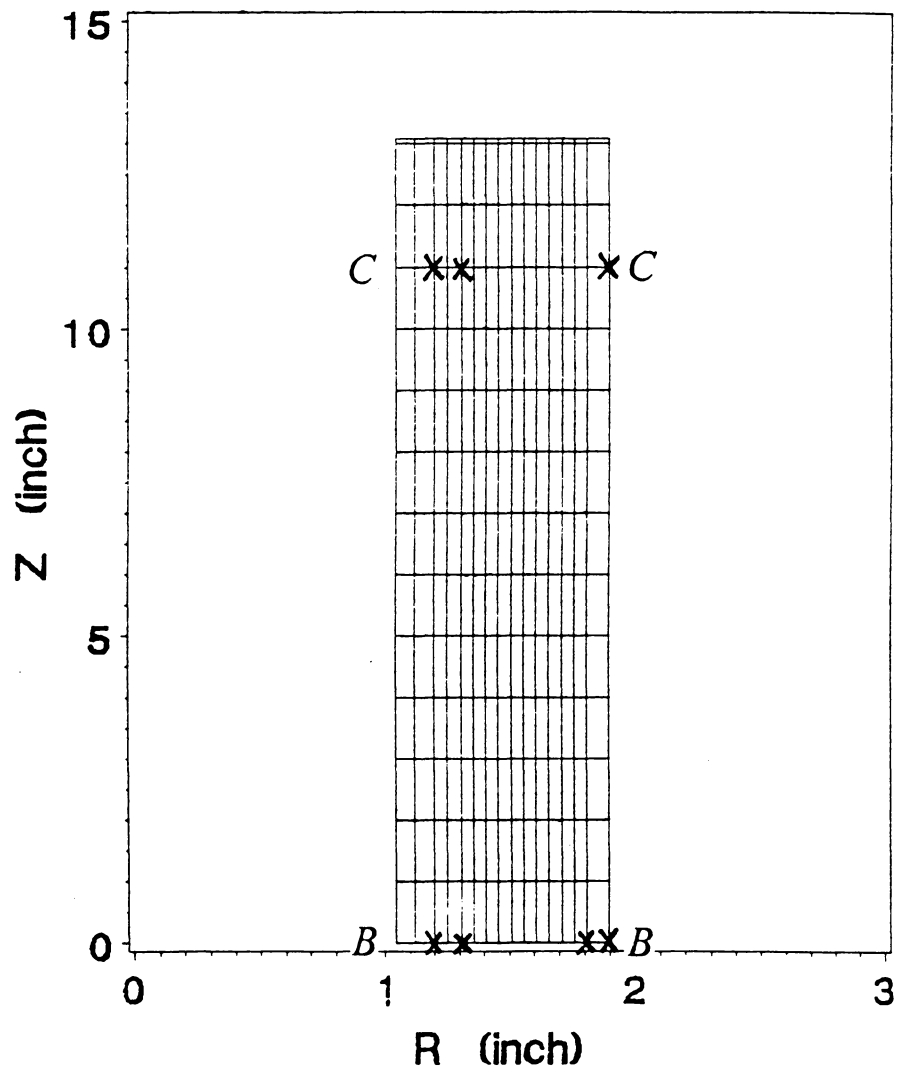

Figure 25. FEM Mesh (4 inch Tube):

The locations where measured temperatures were compared with the finite element solution are denoted by a ' X ' in the mesh.

5.1.3 Results

The calculated and measured temperatures were compared at two locations along the cylindrical tube (Fig. 25). The temperatures were compared at 4 points in section "BB" as follows :

1. the outer surface of the outer layer,
2. the composite case / outer layer interface,
3. the insulator / composite case interface, and
4. the mandrel / insulator interface.

The temperature in section "BB" as a function of time is plotted in Figs. 26 and 27. The symbol "star" represents the measured cure temperature. The temperatures measured at the various locations are represented by different symbols in the plots.. The solid lines represent the calculated temperatures at the corresponding locations. A comparison of the measured and calculated temperatures shows a very good correlation at the four locations.

The assembly was heated from room temperature (21 °C) with a two-step cure cycle as described previously. From the 6th hour to the 12th hour during cure, the temperatures inside the composite case are significantly higher than the oven temperature. The exotherm is due to a large amount of heat generation occurring in the chemical reaction. Results show that the kinetics model is able to simulate the cure rate and heat generation quite well.

In general, the correlation between the measured and calculated temperatures was good. However, the calculated temperature does not perfectly match the measured

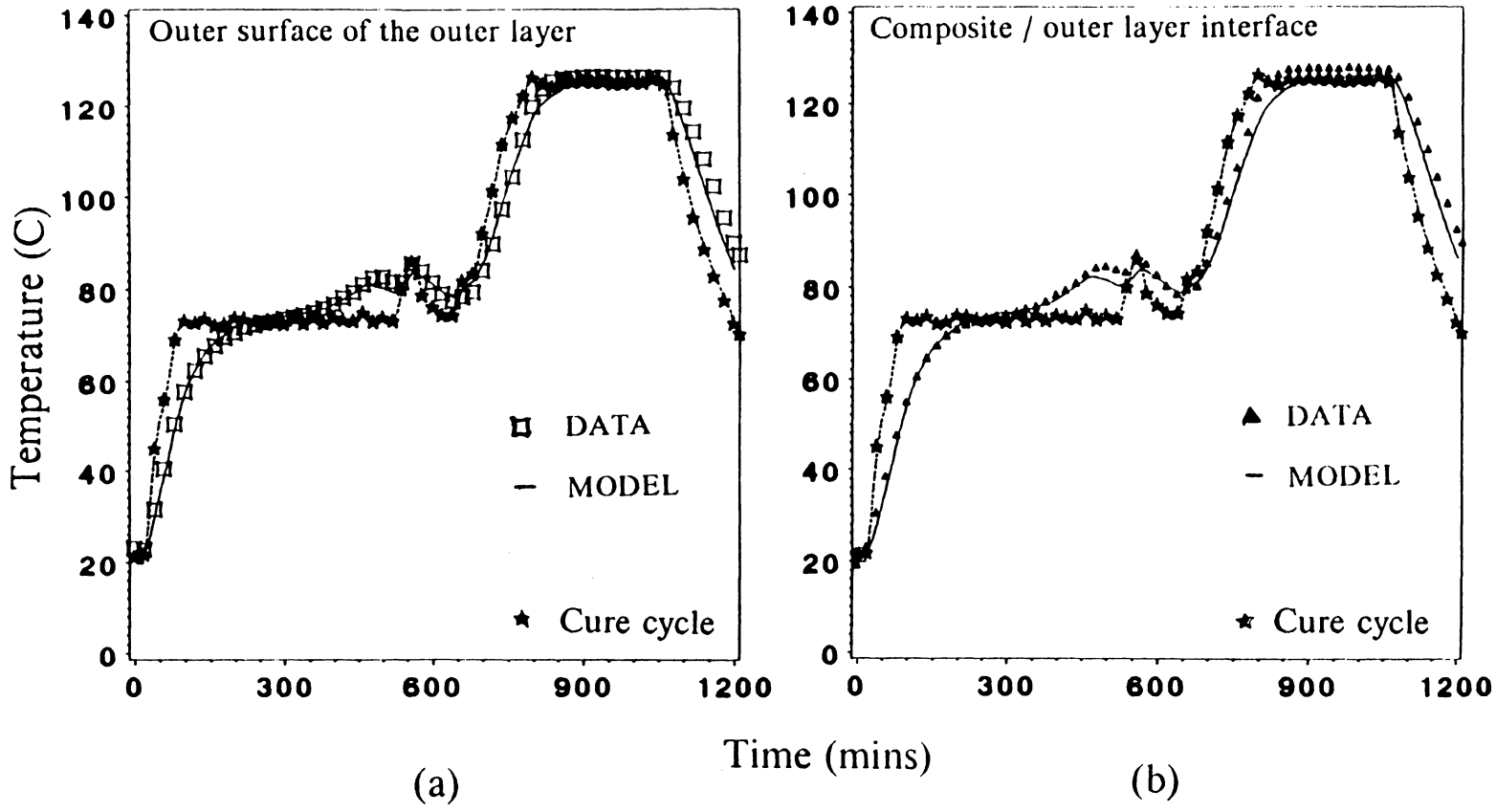

Figure 26. Temperature vs Time at Section "BB" (4 inch Tube) - I:

The measured and calculated temperatures are compared at the locations : (a) the outer surface of the outer layer and (b) the outer layer / composite interface. The measured temperatures are represented by symbols marked in the plot. The solid line represents the calculated solution using the model.

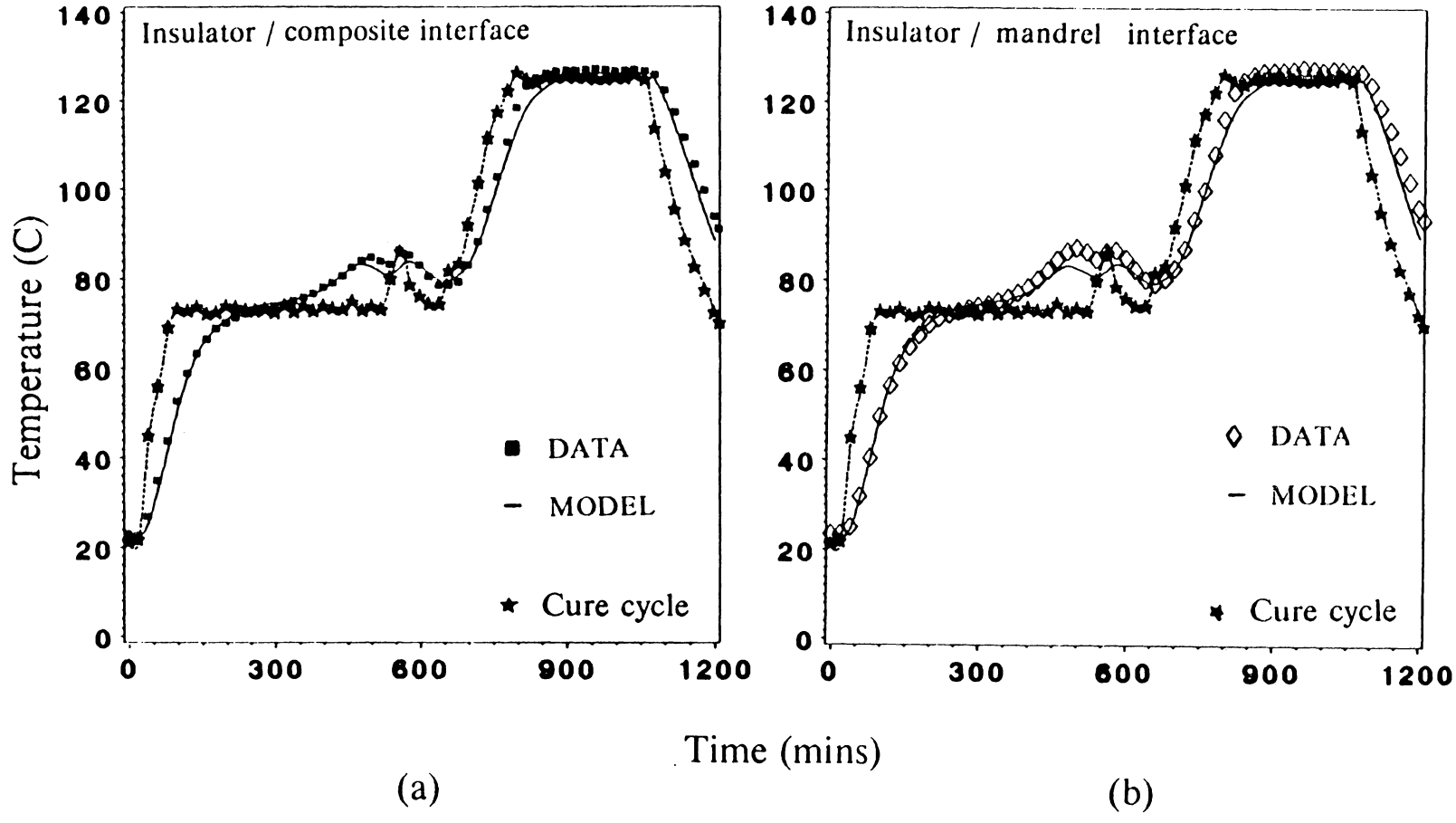

Figure 27. Temperature vs Time at Section "BB" (4 inch Tube) - II:

The measured and calculated temperatures are compared at the locations : (a) the composite / insulator interface and (b) the insulator / mandrel interface. The measured temperatures are represented by symbols marked in the plot. The solid line represents the calculated solution using the model.

data in some regions. The calculated temperatures in the exothermic region were slightly lower than the measured temperatures. This may be due to a low cure rate predicted by the kinetics model; therefore, the heat generation was low resulting in a lower temperature in the simulation.

In the cooling stage, the calculated temperatures were also lower than the measured temperatures. This is most likely due to the assumption of constant specific heat capacity of the composite and heat transfer coefficient in the simulation. In fact, the heat transfer coefficients decreased and the specific heat capacity of the composite increased in the final stage during cure.

The comparison of the measured and calculated temperatures solution at section "CC" is presented in Fig. 28. The temperatures were compared at the following 3 points :

1. the outer surface of the outer layer,
2. the insulator / composite case interface, and
3. the mandrel / insulator interface.

Since the length of the tube is much longer than the radius, the temperature gradient in the longitudinal direction (z-direction) is small. Therefore, the temperature distribution at section "CC" is very similar to the temperature distribution at section "BB". The symbol "star" again represents the measured cure temperature. The temperatures measured at the various locations are represented by different symbols in the plots. The symbol "diamond", "solid triangle", and "circle" represent the measured temperatures at the outer surface of the outer layer, composite / insulator

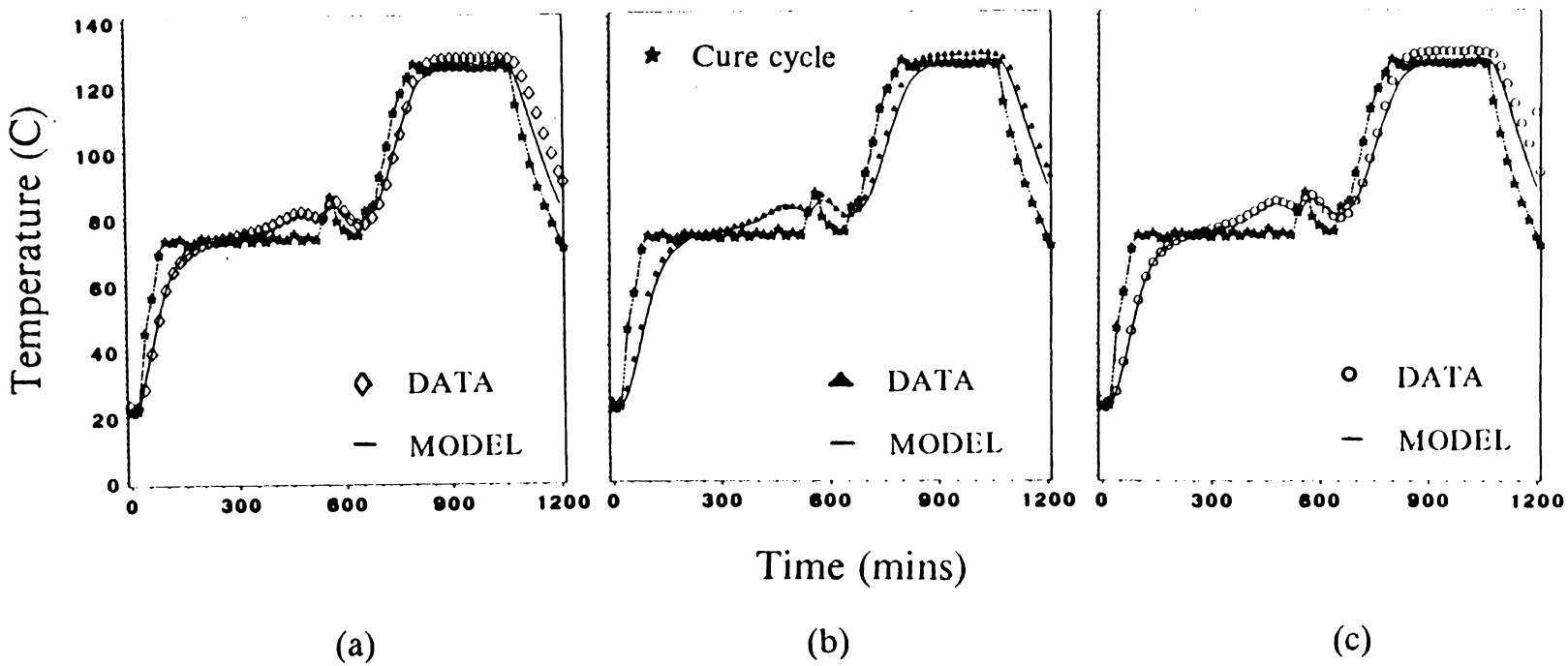

Figure 28. Temperature vs Time at Section "CC" (4 inch tube):

The measured and calculated temperatures are compared at the locations : (a) the outer surface of the outer layer, (b) the composite / insulator interface, and (c) the insulator / mandrel interface. The measured temperatures are represented by symbols marked in the plot. The solid line represents the calculated solution using the model.

interface, and insulator / mandrel interface, respectively. The solid lines represent the calculated temperatures at the corresponding locations.

The comparison shows good agreement between the experimental data and calculated temperatures. However, the calculated temperature did not perfectly match the measured data at the final hold and cool down stages. The differences are due to the same reasons described for the cross section "BB" previously. Additionally, because heat was also transferred from the end surface, a poorer result was obtained at section "CC" than at section "BB".

The degree of cure vs time at section "BB" is illustrated in Fig. 29. The difference in the degree of cure between the innermost and the outermost composite elements is small due to the low heating rate and uniform temperature distribution in the case. The degree of cure approaches to 0.72 at the end of cure. The low degree of cure indicates that the tube would not be completely cured and the cure cycle should be extended.

The resin viscosity vs time at section "BB" calculated using the model is presented in Fig. 30. The viscosity decreases as the composite case is heated and then increases as the resin starts to gel. The magnitude of the viscosity is quite high resulting in a small amount resin flow, fiber motion, and compaction during cure.

Similar results for the degree of cure and resin viscosity were obtained at section "CC".

The fiber tension variation vs time is shown in Fig. 31. Initially, the tube was wound with a uniform winding tension of 35.5 nt (8 lb) per fiber bundle. In the first heating

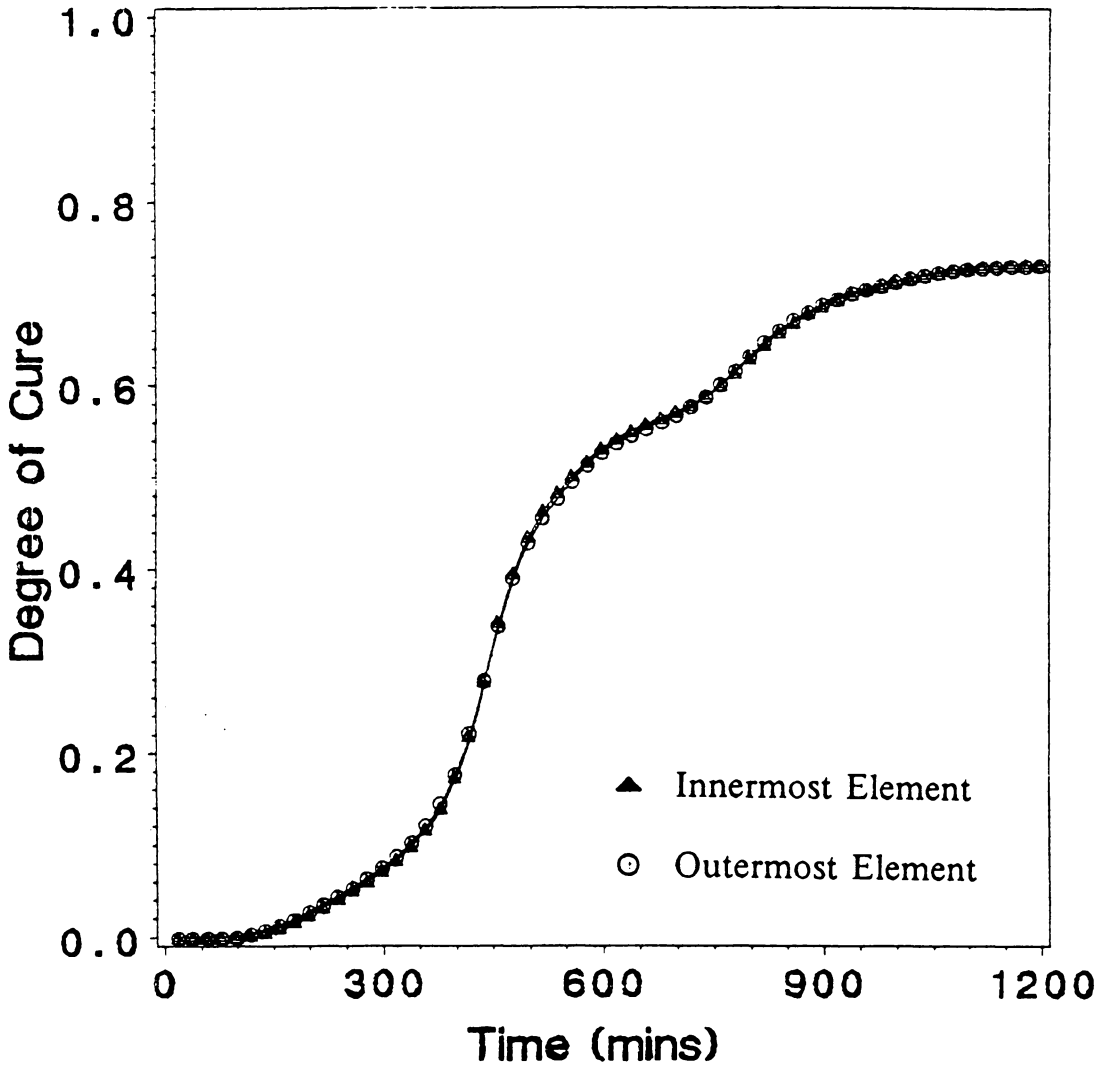

Figure 29. Degree of Cure vs Time (4 Inch Tube):

The plot shows the degrees of cure at the innermost element and the outermost element of composite case in section "BB". The symbol "circle" and "triangle" represent the degree of cure at the outermost and innermost element, respectively. Results were calculated using the model.

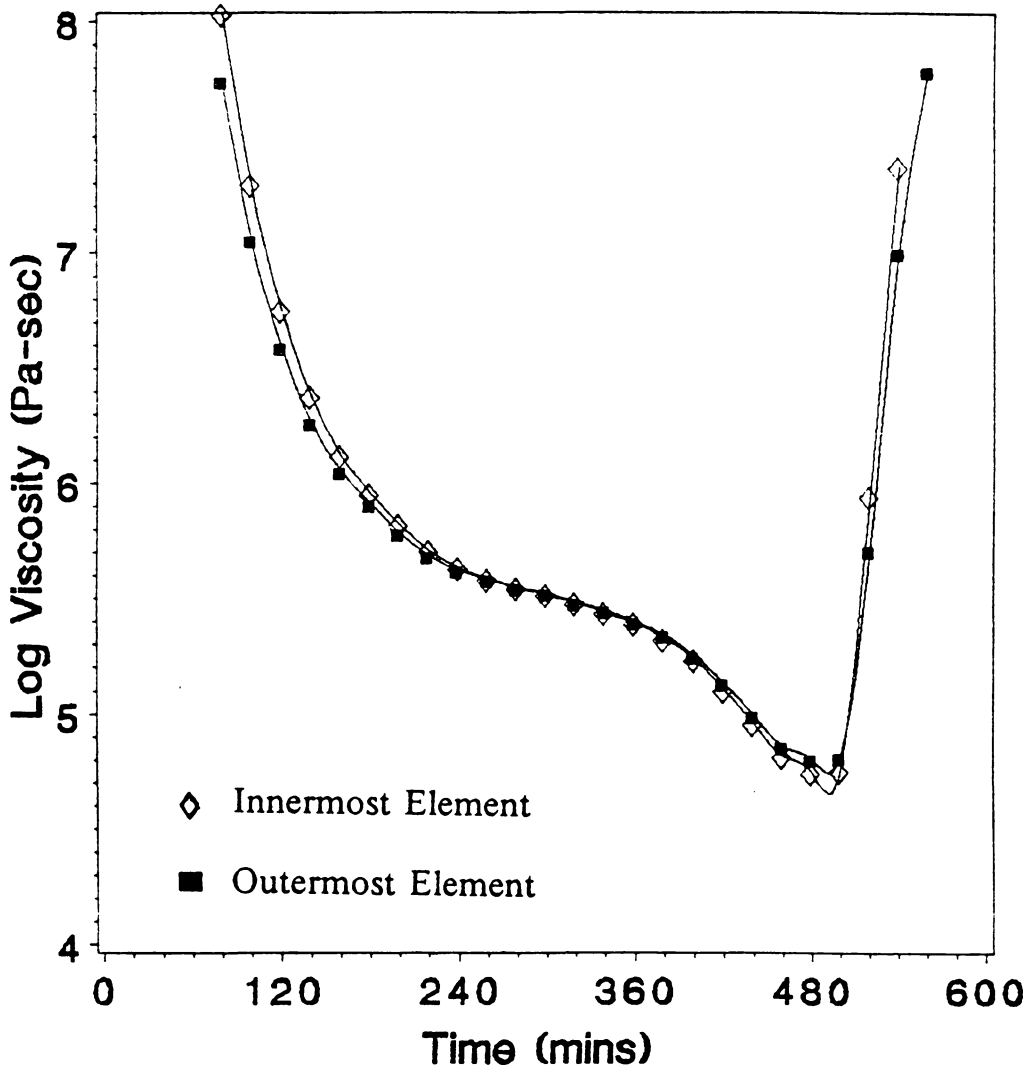

Figure 30. Log Viscosity of Resin vs Time (4 inch Tube):

The figure shows the resin viscosity at the innermost element and the outermost element of the composite in section "BB". The symbol "diamond" and "square" represent the viscosity at the outermost and innermost element, respectively.

stage, the decrease in resin viscosity results in resin flow / fiber motion causing a decrease in fiber tension. Resin flow causes compaction of the composite layer and a corresponding decrease in the permeability and an increase in flow resistance. The lower pressure gradient and decreased permeability reduces fiber motion and consequently fiber tension approaches an equilibrium value.

Since Fiberite 982 resin is a very viscous resin (Fig. 30), very little resin flow and compaction occurs during fabrication. Hence, the fiber tension loss is controlled almost entirely by the magnitude of the pressure gradient. The inner layer has a large curvature which causes a large pressure gradient across the layer. Furthermore, the tensioned outer layers can generate an additional pressure gradient on the inner layer. Therefore, the inner layers have a greater tension loss than the outer layers.

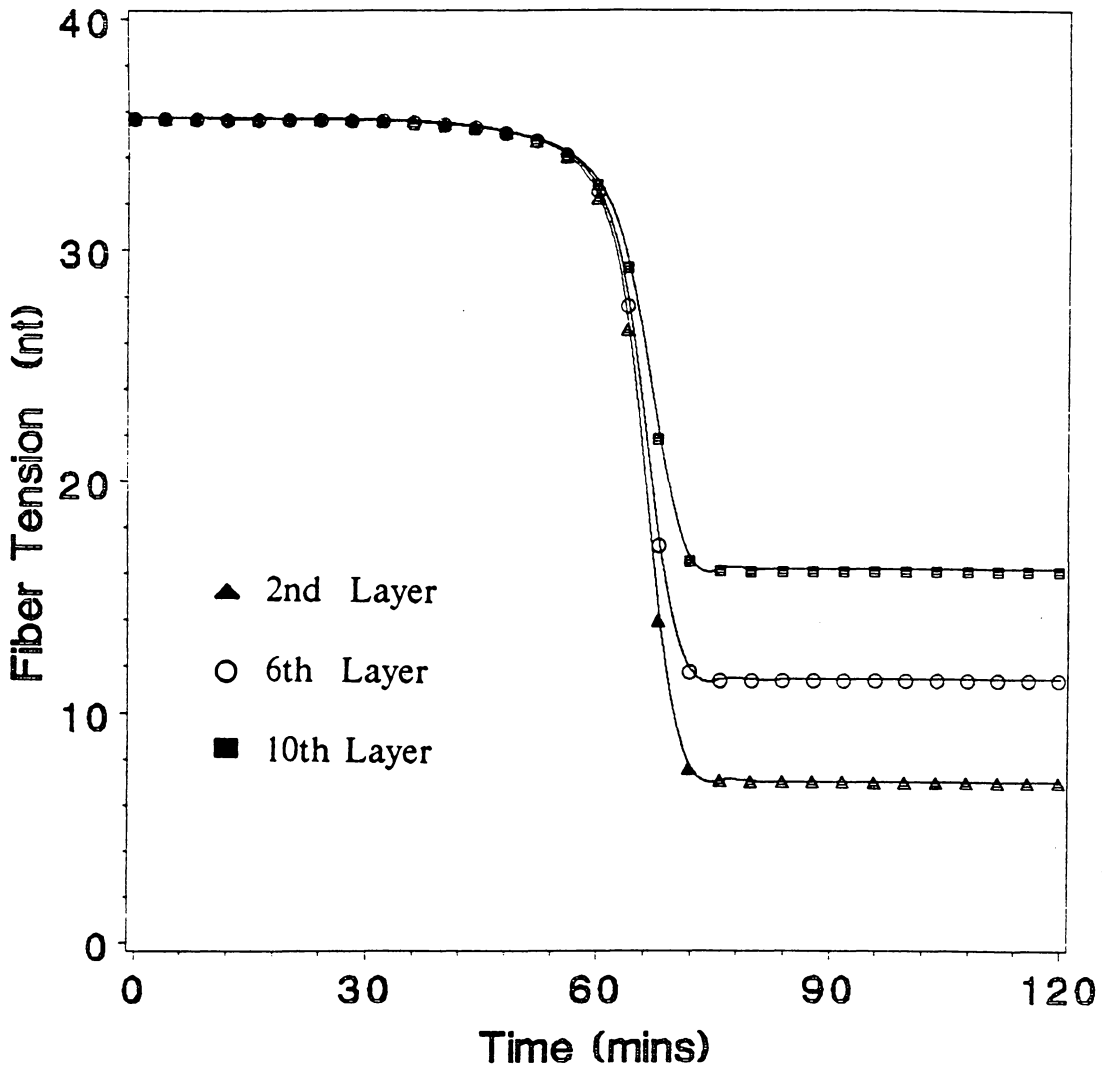

Figure 31. Fiber Tension Variation vs Time (4 inch Tube):

The fiber tension variation through the thickness shows that the inner layer loses more tension. This is due to a large curvature in the inner layer causing a large pressure gradient, resin flow, and fiber motion.

5.2 5.75 inch Bottle

5.2.1 Experiment

A 5.75 inch diameter test bottle was wound using Fiberite T300 / 934 prepreg roving.

A. Materials

1. Mandrel

The mandrel material was ASTM 6061 wrought aluminum pipe. The outer diameter was 0.14605 m (5.75 in.) and the total end to end length was 0.1799 m (7.683 in.). Both the ends of the cylindrical pipe were covered with end caps made of the same material. A schematic of the mandrel is shown in Fig. 32.

2. Insulator

The mandrel was wrapped with an elastomeric insulator made up of 30% filled silicon dioxide, nitrile butadiene rubber (NBR), having a nominal thickness of $6.096x10^{-3}m$ (0.24 in.).

3. Composite Case

The composite case was formed by winding the prepreg rovings in a helical pattern at an angle of 24.2° with respect to the longitudinal axis of the mandrel in the cylindrical region. Totally, 32 layers were wound to form the bottle.

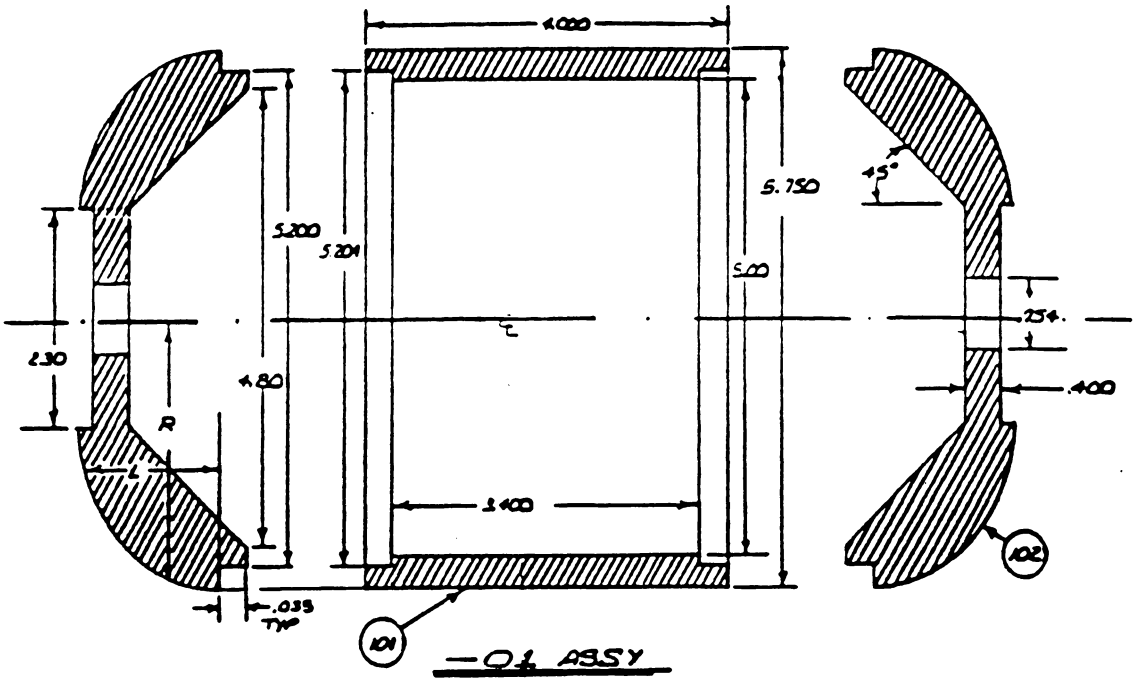

Figure 32. Schematic of Mandrel (5.75 Inch Bottle):

The mandrel was made of aluminum. All dimensions are in inches. (Courtesy: Morton Thiokol Inc, Wasatch Operations)

The preconsolidated roving thickness was measured to be $3.048x10^{-4}$ m (0.012 in.) and the resin weight percentage was 30 %. The case thickness was measured to be $0.9550x10^{-2}$ m (0.376 in.) in the cylindrical region. In dome region, the case thickness varied from $6.35 \times 10^{-3} m$ (0.25 in) to about $1.82 \times 10^{-2} m$ (0.72 in) at the polar boss.

The applied winding tension was measured to be approximately 35.56 nt (8 lbs) per fiber bundle with cross-sectional area of $4.45 \times 10^{-7}\ m^2$ ($6.9 \times 10^{-4}\ in^2$). The tensile stress in the fiber was about $7.997x10^7\ N/m^2$.

4. Outer Layer

The outer layer comprised of a perforated FEP film, Airweave breather cloth, and a silicon vacuum bag for a total thickness of $3.175x10^{-3}$ m (0.125 in.).

B. Temperature Measurement

The temperature measurements were obtained by using thermocouples embedded at various radial locations in the composite assembly. Additional thermocouples were placed on the inner and outer surfaces of the assembly. The thermocouple locations, where the measured and calculated temperatures are compared, are shown in Fig. 33. All thermocouples were connected to a Molitek recorder which recorded the temperatures of each thermocouple onto a strip chart plotter at time intervals of 5 minutes.

C. Cure Cycle

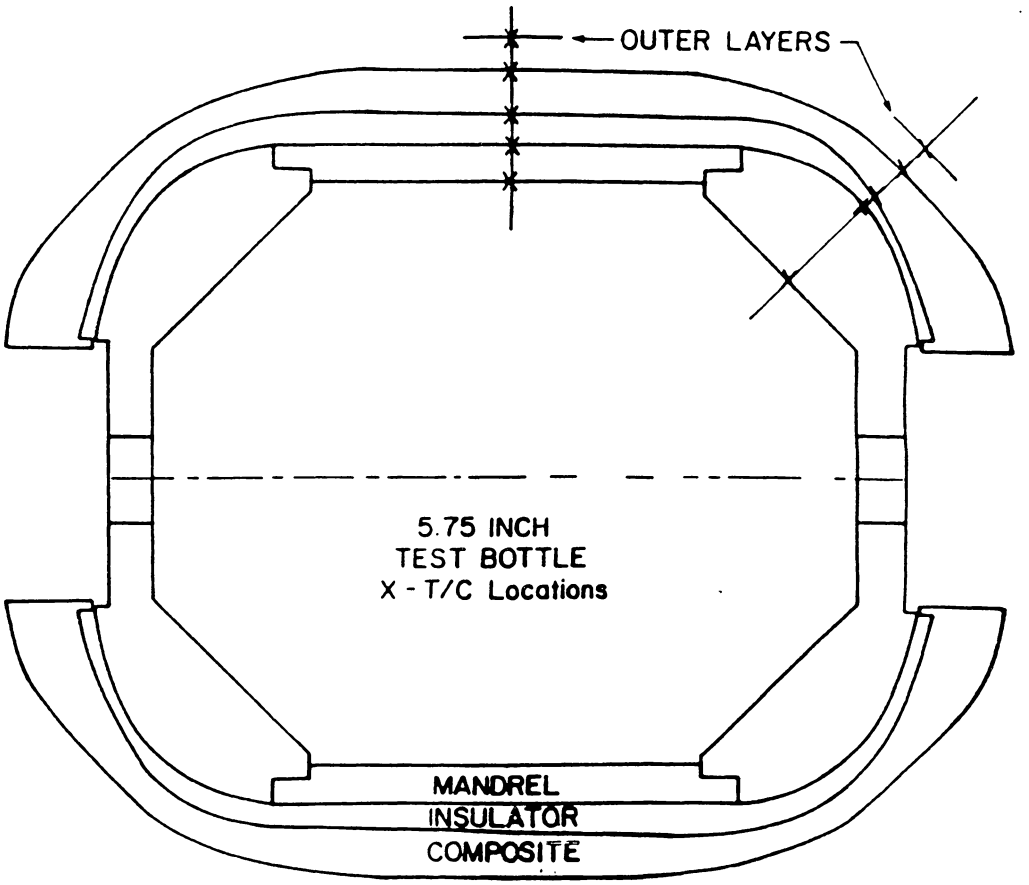

Figure 33. Schematic of 5.75 Inch Bottle Assembly:

Thermocouples are placed to sense the temperature at various locations in the FWC assembly. The locations of the thermocouples are indicated by a ' X ' on the assembly.

The oven was heated at a constant rate of 2.8° C (5°F/ min) from an ambient temperature of 21°C to the final hold temperature of 176°C. The oven was held at the cure temperature for a period of 5 hours.

5.2.2 Analysis

The simulation was carried out using the models. The properties of the materials used in the simulation are summarized in Table 3. The kinetics model and the viscosity model used in the analysis are given in reference [23].

A. Finite Element Mesh

Because of the symmetry, only a quarter of the assembly was analyzed in the simulation. The finite element model of the assembly is illustrated in Fig. 34. The domain is divided into 252 elements with 286 nodes.

In composite region, each element has a winding angle and a polar angle which depend on the fiber path and the geometry of the case. The winding angle for each element is calculated using the model described in the Appendix A. The polar angle is calculated from the relative position between the center of the element and center of the dome.

The center of the dome is located at coordinates (1.1, 0.0) shown in Fig. 34. The center of the element was defined in Section 3.3 previously. Accordingly, a vector can be defined by the two centers. The direction normal to the dome surface (i.e.

Table 3. Material Properties for 5.75 Inch Bottle

	Density	Heat Capacity	Thermal Conductivity
	ρ	C_p	K
	kg/m^3	$J/kg\,°K$	$W/m\,°K$
Mandrel	0.280×10^4	0.960×10^3	0.171×10^3
Insulator	0.110×10^4	0.176×10^4	0.276×10^0
Composite	0.159×10^4	0.875×10^3	0.710×10^0 (K_{11}) 0.710×10^0 (K_{22}) 0.160×10^2 (K_{33})
Outer layer	0.137×10^4	0.105×10^4	0.199×10^0

Constants for permeability model : $C' = C'' = 5$
Fiber diameter : $8\mu m$
Thermal expansion coefficient : -0.36×10^{-6} /°C
Young's modulus of the fiber : 2.34×10^{11} Pa

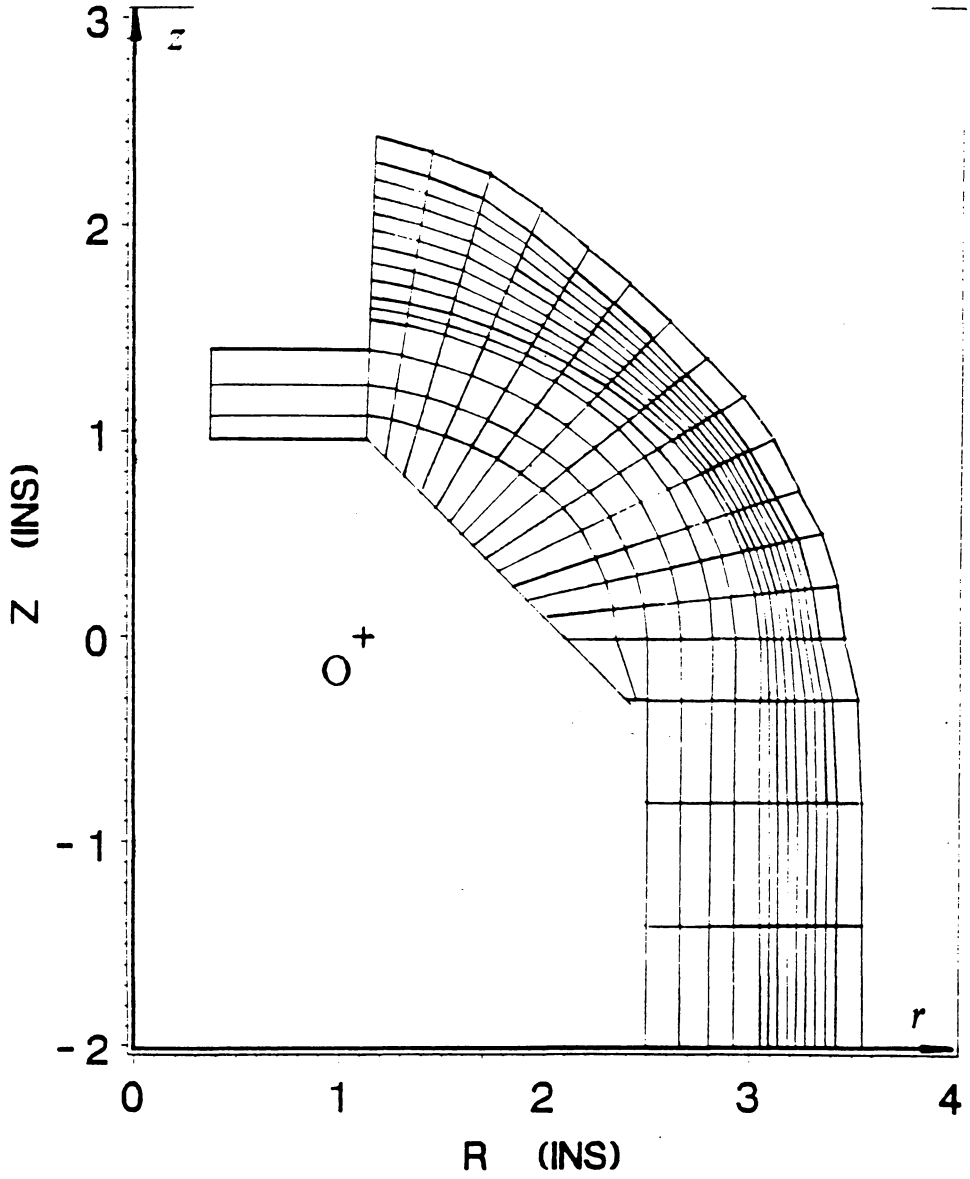

Figure 34. Finite Element Mesh (5.75 Inch Bottle):

Due to symmetry, only a quarter of the case is analyzed in the simulation. The center of the dome is indicated by "O" in the plot. All dimensions are in inch.

direction of the polar angle) is along the direction of the vector. Therefore, the polar angle can be determined for each element in the FEM mesh.

B. Boundary Condition

Because the FWC assembly was vacuum bagged and the inner surface of the mandrel was not heated directly, the calculations were performed using a heat transfer coefficient of 0 W/m^2K on the inner surface of the hollow mandrel. The outer surface of the assembly had direct contact with the oven fluid and heated by forced convection. The heat transfer coefficient is 40 W/m^2K in the cylindrical region and 69 W/m^2K in the dome region.

The heat transfer coefficients are obtained by matching the calculated and measured temperatures in the dome and cylindrical regions. The heat transfer coefficient over the outer surface of the assembly was higher in the dome region than in the cylindrical region. This is most likely due to a higher local velocity of the air stream over the dome surface.

5.2.3 Results

The finite element solution and the experimental temperature data were compared at four relevant points in cylindrical region and at three relevant points in dome region.

In cylindrical region, the four points were

1. the inner surface of the mandrel,

2. the insulator / composite case interface,
3. the composite case / outer layer interface, and
4. the outer surface of the outer layer.

In dome region, the three points were

1. the inner surface of the mandrel,
2. the composite case / outer layer interface, and
3. the outer surface of the outer layer.

Fig. 35 shows the temperature vs time in the cylindrical region. The symbol "hollow circle" represents the oven temperature. The symbols "solid square", "diamond", "solid circle", and "solid triangle" represent the measured temperatures at the outer surface of the outer layer, the composite case / outer layer interface, the insulator / composite case interface, and the inner surface of the mandrel, respectively. The calculated temperatures at corresponding locations are represented by solid lines.

The temperature vs time at the various locations indicate that a very good correlation between the calculated results and the experimental data. In the final hold stage, the calculated temperatures are higher than the measured data. This is due to the kinetics model used in the simulation. The kinetics model for Fiberite 976 resin system was used in the calculation. Fiberite 976 has a similar kinetic behavior as Fiberite 934. However, they are not exactly same. A larger amount of heat generation was obtained using the Fiberite 976 model. Therefore, the calculated temperatures were higher than the measured temperatures.

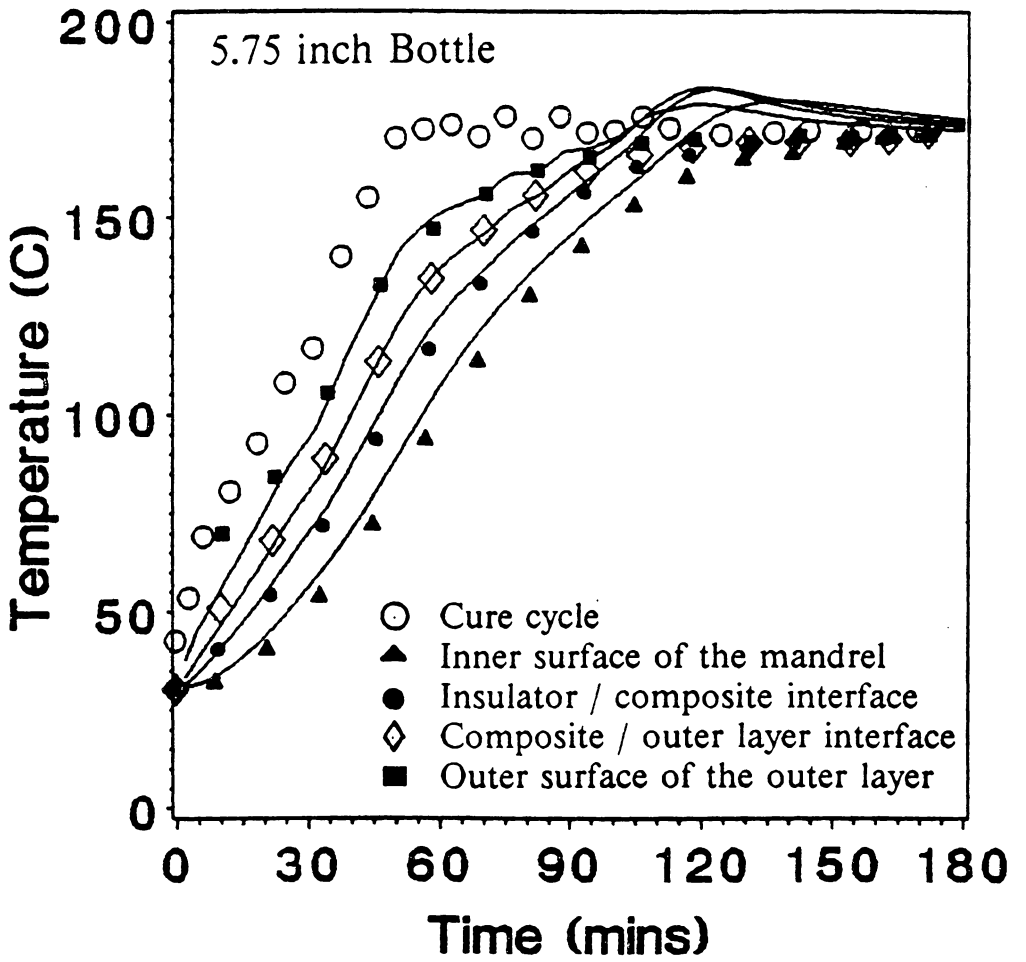

Figure 35. Temperature vs Time in Cylindrical Region:

The experimental data and the finite element analysis results are plotted as a function of time. The symbols indicate the experimental data at various locations and the solid lines present the calculated solution.

Fig. 36 illustrates the temperature vs time in the dome region. The symbol "hollow circle" again represents the oven temperature. The symbols "solid square", "diamond", and "solid triangle" represent the measured temperatures at the outer surface of the outer layer, the composite case / outer layer interface, the inner surface of the mandrel, respectively. The finite element solutions at corresponding locations are represented by solid lines.

The temperature is about 10°C higher in the dome region than in the cylindrical region. This indicates that the variations in the local heat transfer coefficient are significant. The calculated temperatures on the inner surface of the mandrel are slightly higher than the measured data for both the dome and cylindrical regions. This is most likely due to the assumption of a zero heat transfer coefficient on the inner surface of the mandrel.

The temperature distribution through thickness as a function of time for the FWC assembly is shown in Figs. 37 and 38. The temperature vs the normalized radius in the cylindrical region along the radial line "XX" is presented in Fig. 37. Fig. 38 illustrates the temperature distribution in the dome region along the radial line "YY". The symbols represent the measured temperatures. The two plots show a significant temperature gradient through the thickness of the assembly. The magnitude of temperature gradient depends on the thermal conductivity of material. Thermal conduction in the aluminum mandrel is quite fast. Therefore, a uniform temperature is obtained in the mandrel.

The temperature distributions along the outer surface of the outer layer and the definition of the global angle are illustrated in Fig. 39. The temperature distribution along the composite / outer layer and mandrel / insulator interfaces are shown in Fig. 40.

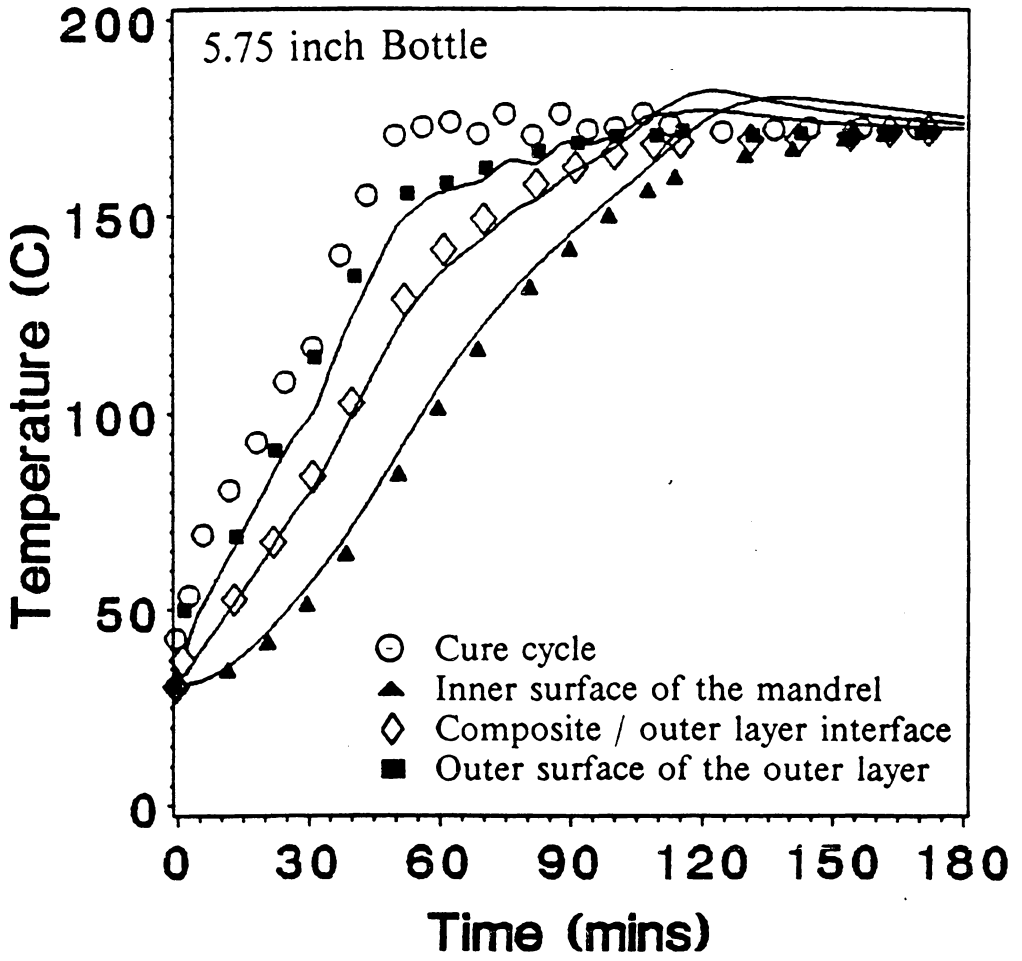

Figure 36. Temperature vs Time in Dome Region:

The experimental data and the finite element analysis results are plotted as a function of time. The symbols indicate the experimental data at various locations and the solid lines present the calculated solution.

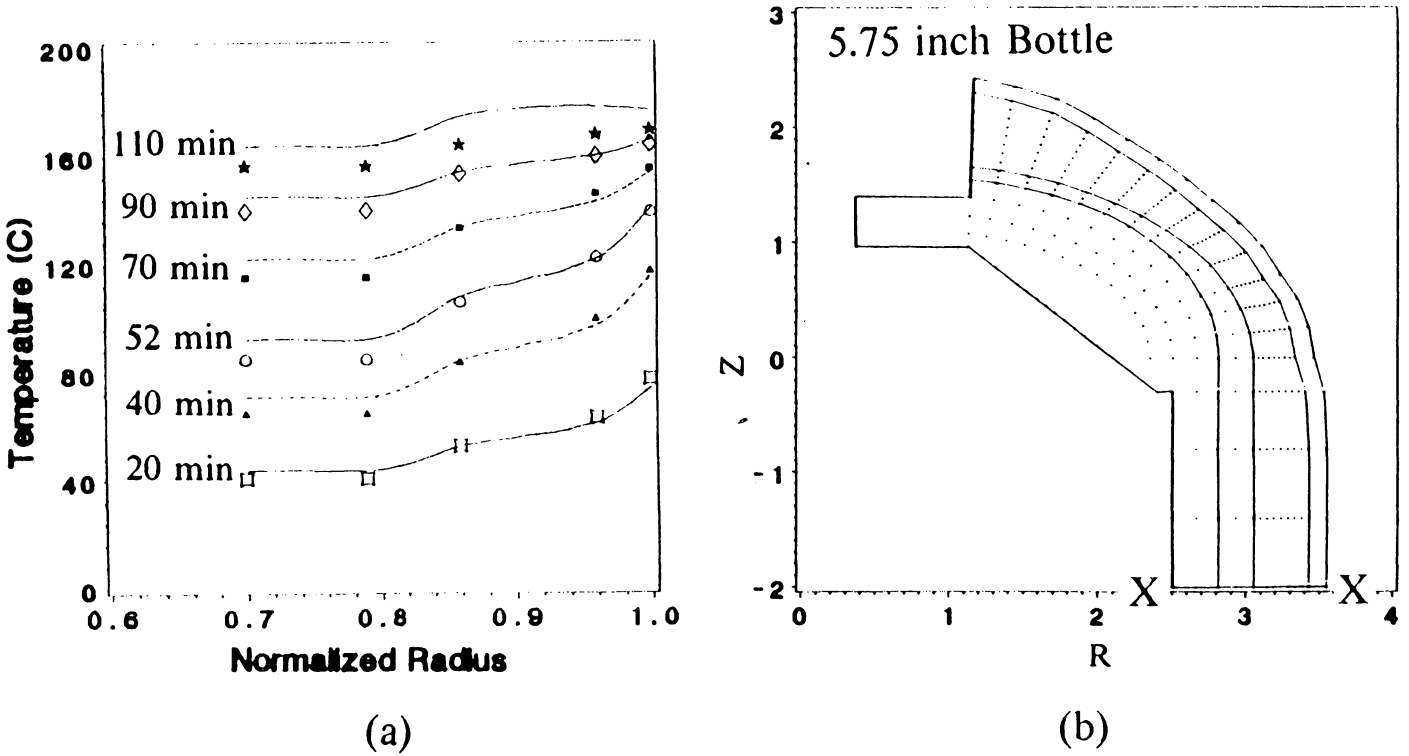

Figure 37. Temperature Distribution (Cylindrical Region):

Temperature variation through thickness at section "XX" is shown in plot (a). Plot (b) shows the location of section "XX".

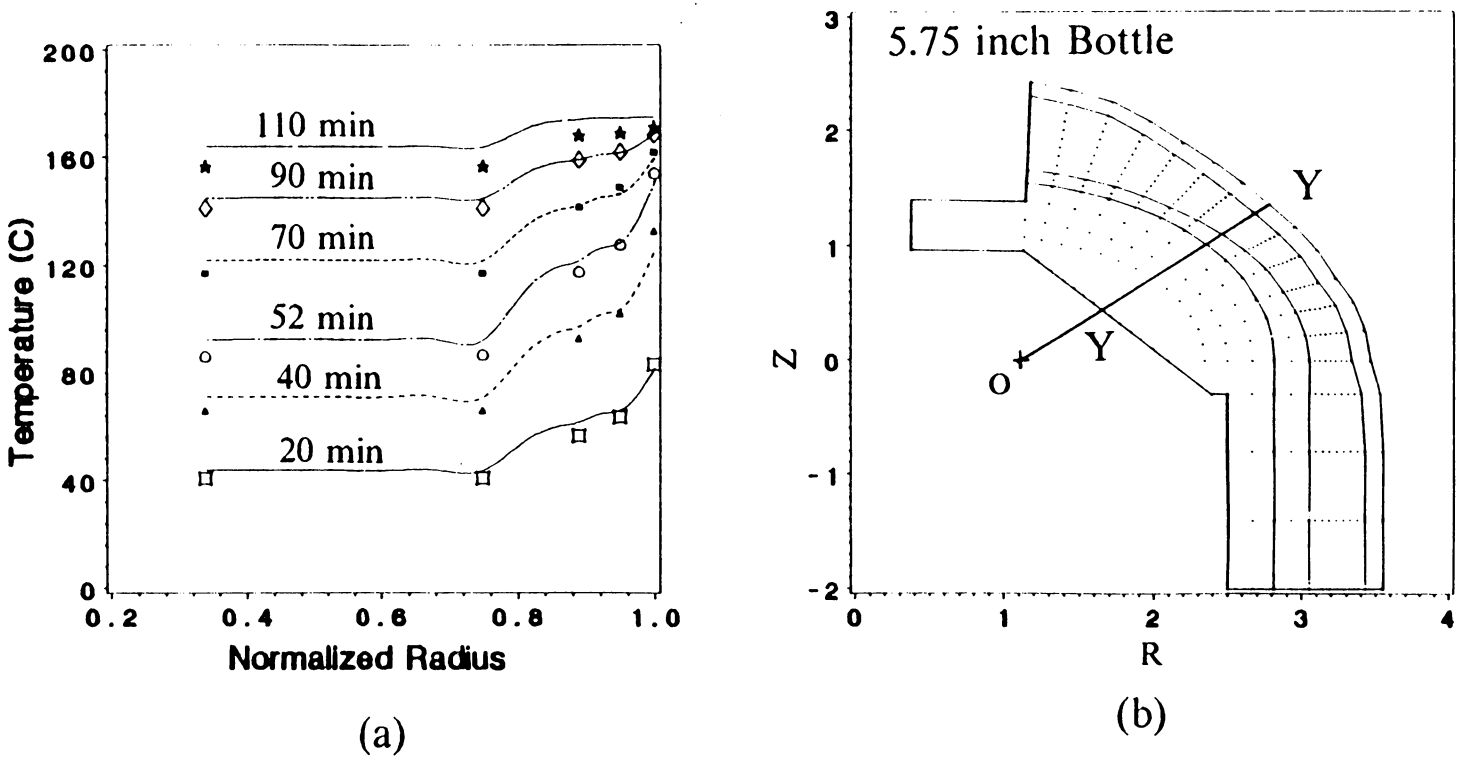

Figure 38. Temperature Distribution (Dome Region):

Temperature variation through thickness at section "YY" is shown in plot (a). Plot (b) shows the location of section "YY".

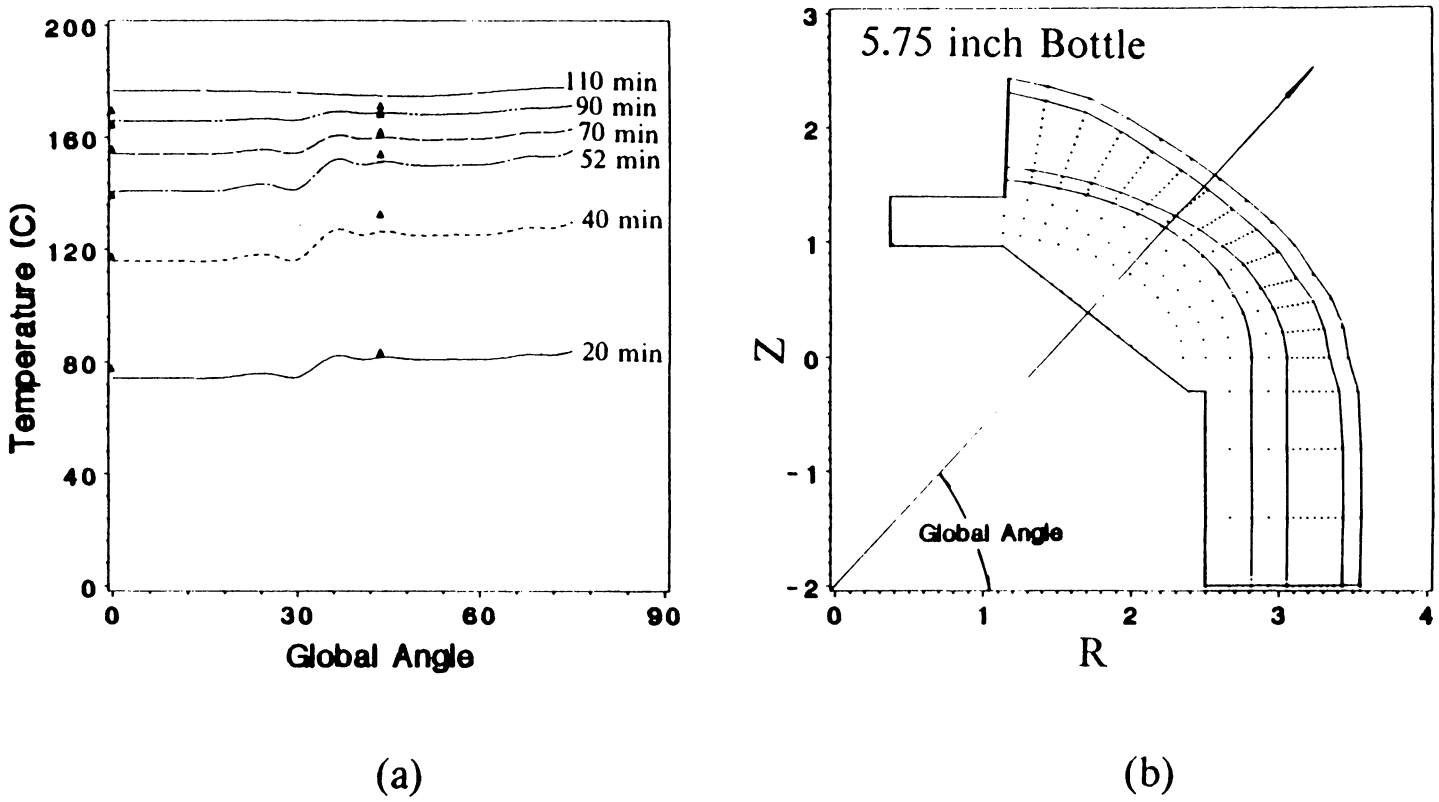

Figure 39. Temperature Variation along the Interface (I):

The temperature along the interface was presented in (a) the outer surface of the assembly. Plot (b) shows how to determine the "global angle".

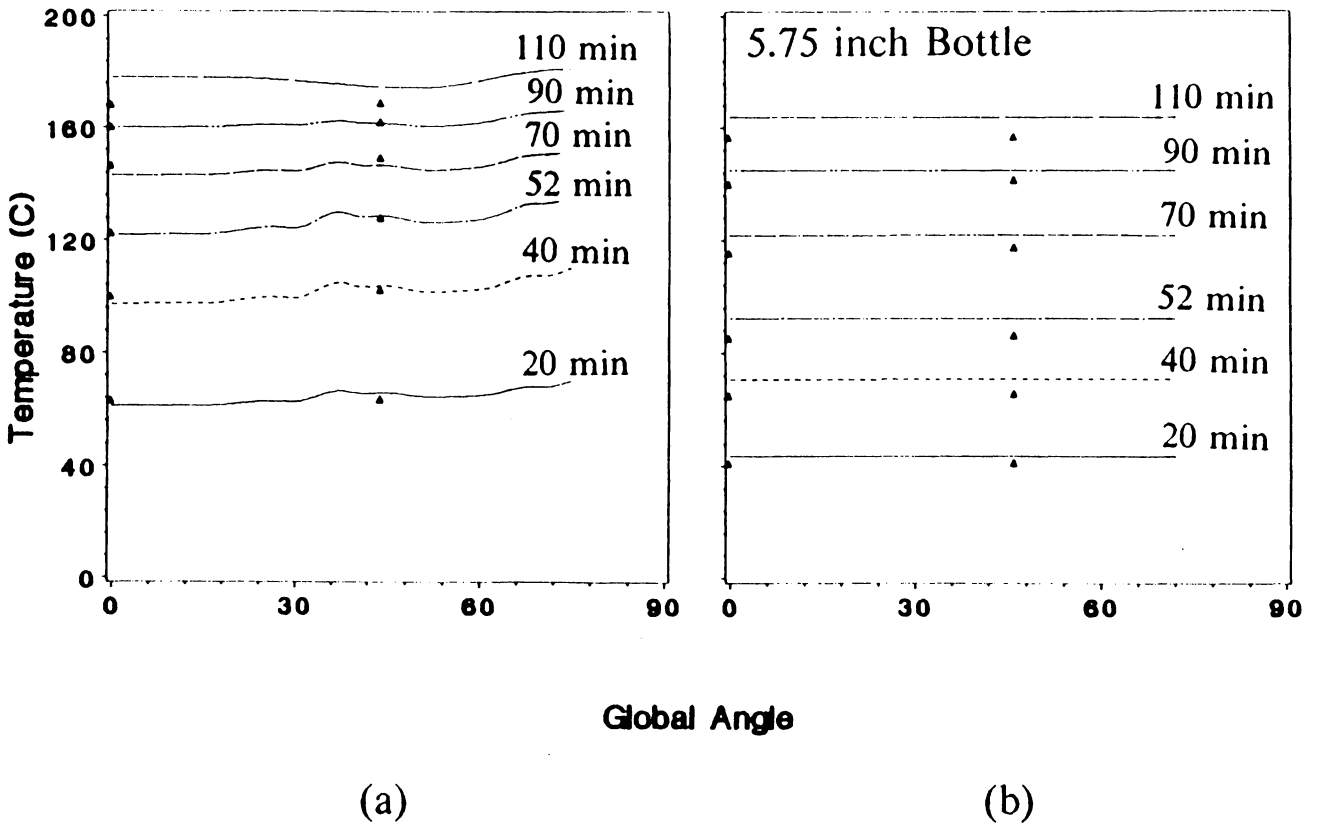

Figure 40. Temperature Variation along the Interface (II):

The temperature along the interface was presented as follows: (a) the outer layer / composite interface and (b) the mandrel / insulator interface.

The results show variations in temperature along the interfaces of the FWC assembly from the cylindrical region to the dome due to differences in the heat transfer coefficient, thickness, and geometry. Due to the high thermal conductivity of aluminum, a uniform temperature was obtained again in the mandrel region. The temperature difference along the interface is smaller for the inner region than for the outer region. The result also indicates the significance of axial heat conduction in the assembly.

The resin degree of cure vs time calculated using the model is plotted in Fig. 41. The composite case was heated faster in the outer region than the inner region. Therefore, the composite case was cured faster in the outer region than the inner region. Variations in the degree of cure indicates that the temperature gradient inside the composite case causes nonuniform cure. A similar result was found between the dome and cylindrical regions.

Resin viscosity as a function of time calculated using the model is illustrated in Fig. 42. The viscosities at points on the inner and outer surface of the case reach a minimum value at approximately the same time. As the cure proceeds, the viscosity at the outer surface of the case increases and gels faster than at the inner surface. However, since the degree of cure and viscosity were not measured experimentally, data were not available for comparison.

Fiber tension variation vs time is shown in Fig. 43. The composite case was divided into 6 layers in the simulation. The result indicates that the outer layers lose more tension than the inner layers. This is due to more compaction occurring in the inner layers of the case.

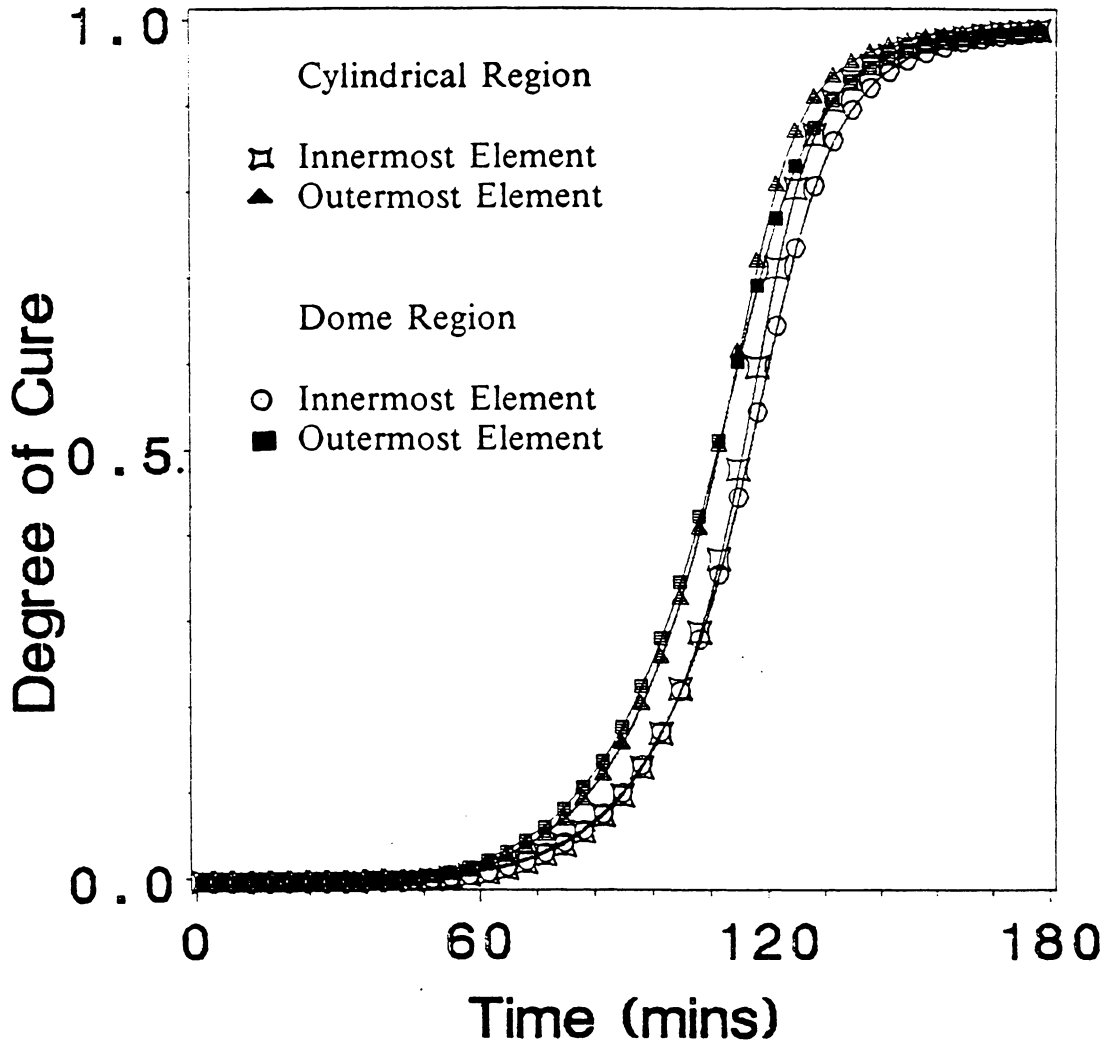

Figure 41. Degree of Cure vs Time (5.75 inch Bottle):

The degree of cure of the inside and outside surfaces of the composite case at one location in the cylindrical region and one location in the dome region are denoted by various symbols.

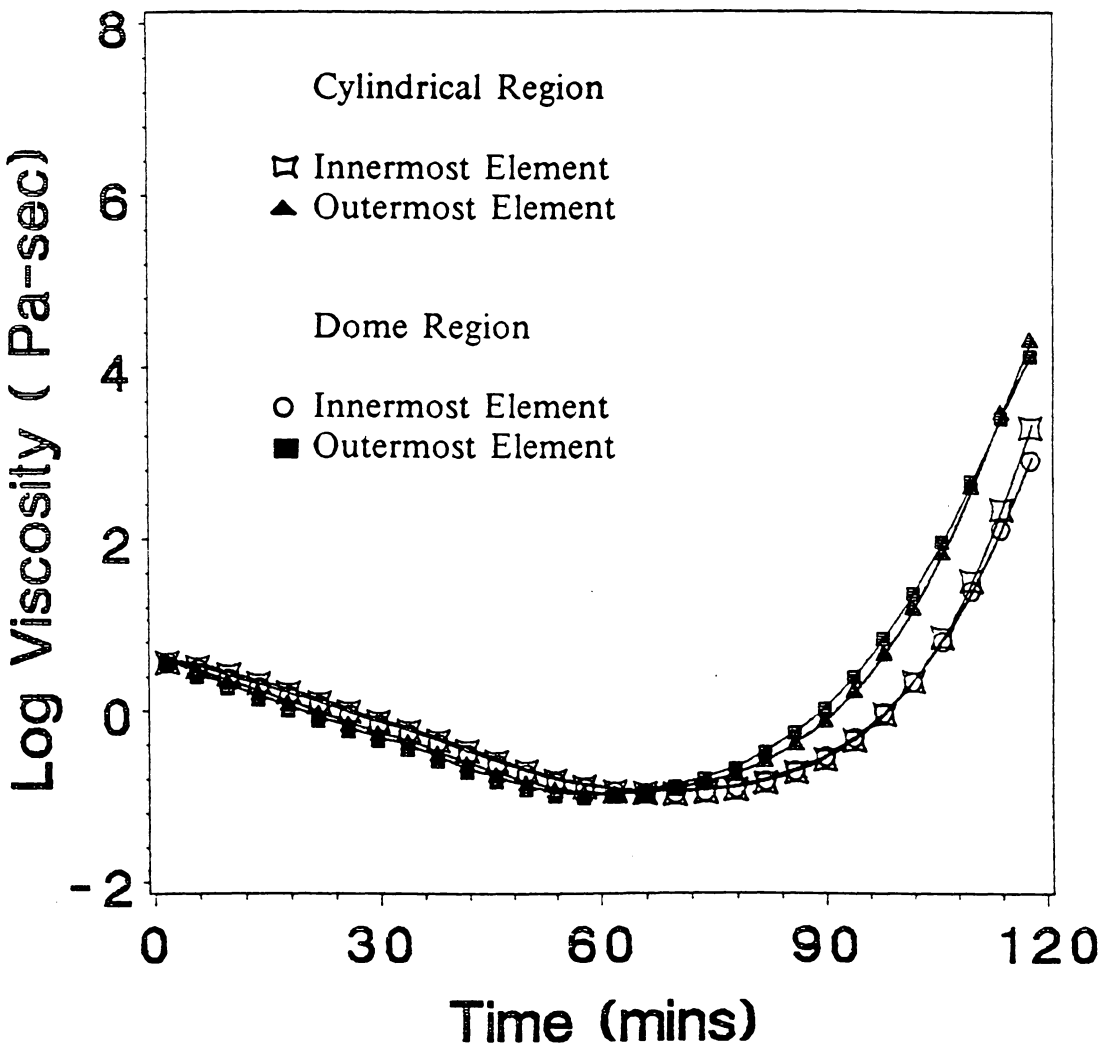

Figure 42. Log Viscosity vs Time (5.75 inch Bottle):

The resin viscosity of the inside and outside surfaces of the composite case at one location in the cylindrical region and one location in the dome region are denoted by various symbols.

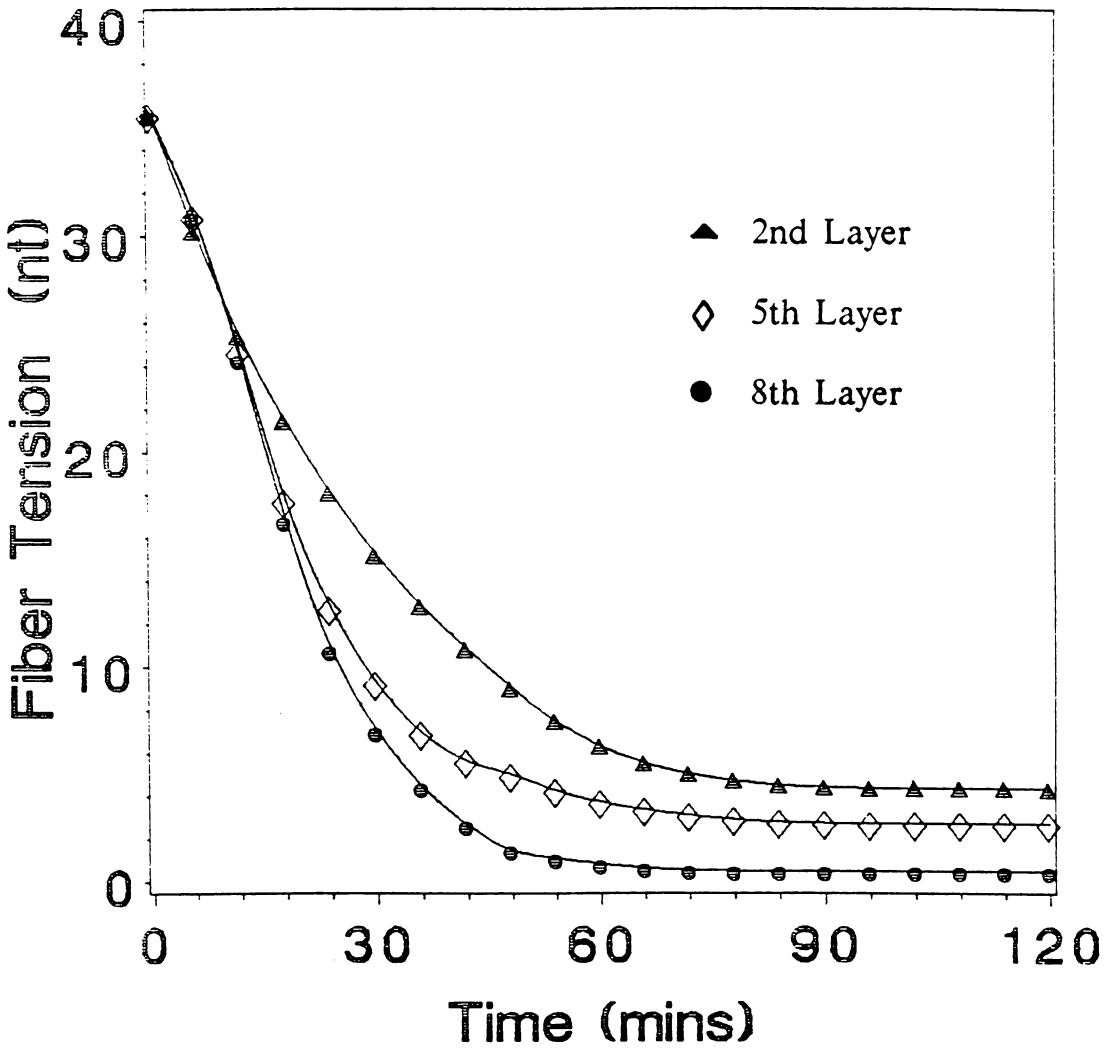

Figure 43. Fiber Tension vs Time (5.75 inch Bottle):

The compaction caused by resin flow starts from the inner layers; therefore, the fiber tension variation shows the outer layers lose more tension than the inner layers.

The case was helically wound and the curvature of the fiber path is small. Therefore, the variation in the pressure gradient through the case is small and does not greatly affect the fiber tension loss. Fiber tension loss is mainly due to the low resin viscosity which results in a considerable amount of resin flow and layer compaction. Accordingly, as the composite layer is compacted, the permeability of the composite decreases, and the resistance to additional resin flow increases.

Since the magnitude of the resin viscosity is very low and almost constant (Fig.42) during the compaction process, each layer of the case will reach an equilibrium value of fiber tension before the resin gels. Hence, fiber tension loss is controlled by permeability. The inner layers compact faster than the outer layers and therefore retain a higher percentage of the original fiber tension.

5.3 18 inch Bottle

A parametric study was performed using an 18 inch diameter test bottle. The winding and curing processes were simulated using the model and associated computer code for various processing variables and material properties.

5.3.1 Geometry and Finite Element Mesh

A schematic of the 18 inch diameter bottle is illustrated in Fig. 44. The FWC assembly consists of four regions: mandrel, insulator, composite case, and outer layer.

Due to symmetry, only a quarter of the assembly needs to be analyzed. The finite element mesh for the 18 inch bottle has 1404 elements with 1551 nodes (Fig. 45).

In the composite region, each element has a winding angle and a polar angle. The polar angle varies from 0° for an element in the cylindrical region and approaches 90° for an element adjacent to the polar boss. The winding angle varies from 77° in the cylindrical region to 0° at the edge of the polar boss.

5.3.2 Material

The mandrel material was taken to be PVA sand with an average thickness of $3.81 \times 10^{-2} m$ (1.5 in). The three thick layers of the inner region of the mesh represent

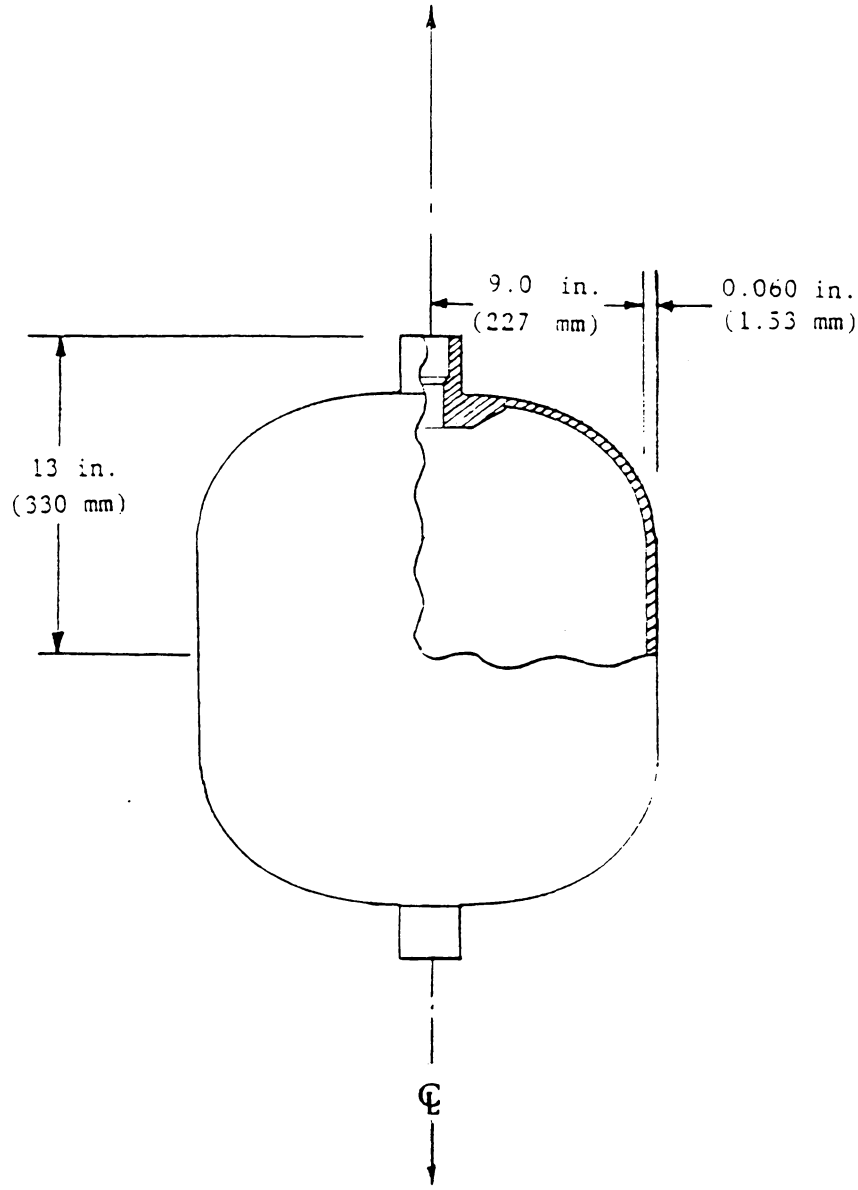

Figure 44. Schematic of 18 inch Bottle

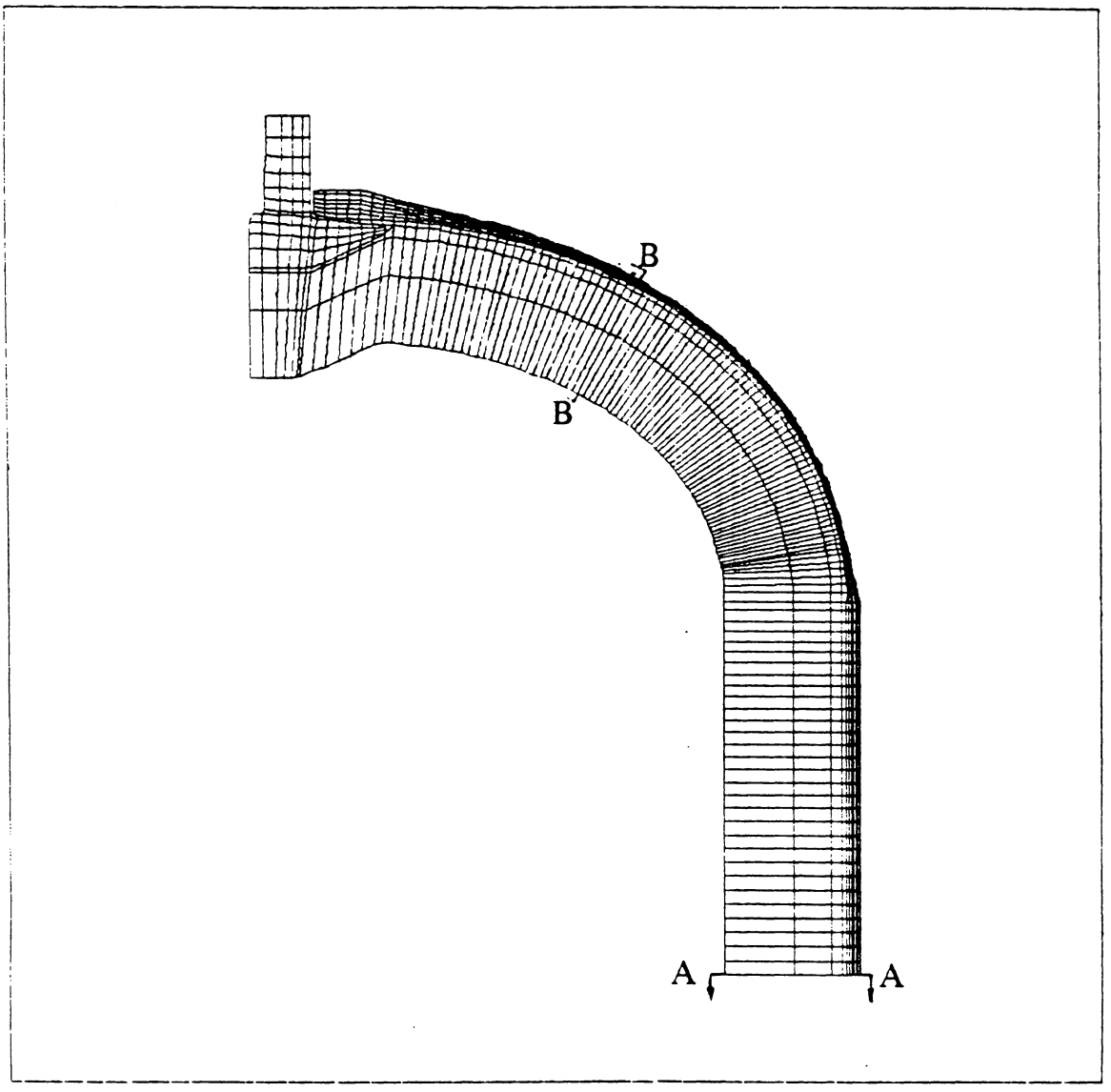

Figure 45. FEM Mesh of 18 Inch Case

mandrel elements. The mandrel surface was wrapped with an elastometric insulator made up of EPDM rubber. The insulator thickness was 1.52×10^{-3} *m* (0.06 in).

A composite case was formed by winding six prepreg layers over the insulator. The 1st, 2nd, 5th, and 6th layers were wound using a helical pattern. The 3rd and 4th layers was hoop wound in the cylindrical region only. Each layer has a thickness of 7.23×10^{-4} *m* (0.0285 in). Simulations were performed using properties of Fiberite T300/976 prepreg with a resin volume fraction of 0.4.

The outer layer consists of a perforated FEP film, breather cloth, and a silicon vacuum bag for a total thickness of 3.175×10^{-3}*m* (0.125 in). The mandrel, insulator, composite, and outer layer properties used in the simulation are listed in Table 4.

5.3.3 Cure Cycle and Winding Tension

The cure cycle was selected according to the recommended cure temperature for the matrix resin used in the composite. Since the composite case is relatively thin, a one-step cure cycle was used in the simulation.

The case was heated at a constant rate (2.6°C/ min) from ambient temperature (21°C) to the final cure temperature (176°C) in 60 minutes. The temperature was held at the final cure temperature for four hours.

Because the FWC assembly was vacuum bagged and the inner surface of the mandrel was not heated directly, the calculations were performed using a heat

Table 4. Material Properties for 18 inch Case

	Density	Heat Capacity	Thermal Conductivity
	ρ	C_p	K
	kg/m^3	$J/kg\,°K$	$W/m\,°K$
Mandrel	0.223×10^4	0.837×10^3	0.185×10^1
Insulator	0.110×10^4	0.176×10^4	0.207×10^0
Composite	0.159×10^4	0.148×10^4	0.710×10^0 (K_{11}) 0.710×10^0 (K_{22}) 0.160×10^2 (K_{33})
Outer layer	0.137×10^4	0.105×10^4	0.199×10^0

Constants for permeability model : $C' = C'' = 5$
Fiber diameter : $8\mu m$
Thermal expansion coefficient : -0.36×10^{-6} $/°C$
Young's modulus of the fiber : 2.34×10^{11} Pa

transfer coefficient of 0 W/m^2K on the inner surface of the hollow mandrel. The outer surface of the assembly had direct contact with the oven fluid and is heated by forced convection. The heat transfer coefficient is 40 W/m^2K over the entire outer surface of the assembly.

The initial winding tension was taken to be 35.6 nt (8/bs) per fiber bundle with a tow cross-section area of $4.45 \times 10^{-7}\ m^2$ ($6.9 \times 10^{-4}\ in^2$) .

5.4 Parametric Study

A parametric study was performed for the following cases.

1. Case 1 is the baseline case which uses the cure cycle and boundary conditions described in Section 5.3.3.
2. Case 2 uses the same parameters as Case 1 except that the heating rate is doubled to 5.2°C/ min. The oven was heated from room temperature of 21°C to the cure temperature of 176°C in 30 minutes and held at the final temperature for 4.5 hours.
3. Case 3 uses the same parameters in Case 1 except that a uniform heat transfer coefficient of 100 W/m^2K over the entire outer surface of the assembly is assumed.

The temperature distributions are compared at two locations : one in the cylindrical region (section AA) and one in the dome region (section BB). Section AA and BB are shown in the finite element mesh (Fig. 45).

The resin degree of cure and resin viscosity were compared on the inside and outside surfaces of the composite case at one location in the cylindrical region (section AA) and at one location in the dome region (section BB). The fiber tension variation in each layer is also plotted and discussed for the three cases.

5.4.1 Temperature Distribution

Simulations of the winding and curing processes were performed using the model and the associated computer code. In both the cylindrical and dome regions, temperature vs time was plotted at the following five points :

1. the inner surface of the mandrel,
2. the mandrel / insulator interface,
3. the insulator / composite case interface,
4. the composite case / outer layer interface, and
5. the outer surface of the outer layer.

The temperature distributions for Case 1, Case 2, and Case 3 are presented in Fig. 46, Fig. 47, and Fig. 48, respectively. The temperature is higher in the dome region than in the cylindrical region for the three cases during heating. This is most likely due to a larger outer surface in the dome region than in the cylindrical region. More heat is convected into the dome region than into the cylindrical region resulting in a higher temperature distribution in the dome. Also the case is thinner in the dome region.

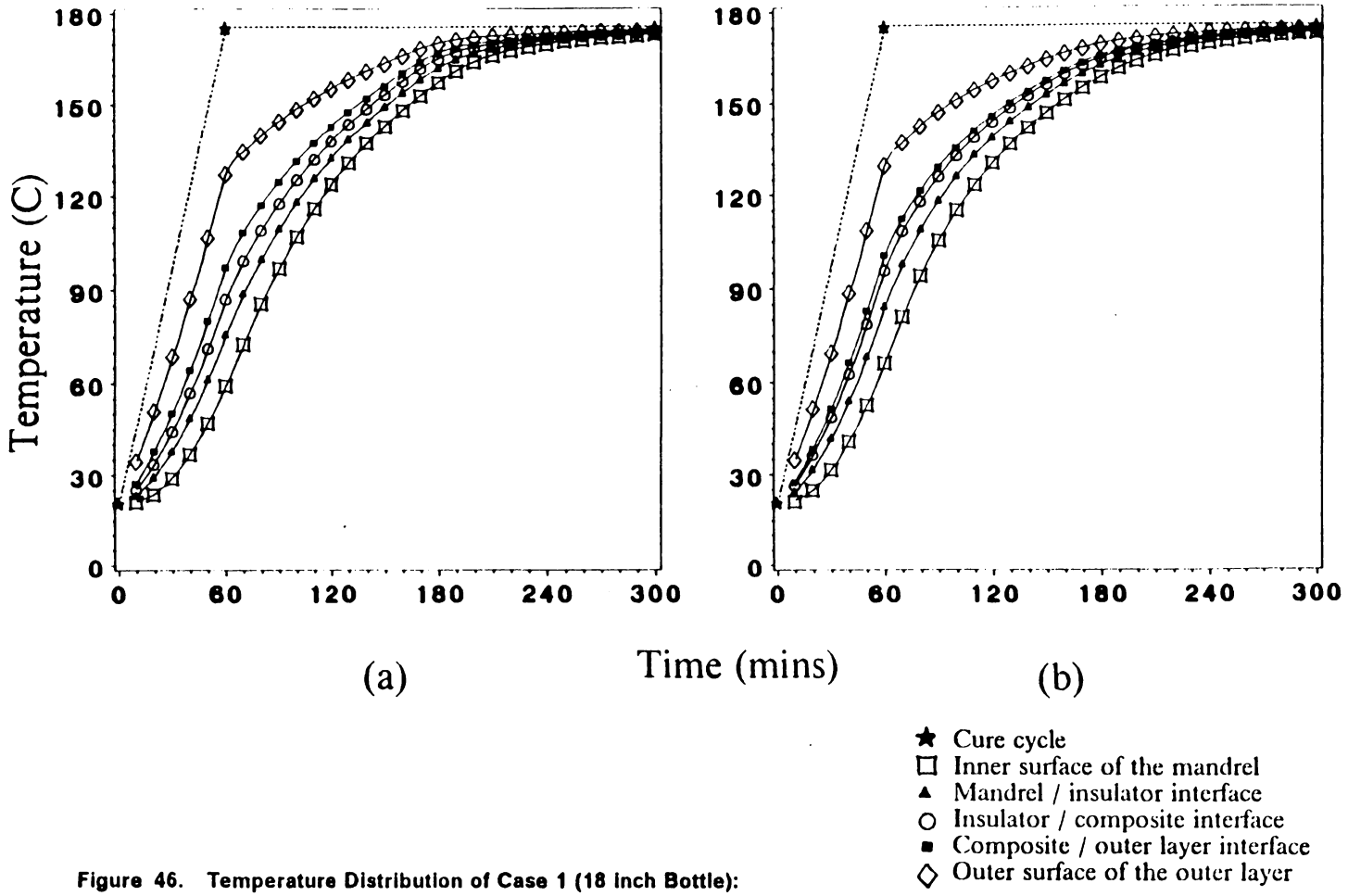

Figure 46. Temperature Distribution of Case 1 (18 Inch Bottle):

The temperature distributions in the cylindrical and dome regions are shown in (a) and (b), respectively. The dash line represents the cure temperature.

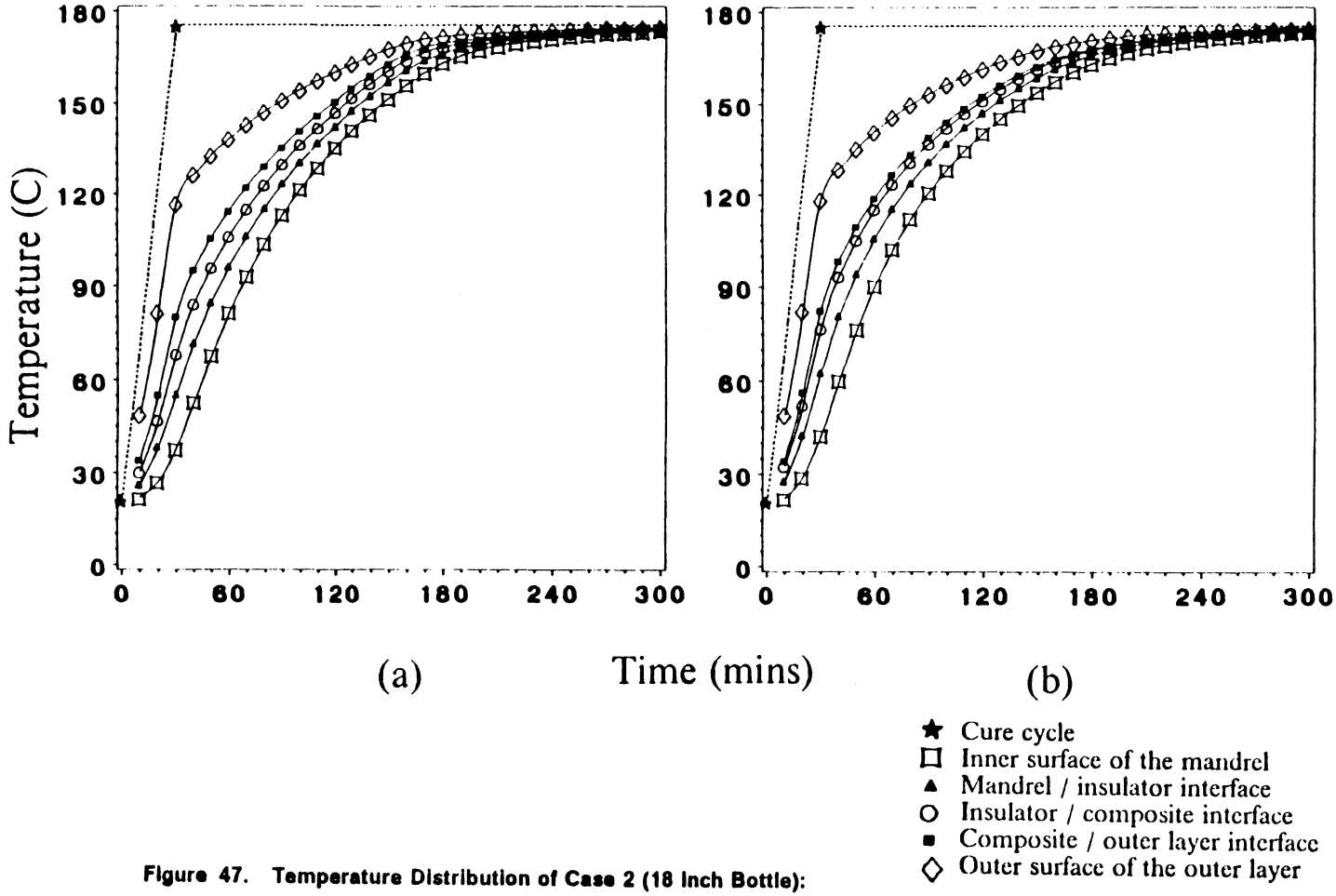

Figure 47. Temperature Distribution of Case 2 (18 Inch Bottle):

The temperature distributions in the cylindrical and dome regions are shown in (a) and (b), respectively. The dash line represents the cure temperature.

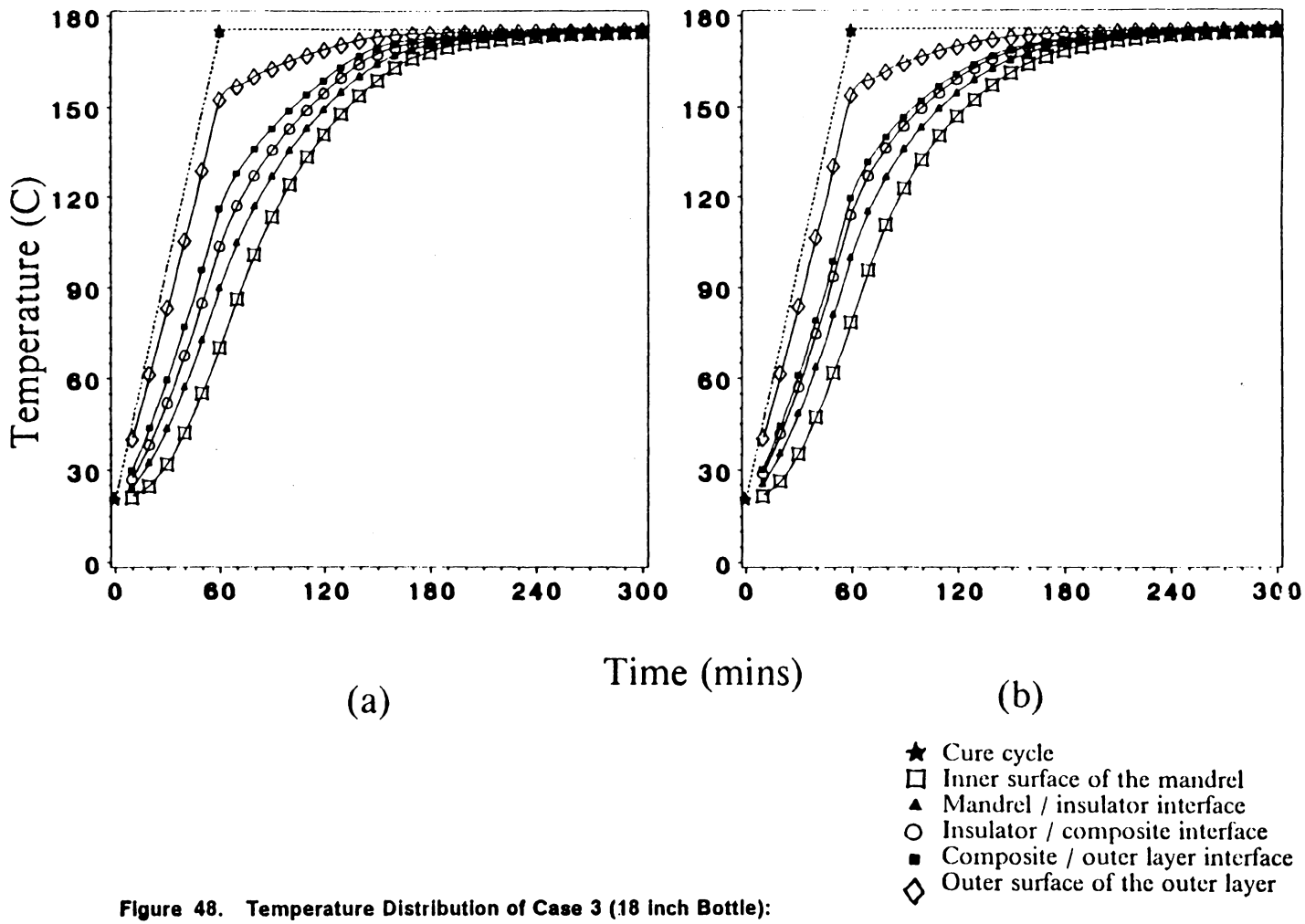

Figure 48. Temperature Distribution of Case 3 (18 inch Bottle):

The temperature distributions in the cylindrical and dome regions are shown in (a) and (b), respectively. The dash line represents the cure temperature.

Because the case is very thin, heat generation is small and quickly released from the composite case. Therefore, exotherms do not occur even when the heating rate is doubled. Furthermore, in Case 2 where the composite assembly is heated at a high rate, the temperature distribution in the composite case remains quite uniform.

Faster heating of the FWC assembly due to an increased heating rate (case 2) or a higher heat transfer coefficient results in only a slight increase in the temperature drop across the composite case. This is most likely due to a very thin composite case used in the study.

The temperature drop across the composite case is greatly affected by the thermal conductivity of the composite and an amount of heat convected into the assembly. It takes more time for heat to be conducted into the inner region for a thick case than for a thin case. Therefore, a higher heating rate and heat transfer coefficient results in more heat convected into the assembly causing a larger great temperature drop across the composite case during heating stage.

The results of the study also shows that the composite case is cured faster by increasing the heat transfer coefficient (Case 3) than doubling the heating rate (Case 2). The composite case reaches the cure temperature earlier in Case 3 than in Case 2.

5.4.2 Degree of Cure and Viscosity

The degree of cure and viscosity are shown in Fig. 49 and Fig. 50, respectively. The results show the effects of local geometry, heat transfer coefficient, and axial heat conduction.

Resin degree of cure and viscosity are affected by the temperature distribution in the composite case. The degree of cure increases rapidly when the temperature in the composite case approaches the cure temperature. In the previous section, it was shown that in Case 3 the composite reaches the cure temperature first resulting in the lowest cure time. A similar result is obtained for the dome region.

Resin viscosity is also affected by the temperature distribution in the composite case. Initially, Case 2 is heated fastest among the three cases resulting in the lowest initial viscosity. Case 2 and Case 3 reach the minimum viscosity at the same time about 10 minutes earlier than Case 1. A similar variation of the resin viscosity is obtained in the dome region.

5.4.3 Fiber Tension Variation

The fiber tension variation as a function of time for Case 1 is illustrated in Fig. 51. The results show a small amount fiber tension loss occurring in the layers 1, 2, 5, and 6, while the layers 3 and 4 lose tension completely for the three cases.

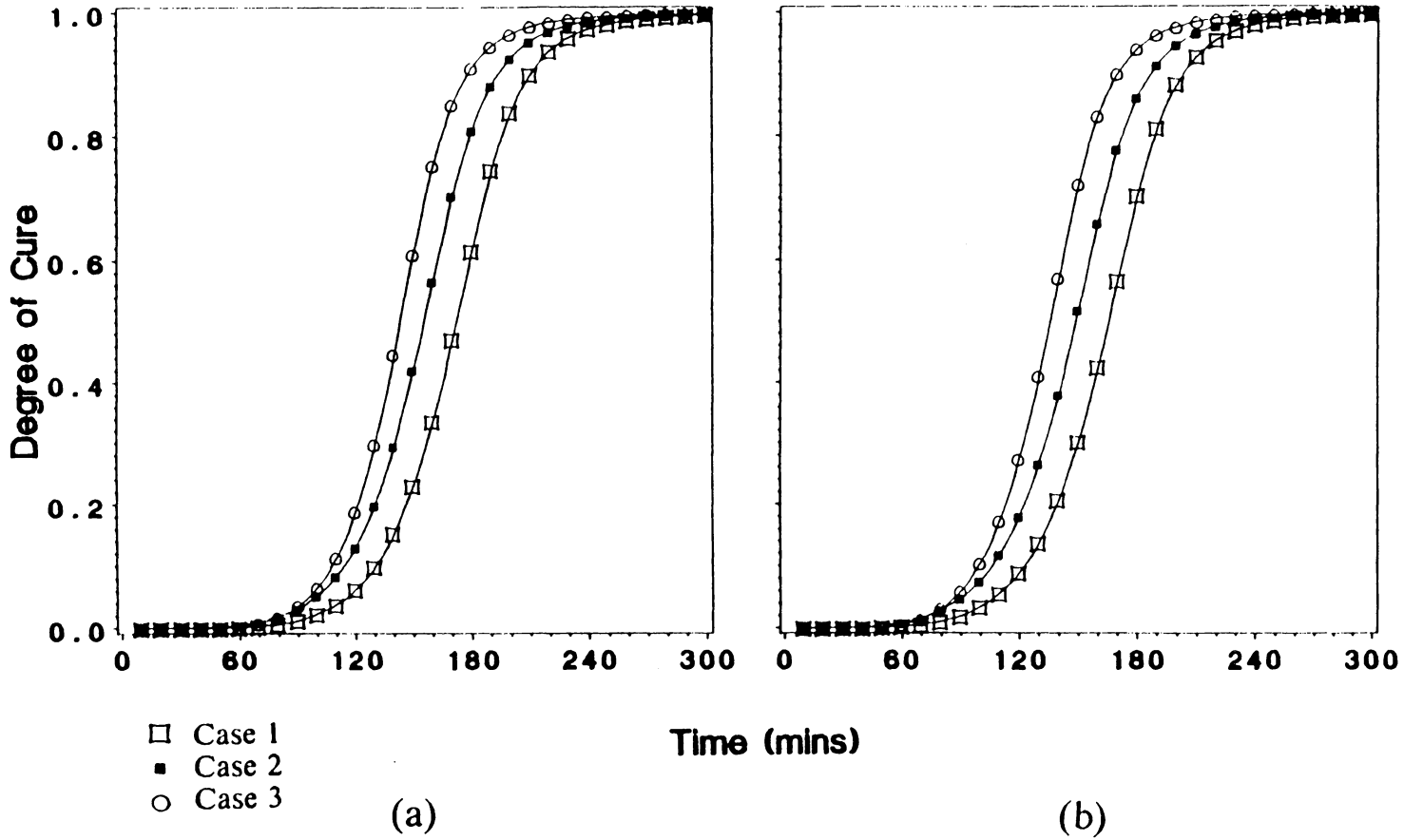

Figure 49. Degree of Cure in Cylindrical Region (18 Inch Bottle):

(a) inner surface in the cylindrical region (b) outer surface in the cylindrical region,

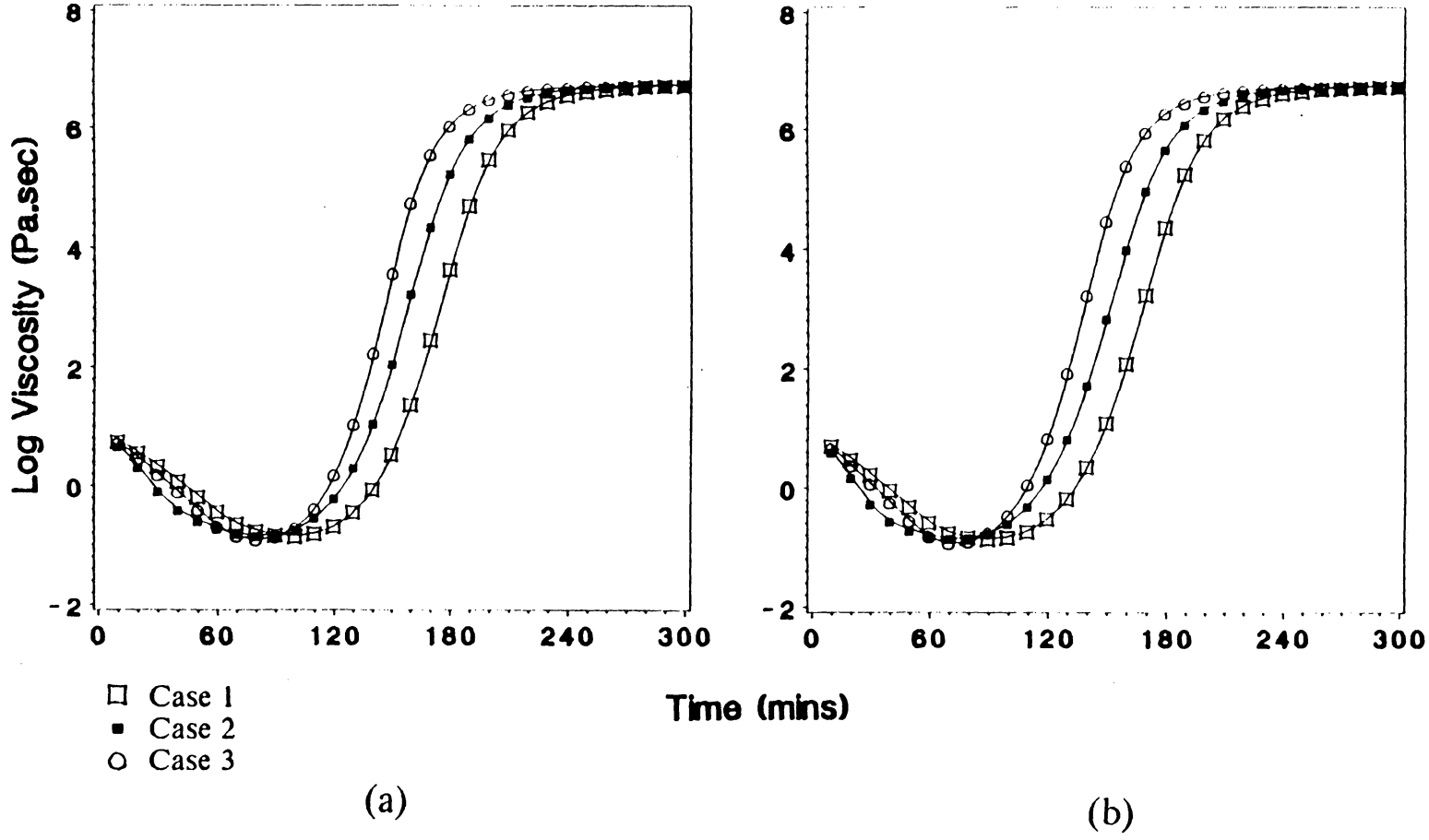

Figure 50. Viscosity in Cylindrical Region (18 inch Bottle):

(a) inner surface in the cylindrical region (b) outer surface in the cylindrical region,

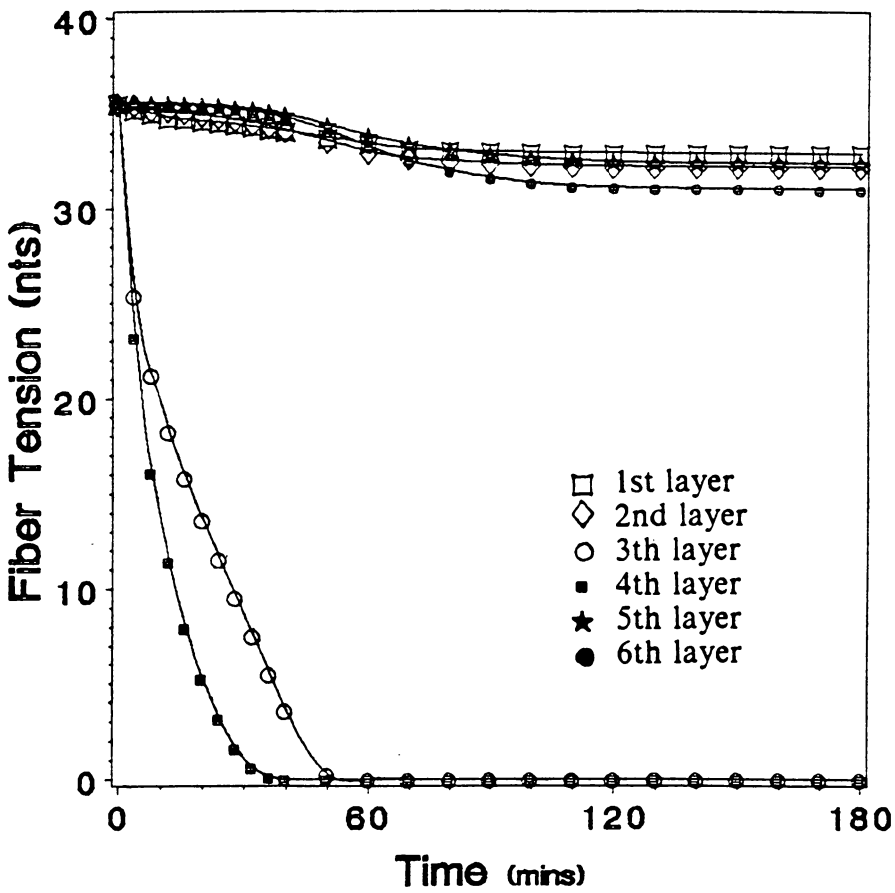

Figure 51. Fiber Tension Variation (18 inch Bottle):
Fiber tension vs time for Case 1.

The 3rd and 4th layers were hoop wound. Hence, the layers have large curvatures which generated large pressure gradients across the layers causing a rapid and complete loss of fiber tension.

Layer 1, 2, 5, and 6 were helically wound. The helical winding pattern has a small fiber curvature and small pressure gradients across the layer. Accordingly, layers 1, 2, 5, and 6 retained more fiber tension.

A similar tension variation is obtained in Case 2 and Case 3 except that the fiber tension loss occurs early.

A comparison of the fiber tension variations of layer 3 and layer 4 for the three cases is shown in Fig. 52. Resin viscosity has a great effect on fiber tension loss. Initially, Case 2 has the lowest viscosity among the three cases resulting in fiber tension loss occurring earlier than the other two cases. Because a compaction occurs earlier in layer 3 than in layer 4, the fiber tension loss occurs more radically in layer 4 than in layer 3.

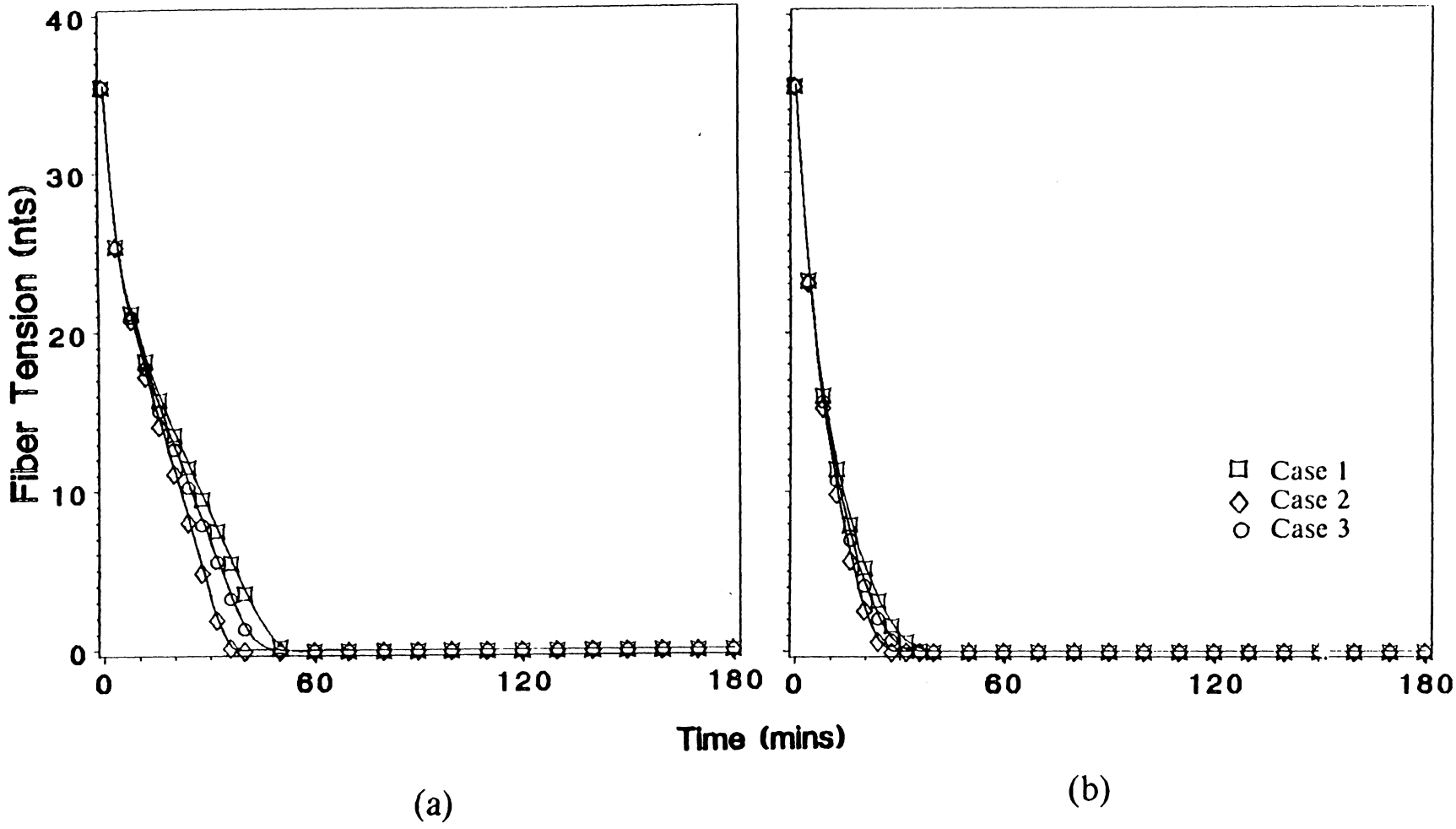

Figure 52. Comparison of Fiber Tension (18 Inch Bottle):

Fiber tension variation as a function of time in the 3rd layer (a) and the 4th layer (b).

6.0 SUMMARY AND CONCLUSION

6.1 Summary

The following major tasks were completed during the course of this investigation.

1. Models were developed which simulate the winding and curing processes of an axisymmetric filament wound composite structure. The cure model relates the cure cycle, applied at the boundaries of the composite assembly, to the thermal, chemical, and physical processes occurring in the composite during cure. The layer tension loss model relates the winding and curing process variables to the instantaneous position and tension of the fibers in each layer of the composite case. The models include :

   a. anisotropic heat conduction due to material anisotropy,
   b. heat generation caused by chemical reaction,
   c. effects of structural curvature and complex geometry including integrally wound end closures,

d. anisotropic resin flow due to various fiber orientation,

e. compaction resulting from the outer tensioned fiber layers and external pressure, and

f. variation in composite permeability caused by consolidation.

2. On the basis of the models, a computer code was developed which can be used to generate the following information for axisymmetric filament wound composites cured by a specified cure cycle :

   a. the temperature distribution in the composite assembly as a function of position and time,

   b. the degree of cure of the resin as a function of position and time,

   c. the resin viscosity as a function of position and time, and

   d. the fiber tension variation as a function of layer and time.

3. The input parameters required in the computer code were specified. The methods and submodels used to determine these parameters were described. The submodels include :

   a. the winding angle as a function of position on the surface of a spherical dome,

   b. the kinetics model and viscosity model for the resin system used in this study,

   c. the permeability as a function of resin volume fraction of the composite, and

   d. the compaction and calculation of fiber/resin content due to the resin flow.

4. Experimental verifications for the cure model were performed by using a 4 inch graphite/epoxy tube and a 5.75 inch diameter graphite/epoxy bottle. The temperatures calculated using the computer code were compared with experimental data. The comparison showed that the model describes adequately the temperature distribution for both cases. Calculation of the layer tension loss was performed using the models for both the 4 inch tube and the 5.75 inch bottle. However, tension loss data were not available for comparison.

5. A parametric study was performed using an 18 inch bottle to show the effects of various processing parameters on the cure and fiber tension loss in the composite case during fabrication.

6. Applications of the model in the fabrication of filament wound composites are summarized as follows :

   a. to select optimum fabrication cycle,
   b. to access the processing characteristics of new material systems used in fabrication,
   c. to identify material properties and processing parameters which have the greatest effect on fabrication,
   d. to identify parameters that must be controlled and monitored during processing, and
   e. to simulate the manufacturing process for real-time, closed-loop process control.

6.2 Conclusion

The cure / layer tension loss model can adequately simulate the manufacturing processes for axisymmetric filament wound composites. Important issues such as heat transfer, cure kinetics, composite permeability, winding pattern, resin flow, fiber motion, compaction, and fiber tension loss were included in the model formulation. The main conclusions drawn from this investigation are summarized as follows.

Results of the cure model showed that the temperature distribution inside the FWC assembly depends on the thermal conductivities of materials as well as curvature and shape of the assembly. Anisotropic conductivity of the composite and axial heat conduction can greatly affect the temperature distribution. A higher thermal conductivity in the direction parallel to the fibers results in a more uniform temperature distribution for a helically wound case than for a hoop wound case.

For thermoset composites, heat generation due to exothermic chemical reactions can cause substantial temperature "overshoots" and a nonuniform temperature distribution and must be controlled during cure. Heat transfer coefficients are greatly affected by the fluid circulation surrounding the FWC assembly. The relatively low heat transfer coefficients commonly measured in forced air ovens and autoclaves results in a large difference between the cure temperature and the surface temperature of the assembly.

Composite permeability, resin viscosity, and pressure due to fiber tension can affect resin flow and the final fiber tension level of each layer in the case. Resin displacement is caused not only by the fiber tension in each layer but also by pressures re-

sulting from tension in the outer layers and external pressure applied during cure. Compaction due to the outer layers can cause a significant amount of resin flow resulting in fiber tension loss and consolidation of the composite for a thick case.

Anisotropic resin flow due to fiber orientation becomes important since composite permeability is much greater in the direction parallel to the fibers than normal to the fibers. Accordingly, axial resin flow can not be neglected for a helically wound case.

A low resin viscosity usually causes a large amount of resin flow resulting in decreases in composite permeability. The final fiber tension level is related to the compaction and permeability of the composite. On the other hand, only a small amount of resin flow occurs in a composite case which uses a high melt viscosity resin. No significant decrease in the composite permeability occurs and the final fiber tension level depends mainly on the pressure. Therefore, the fiber tension distribution in the filament wound composite can be controlled by properly choosing the resin system, initial winding tension, winding pattern, and cure cycle.

Structural defects such as delaminations, local fiber buckling, resin accumulation, and nonuniform cure, due to improper processing parameters were discussed previously. Improvement in the processing of filament wound composite can be accomplished by using the cure / layer tension loss model which can eliminates the need for trial and error selection of the optimal processing parameters.

6.3 Future Research

In order to have a complete and comprehensive fabrication model, the following recommendation are made for future research.

An experimental program will be required to determine the coefficients for the permeability model and to verify the layer tension loss model. This can be accomplished by winding a single fiber layer impregnated with resin on a thin-walled cylindrical mandrel. During winding, strain on the inner surface of the mandrel will be measured and used to calculate fiber tension variation.

A comprehensive cure/stress model requires integration of the cure/layer tension loss model into the thermomechanical model The thermomechanical model, based on elasticity theory, can calculate the residual stresses due to elastic and thermal deformation during winding and cure [1].

The temperature and degree of cure calculated by the cure model will be used to calculate the thermal stresses and material properties in the mechanical model. The stress field obtained by the mechanical model will be used to determine the pressure field in the layer tension loss model.

BIBLIOGRAPHY

1. Nguyen, V. D. "A Fabrication Stress Model for Filament Wound Composite", Thesis, Virginia Tech, (1988)
2. Billmeyer, Fred W., "Textbook of Polymer Science", 2nd edition, John Wiley and Son, (1971)
3. Ryan, M. E. and Dutta, A., "Kinetics of Epoxy Cure: A Rapid Technique for Kinetic Parameter Estimation", Polymer, Vol. 20 (1979)
4. Lee, W. I., Loos, A. C., and Springer, G. S., "Heat of Reaction, Degree of Cure, and Viscosity of Hercules 3501-6 Resin" , J. Composite Material Vol. 16, (1982)
5. Hou, T. H., "Chemoviscosity Modeling for Thermosetting Resin", NASA Langley, CR-172443, (1984)
6. Halpin, J.C., Kardos, J. L., and Dudukovic, M. P., "An Approach for Prepreg Composite System", Interrelations between Processing Structures and Properties of Polymeric Material, (1984)
7. Loos, A. C. and Springer, G. S., "Curing of Epoxy Matrix Composite", Journal of Composite Material, 17 135-169, (1983)

8. Callius, Emilio P. and Springer, G. S., "Modeling the Filament Wound Process", 5th International Conference on Composite Material, (1985)
9. Grigull, U. and Sandner, H., "Heat Conduction" , Springer-Verlag, (1983)
10. Jones, R. M., "Mechanics of Composite Material", McGraw-Hill, (1980)
11. Springer, G. S. and Tsai, S. W., "Thermal Conductivity of Unidirectional Material", J. of Composite Material, Vol.16, (1967)
12. Reddy, J. N., "Energy and Variational Methods in Applied Mechanics", John-Wiley N.Y., (1984)
13. Reddy, J. N., "An Introduction to the Finite Element Method", McGraw-Hill Book Company, (1984)
14. Zienkiewicz, "The Finite Element Method", McGraw-Hill Book Company
15. Bathe, K. J. and Wilson, E. L., "Numerical Method in Finite Element Analysis", Prentics - Hall, Inc., Englewood Cliffs, (1976)
16. Lambert, J. D., "Computational Method in Ordinary Differential Equations", Wiley, (1973)
17. Lindt, J. T., "Engineering Principles of of the Formation of Epoxy Resin Composite", SAMPE Quartely, (1982)
18. Hou, T.H., "A Theoretical Study of Resin Flows for Thermosetting Materials during Prepreg Processing", (1984)
19. Gutowski, T. G. and Morigaki, T., and Cai, Z., " The Consolidation of Laminate Composite", J. of Composite Material, (1987)
20. Dave, R., Kardos, J. L., and Dudukovic, "A Model for Resin Flow during Composite Processing: Part 1 - General Mathematical Development", Polymer Composite, Vol.8 NO.8, (1987)
21. Scheidegger, A. E., "The Physics of Flow Through Porous Media", 3rd edition, University of Toronto Press, (1974)

22. Lubin, G., "Handbook of Composite Material", Van Nostrand Reinhold, (1982)

23. Dusi, M. K., Lee, W. I., Ciriscioli P. R., and Springer G. S., "Cure Kinetics and Viscosity of Fiberite 976 Resin", J. of Composite Material, Vol 21, (1987)

24. Hildebrand, F. G. "Advanced Calculus for Application", 2nd edition, Prentice - Hall, Inc. (1977)

Appendix A. WINDING PATTERN

A.1 Winding Path

The winding pattern is the most important and complex variable in the manufacturing process of filament wound composites. Depending on the structural geometry and strength requirements, the winding pattern is designed by choosing suitable winding paths. The winding path may vary from layer to layer to meet the design requirements. For pressure vessels or rocket motor cases with integrally wound end closures, two winding patterns are commonly used. These include a geodesic path and a planar path (Fig. 53).

For a geodesic path, the fiber bands are wound along the shortest (or geodesic) path on the mandrel surface. The tensioned fibers tend to move onto and stay on the geodesic path to maintain force equilibrium conditions. Accordingly, the fiber bundles wound on the geodesic path are stable with less slippage. The geodesic path is referred to as a stationary path. The geodesic winding pattern usually includes a

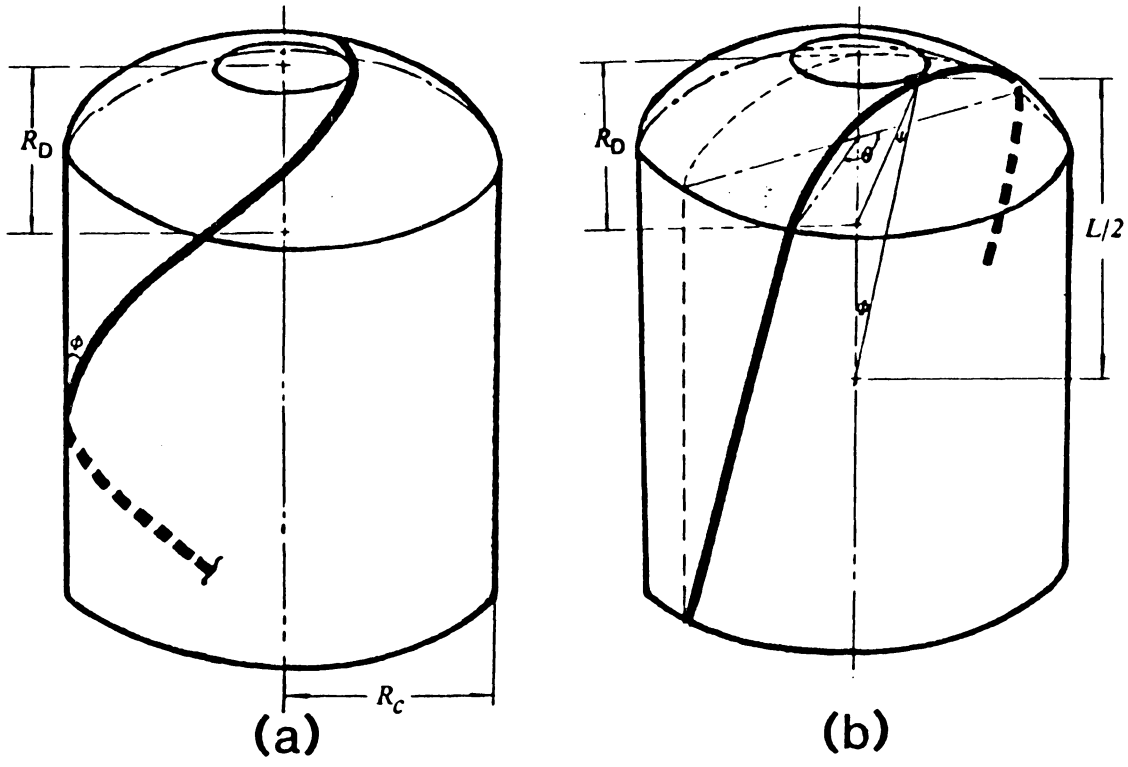

Figure 53. Geodesic and Planar Winding Path:
(a) Geodesic Path and (b) Planar Path

helical winding pattern on the cylindrical surface of the case with a geodesic path at dome region.

For a planar path, the fiber path on the dome region is located by the intersection of a plane with the dome. Hence, the winding path is referred to as a planar path. The tensioned fiber is balanced not only by the resistant normal force from mandrel but also by friction. The planar path is not a stationary path thus limiting the number of applications in the filament winding. Usually, the planar path is wound on a case which has a large diameter and a relatively short length. Slippage of the fiber bundles often occurs in a planar winding path during cure due to a decrease in the balancing friction when the matrix resin melts.

The winding pattern affects not only the final mechanical strength and residual stresses of the composite case but also influences to many parameters in the manufacturing process. The pressure distribution and amount of layer compaction inside the case greatly depend on the winding pattern. During cure, anisotropic heat conduction and resin flow are also affected by the fiber path.

A.2 Winding Angle

The winding angle at any point along the fiber path is defined as the angle between the fiber path and the latitude drawn through the point of path (Fig. 54). The winding path and winding angle on the dome surface are determined by the polar boss and geometry of the mandrel. The winding angle on the surface of the cylindrical region is determined by the winding path on the dome region.

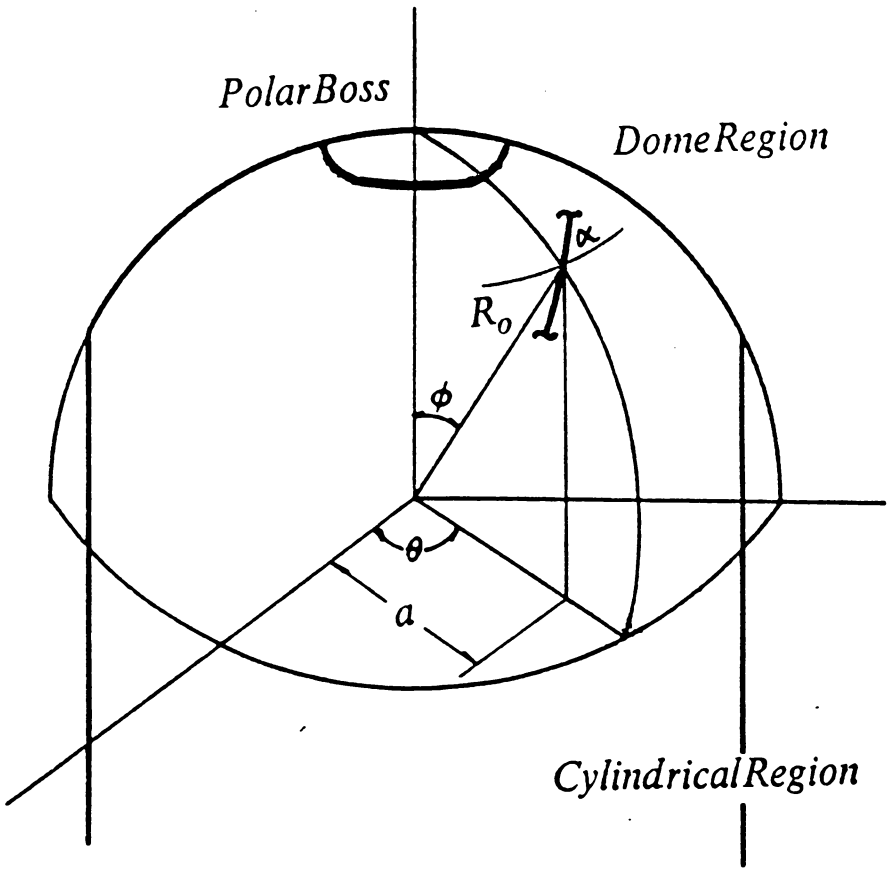

$$\min \quad L = \int_{\phi_0}^{\phi_1} \sqrt{1 + \sin^2\phi\,\dot{\theta}^2}\; r\,d\phi$$

Figure 54. Calculation of Winding Angle

In order to estimate the winding angle along the fiber path, a geodesic winding path is assumed to be wound on a spherically shaped dome. The winding path can be calculated from the definition of the geodesic path on a spherical surface.

In spherical coordinates (r, θ, ϕ), the arc length of the fiber path can be written as:

$$dl = \sqrt{dr^2 + r^2 d\phi^2 + r^2 \sin^2\phi \, d\theta^2} \qquad (a.1)$$

where dr is the increment of the fiber path along r-direction, $r\,d\phi$ is the increment of the fiber path along ϕ-direction, and $r \sin\phi \, d\theta$ is the increment of fiber path along θ-direction. Since the fiber path is on a spherical surface of constant radius. Eq.(a.1) can be simplified as follows:

$$\begin{aligned} dl &= \sqrt{r^2 d\phi^2 + r^2 \sin^2\phi \, d\theta^2} \\ &= \sqrt{1 + \sin^2\phi \left(\frac{d\theta}{d\phi}\right)^2} \; r \, d\phi \end{aligned} \qquad (a.2)$$

Let $\theta = \theta(\phi)$ represent a geodesic path on the surface of dome. The length of the fiber path between two arbitrary points, ϕ_0 and ϕ_1, can be calculated by integration the expression for the arc length as :

$$L = \int_{\phi_0}^{\phi_1} \sqrt{1 + \sin^2\phi \, \dot{\theta}^2} \; r \, d\phi \qquad (a.3)$$

The minimized length L is obtained by solving the Euler equation of Eq.(a.3) from calculus of variations [24]. The Euler equation can be derived from the following expression.

$$\frac{d}{d\phi}\left(\frac{\partial\, r\sqrt{1+\sin^2\phi\,\dot{\theta}^2}}{\partial\dot{\theta}}\right)-\frac{\partial\, r\sqrt{1+\sin^2\phi\,\dot{\theta}^2}}{\partial\theta}=0 \qquad (a.4)$$

The calculation results in the following governing equation of the fiber path.

$$\sin\phi\,\ddot{\theta}+\sin^2\phi\,\cos\phi\,\dot{\theta}^3+2\cos\phi\,\dot{\theta}=0 \qquad (a.5)$$

The solution of Eq.(a.5) is

$$\theta=\sin^{-1}(c_1\cot\phi)+c_2 \qquad (a.6)$$

Where the coefficients c_1 and c_2 can be determined from the boundary conditions at Point A and Point B in the fiber path (Fig. 55).

At Point A, the boundary condition is

$$\phi=\frac{\pi}{2} \qquad when \quad \theta=0 \qquad (a.7.a)$$

At Point B, the boundary condition is

$$\phi=\phi_i \qquad when \quad \theta=\frac{\pi}{2} \qquad (a.7.b)$$

where ϕ_i is the angle measured from the edge of polar boss to longitudinal axis of the case.

The winding angle at any point along the fiber path is obtained from the slope of the fiber path. Taking the derivative of Eq.(a.6) with respect to ϕ gives the following expression

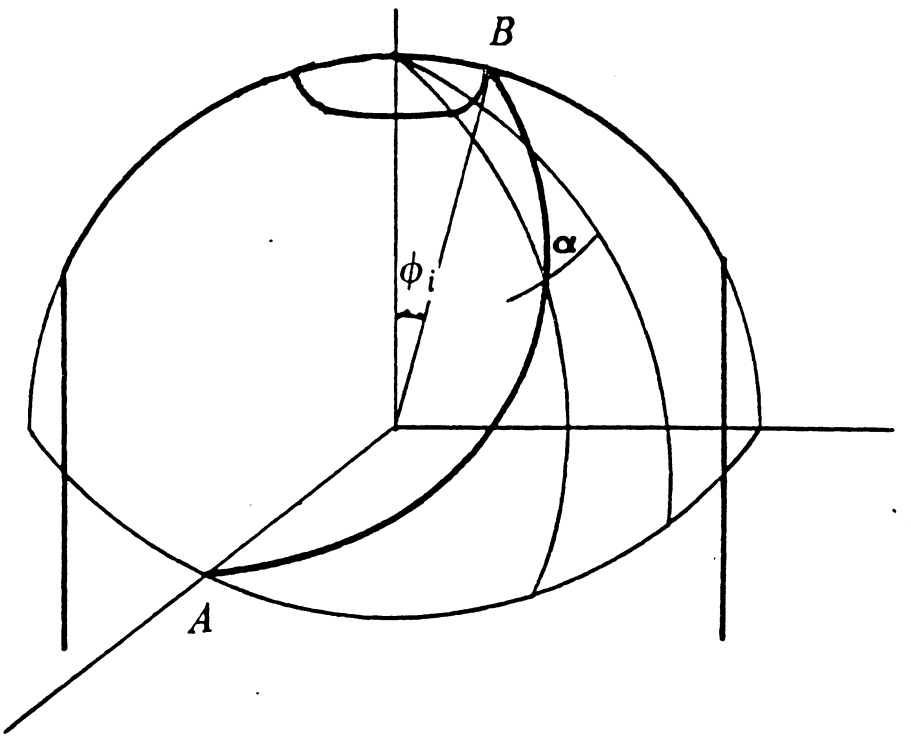

Boundary Condition

$$A\ (R_o\ ,\ 0\ ,\ \frac{\pi}{2})$$

$$B\ (R_o\ ,\ \frac{\pi}{2},\ \phi_i)$$

Figure 55. Boundary Conditions for Winding Path

$$\cot\alpha \simeq \lim_{\Delta\phi \to 0} \frac{\Delta\theta}{\Delta\phi} \frac{a}{R_o} \tag{a.8}$$

where R_o is the radius of the sphere and a is the distance between the fiber path and the longitudinal axis of case. Therefore, the winding angle at any point along the path can be calculated from the following expression.

$$\alpha = \cot^{-1} \left(\frac{a}{R_o} \frac{\frac{c_1}{\sin^2\phi}}{\sqrt{1 - c_1^2 \frac{\cos^2\phi}{\sin^2\phi}}} \right) \tag{a.9}$$

Appendix B. KINETICS AND VISCOSITY MODEL - FIBERITE 982 RESIN

B.1 Kinetics Model

The calorimetric measurements were made using differential scanning calorimetry (DSC) experiments. The rate of heat generation, $\frac{dQ}{dt}$ was measured for isothermal cure at the following temperatures : 93, 102, 107, and 113 °C . A continuous curve (DSC curve) was obtained for each temperature showing the rate of heat generation as a function of time.

Integration of the rate of heat generation with respect to time gives the heat generation, $Q(t)$ from the beginning of cure to any intermediate time, t as follows:

$$Q(t) = \int_0^t \frac{dQ}{dt}\, dt \qquad (b.1)$$

This procedures were carried out by measuring the area enclosed by the DSC curves. The degree of cure is calculated from the ratio of the heat generation to the total heat of reaction

$$\alpha = \frac{Q(t)}{Q_u} \qquad (b.2)$$

where, Q_u is the heat of reaction. The heat of reaction was measured from the dynamic scanning experiment. Differentiating the expression (b.2) with respect to time gives the cure rate

$$\dot{\alpha} = \frac{\dot{Q}(t)}{Q_u} = \frac{dQ/dt}{Q_u} \qquad (b.3)$$

where $\dot{\alpha}$ is cure rate and $\dot{Q}(t)$ is heat generation rate.

Accordingly, we can relate the cure rate to the degree of cure for the isothermal cure experiment. Experimental data of cure rate vs degree of cure for each temperature are listed in Table 5.

The following expression for cure rate was fit to experimental data for Fiberite 982 resin.

$$\dot{\alpha} = (K_1 + K_2\ \alpha^m)\,(1-\alpha)^n \qquad (b.4)$$

where K_1, K_2 are the kinetic rate constants which are functions of temperature and m and n are the kinetics exponents.

The constants in the kinetics model were determined by a non-linear least square curve fit to the $\dot{\alpha}$ versus α data using a Levenberg - Marquardt algorithm. This

Table 5. Isothermal Cure Kinetic Data (Fiberite 982)

85°C		93°C	
$\frac{d\alpha}{dt}$	α	$\frac{d\alpha}{dt}$	α
0.2340E-04	0.2796E-01	0.4793E-04	0.4480E-01
0.3358E-04	0.4941E-01	0.6684E-04	0.6776E-01
0.5292E-04	0.9162E-01	0.1022E-03	0.1141E+00
0.5902E-04	0.1355E+00	0.1312E-03	0.1739E+00
0.5800E-04	0.1832E+00	0.1400E-03	0.2291E+00
0.5397E-04	0.2226E+00	0.1286E-03	0.2953E+00
0.4783E-04	0.2520E+00	0.1097E-03	0.3499E+00
0.3868E-04	0.2771E+00	0.8198E-04	0.3951E+00
0.2851E-04	0.3106E+00	0.4416E-04	0.4382E+00
0.0000E+00	0.3566E+00	0.0000E+00	0.4711E+00
102°C		107°C	
$\frac{d\alpha}{dt}$	α	$\frac{d\alpha}{dt}$	α
0.1060E-03	0.2714E-01	0.1611E-03	0.2438E-01
0.1718E-03	0.6053E-01	0.3058E-03	0.6203E-01
0.2595E-03	0.1128E+00	0.4109E-03	0.1267E+00
0.2997E-03	0.1785E+00	0.4497E-03	0.2117E+00
0.2960E-03	0.2563E+00	0.4331E-03	0.2778E+00
0.2631E-03	0.3242E+00	0.3394E-03	0.3343E+00
0.2083E-03	0.3874E+00	0.2620E-03	0.3807E+00
0.1390E-03	0.4359E+00	0.1846E-03	0.4186E+00
0.7310E-04	0.4722E+00	0.1005E-03	0.4580E+00
0.0000E+00	0.4980E+00	0.0000E+00	0.4896E+00

procedure gives values for the constants K_1, K_2, m, and n, which are temperature dependent, as follows

$$K_1 = A_1 \exp(-E_1/RT) \tag{b.5}$$

$$K_2 = A_2 \exp(-E_2/RT) \tag{b.6}$$

$$m = -0.0333 \times T + 14.733 \tag{b.7}$$

$$n = 9.0 \tag{b.8}$$

where R is idea gas constant and T is absolute temperature.

Constants A_1, E_1, A_2, and E_2 were obtained by linear squares curve fits to the K_1 vs $1/T$ and K_2 vs $1/T$ data. The procedures gave the following values

$$A_1 = 2.307 \times 10^9 \ \ sec^{-1} \tag{b.9}$$

$$A_2 = 2.519 \times 10^5 \ \ sec^{-1} \tag{b.10}$$

$$E_1 = 9.526 \times 10^4 \ \ J/mole \tag{b.11}$$

$$E_2 = 4.648 \times 10^4 \ \ J/mole \tag{b.12}$$

The kinetics model is compared with the experimental data in Fig. 56 and Fig. 57 . A good correlation was found between the prediction of the model and experimental data.

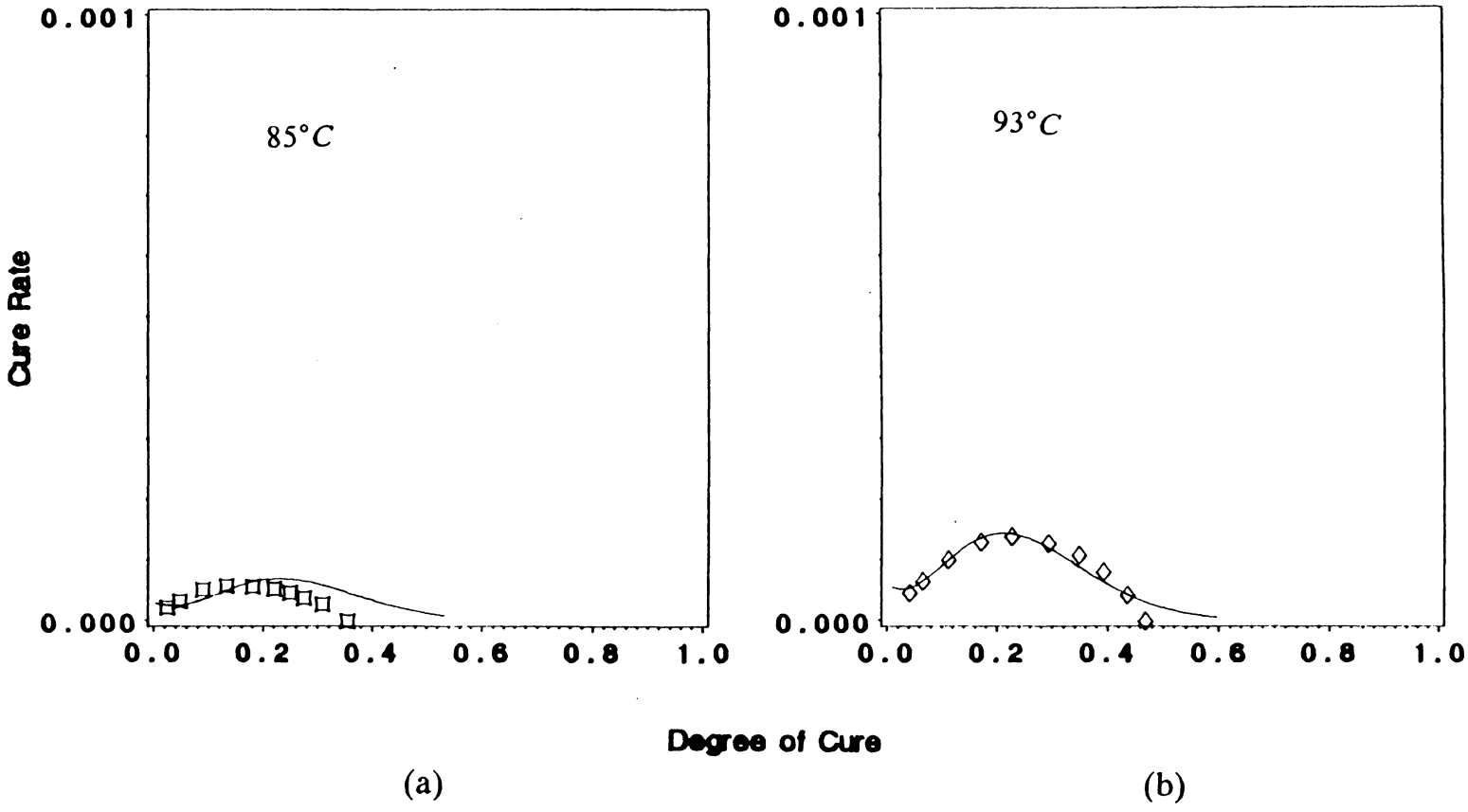

Figure 56. Kinetics Model for Fiberite 982 Resin - I:

Cure rate as a function of degree of Cure are shown at the following temperature : (a) 85°C and (b) 93°C.Solid lines were calculated using the model.

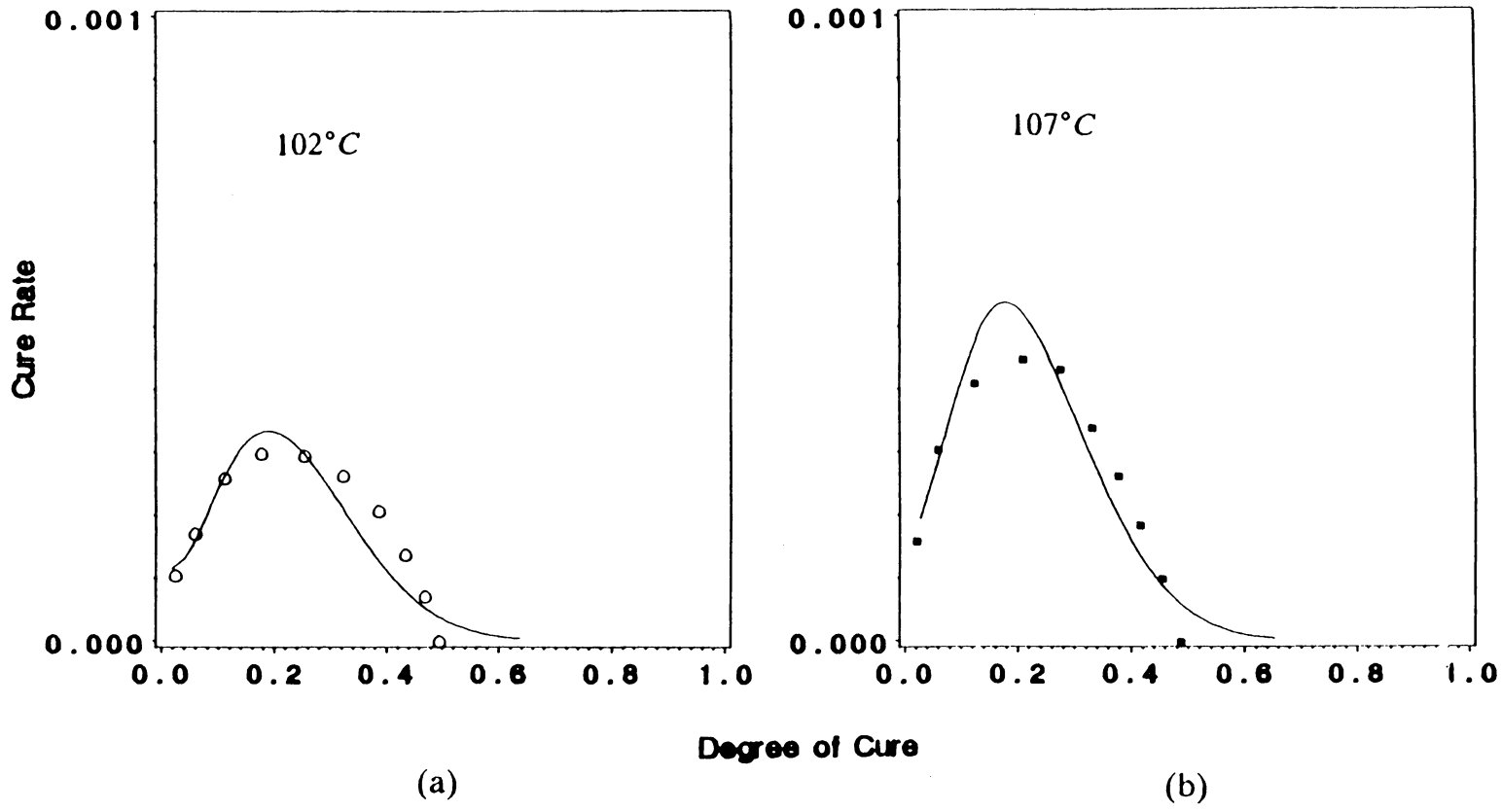

Figure 57. Kinetics Model for Fiberite 982 Resin - II:

Cure rate as a function of degree of Cure are shown at the following temperature : (a) 102°C and (b) 107°C, Solid lines were calculated using the model.

B.2 Viscosity Model

Resin viscosity as a function of time and temperature was measured from isothermal cure experiments. Resin samples were cured at constant temperatures and the viscosity was measured during cure on a rheometer.

Since the degree of cure of the resin is also a function of time and temperature (refer the cure model), the viscosity can be expressed in terms of the degree of cure, α and temperature. The measured viscosity data vs the degree of cure, α used to develop the viscosity model are listed in Table 6.

The viscosity is related to temperature, T and degree of cure, α by the following mathematical model

when $\alpha < \alpha_c$

$$\mu = \mu_\infty \exp(\frac{U}{RT} + K\alpha) \qquad (b.13)$$

when $\alpha \geq \alpha_c$

$$\mu = \mu_\infty \exp(\frac{U}{RT} + K\alpha_c) \exp(M(\alpha - \alpha_c)) \qquad (b.14)$$

where μ_∞ is a constant, U is the activation energy for viscosity, R is the idea gas constant, M is a constant, and K and α_c are are temperature dependent parameters.

Table 6. Isothermal Viscosity Data (Fiberite 982)

	α	log μ (Pa. sec)
93°C	0.1034 0.2148 0.3282 0.3987 0.4425 0.4537 0.4636 0.4726 0.4806 0.4880 0.4947 0.4997	4.389 4.350 4.314 4.290 4.276 4.276 4.340 4.486 4.767 5.197 5.680 5.971
107°C	0.1972 0.4088 0.4748 0.4943 0.5095 0.5229 0.5262 0.5282	3.554 3.534 3.430 3.525 4.145 5.356 5.892 5.985
121°C	0.2829 0.3798 0.4276 0.4577 0.4792 0.4957 0.5090 0.5200 0.5294 0.5375 0.5412 0.5477 0.5480 0.5512	2.941 3.012 3.041 3.048 3.046 3.056 3.065 3.079 3.088 3.111 3.346 4.121 5.235 5.703

The constants μ_{∞}, K, M, α_c, and activation energy U are obtained by fitting the viscosity data to the mathematical model. This procedure results in the following values :

$$\alpha_c = 2.143 \times 10_3 T - 0.3143 \qquad (b.15)$$

$$\mu_{\infty} = 7.29 \times 10^{-19}\ Pa.sec \qquad (b.16)$$

$$U = 1.58 \times 10^{5}\ J/mole \qquad (b.17)$$

$$K = 0.067 \times T - 25.25 \qquad (b.18)$$

$$M = 150 \qquad (b.19)$$

A comparison of the measured data and prediction by the viscosity model is illustrated in Fig. 58 . The comparison shows a very good agreement.

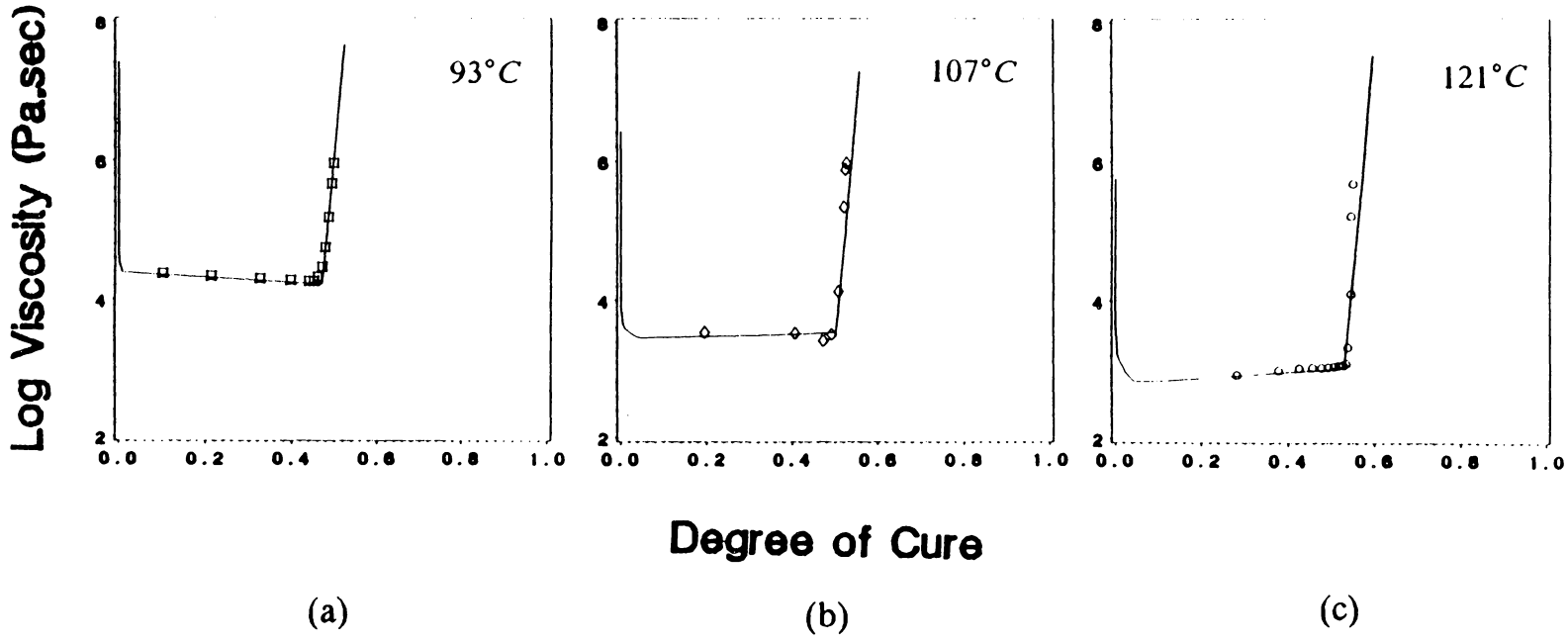

Figure 58. Viscosity Model for Fiberite 982 Resin :

Viscosity as a function of degree of Cure are shown at the following temperature : (a) 93°C , (b) 107°C , and (c) 121°C. Solid lines were calculated using the model.

The vita has been removed from the scanned document